

**STUDY OF TRIBOLOGICAL BEHAVIOR OF
PLASMA SPRAYED RED MUD COMPOSITE
COATINGS**

Thesis Submitted By
Harekrushna Sutar

Doctor of Philosophy

in

Engineering

**Department of Chemical Engineering
Faculty Council of Engineering & Technology
Jadavpur University
Kolkata, India**

2019

JADAVPUR UNIVERSITY

KOLKATA-700032, INDIA INDEX NO: 201/16/E

1. Title of the thesis: Study of Tribological Behavior of Plasma Sprayed Red Mud Composite Coatings.

2. Name, Designation & Institution of the Supervisor/s:

Prof (Dr). Debashis Roy, Department of Chemical Engineering, Jadavpur University, Kolkata, India and **Prof (Dr). Subash Chandra Mishra**, Department of Metallurgical and Materials Engineering, National Institute of Technology, Rourkela, India.

3. List of Publications:

Book Chapter:

- a) Plasma Sprayed Red Mud-Fly Ash Composite Coatings on Mild Steel: A Comprehensive Outline; **H. Sutar**, R. Murmu, D. Roy, S.C Mishra; *Advances and Trends in Physical Science Research*, Chapter-13, Vol-2, 2019, Print ISBN: 978-93-89246-00-1, Editor: Dr. Mohd Rafatullah , **Book Publisher International**, London , UK

Papers Published in Refereed Journal:

- a) *Thermal and Dry Sliding Wear Behavior of Plasma Sprayed Red Mud-Fly Ash Coatings on Mild Steel*; **H. Sutar**, D Roy, S.C Mishra, S. Patra, R. Murmu; *Tribology in Industry*; 40 (1), 117-128, 2018. Scopus Cite Score 1.27
- b) *Sliding Wear Performance Evaluation of Red Mud (RM), RM + Fly Ash (FA) and RM + FA + Al Coatings on Mild Steel*; **H. Sutar**, D Roy, S.C Mishra, R.R Murmu; *Materials Sciences and Applications*; 7(3), 171-179, 2016. Google Based IF: 1.09
- c) *Friction and Wear Behaviour of Plasma Sprayed Fly Ash Added Red Mud Coatings*: **H. Sutar**, D. Roy, S. C. Mishra, A. P. Chakraverty and H. Maharana; *Physical Science International Journal*; 5(1), 61-63, 2016. NAAS Score: 4.69
- d) *Effect of fly ash and carbon reinforcement on dry sliding wear behaviour of red mud*; **H. Sutar**, D Roy and S.C Mishra; *Indian Journal of Materials Science*; Article ID 296324, 7 pages, 2015. Highest Visibility: INSPEC

4. List of Patents: No patent filed.

5. List of Presentations in National/International/Conferences/Workshops:

Not applicable.

CERTIFICATE FROM THE SUPERVISOR/S

This is to certify that the thesis entitled “Study of Tribological Behavior of Plasma Sprayed Red Mud Composite Coatings” submitted by Shri Harekrushna Sutar, who got his name registered on 27/01/2016 for the award of **Ph.D (Engineering)** degree of Jadavpur University is absolutely based upon his own work under the supervision of Prof (Dr) Debashis Roy and Prof (Dr) Subash Chandra Mishra and that neither his thesis nor any part of the thesis has been submitted for any degree/diploma or any other academic award anywhere else before.

Prof. Debashis Roy

Prof. Subash Chandra Mishra

Dedicated
To
My parents

DECLARATION OF ORIGINALITY

I, *Harekrushna Sutar*, bearing index number **201/16/E** hereby declare that this dissertation entitled “*Study of Tribological Behavior of Plasma Sprayed Red Mud Composite Coatings*” represents my original work carried out as a doctoral student of Jadavpur University, Kolkata and, to the best of my knowledge, it contains no material previously published or written by another person, nor any material presented for the award of any other degree or diploma of Jadavpur University, Kolkata or any other institution. Works and writings of other authors; included in this dissertation have been duly acknowledged under the section of "*References*". I am fully aware that in case of any non-compliance detected in future, Jadavpur University, Kolkata may withdraw the degree awarded to me on the basis of the present dissertation.

Date:

Harekrushna Sutar

Jadavpur University, Kolkata

ACKNOWLEDGEMENT

The author wishes to express his deep sense of gratitude to his guide and co-guide, **Dr. Debashis Roy**, Professor (Head), Department of Chemical Engineering, Jadavpur University, Kolkata and **Dr. Subash Chandra Mishra**, Professor, Department of Metallurgical and Materials Engineering, National Institute of Technology, Rourkela for their invaluable guidance, motivation, untiring efforts and meticulous attention at all stages of this research work.

He appreciates the co-operation extended by the scientists at the Laser and Plasma Technology Division, Bhabha Atomic Research Center (B.A.R.C), Mumbai in carrying out the experimental work.

The author is grateful to **Professor Suranjan Das**, vice chancellor, Jadavpur University, Kolkata who has been a constant source of inspiration for him. He is also grateful to all faculty and staff members of the Chemical Engineering Department of Jadavpur University, Kolkata.

The author gratefully appreciates the help and support of Mr. Sasanka Biswas ex-laboratory technician, Grade-I, Department of Electrical Engineering, Jadavpur University, Kolkata. The author also wishes to acknowledge with gratitude the endless inspiration and sacrifice that came from his family members, friends and relatives to see the completion of this work.

Jadavpur University, Kolkata

(Harekrushna Sutar)

ABSTRACT

The present investigation aims at evaluating the effect of fly ash, carbon and aluminium addition on coating characteristics of pure red mud. Plasma sprayed coatings composed of red mud and a varying percentage of fly ash, carbon and aluminium on mild steel are considered for the study. Plasma spraying technique is used with varying levels of power namely 6, 9, 12 and 15 kW. Plasma spray is one of the most widely used techniques involved in surface modification by improvement of wear resistance, which may affirm the great versatility and its application to a wide spectrum of materials. Investigations of the coatings focused on tribological properties like sliding wear behaviour, wear morphology, wear mechanism and frictional force. Different coating characteristics like surface morphology, hardness, porosity, thickness, deposition efficiency, bond strength and new phase formation are studied. The sustainability of these coatings towards high temperature at air environment up to 1000°C is evaluated by finding their adhesion strength. DSC and TGA techniques are implemented to observe the coating behaviour to heat. The coatings show remarkable resistance towards high temperature by virtue of adhesion strength compensation. It is feasible to use these coatings limiting < 800°C otherwise dislodging of coating from metal. Fly ash with 10, 20 and 50% by weight was mixed with red mud. Carbon and Aluminium powder with 20 weight %each are premixed to red mud separately and plasma sprayed. Sliding wear test are performed using a pin on disc wear test machine. The wear test is performed till the survival of coatings with track diameter of 100 mm and at a sliding speed of 100 rpm (0.523 m/s); applying a normal load of 10 N. The variation of wear rate and frictional force with that of sliding distance and time has been presented. The addition of fly ash with red mud reduces the wear rate by enhancing the coating property. But the optimum percentages of fly ash required for better coating material still impact a question mark for the researchers. Addition of aluminium and carbon further reduces the wear rate. It is observed that for the early stage the wear rate increases slowly and then rises drastically with sliding distance for all coating type and finally becomes stagnant. Operating power level proved to be the remarkable variable for different coating property. The observation signifies the coatings wear resistance (reverse of wear rate) increases until an optimum value at 12 kW, afterwards indicating some other dominating parameters. Significant wear resistance was visible with the addition of fly ash due to an increase in bond strength and dense film at the interface. Wear rate decreases with operating power up to 12 kW, thereafter increases

with initiating other dominating parameters. At the end, design of experiment is conducted to analyse the dominating parameters to wear. The present study concludes that, red mud coatings possess acceptable thermal properties. Fly ash, carbon and aluminium are beneficiary reinforcing agent for red mud, and the composite can be coat able with favouring surface properties. These coatings can be operated at high temperature. It is observed that, due to low material cost, these composite coatings can also be employed for suitable tribological applications. Plasma generating power, adversely affect the coating morphology. This work is a portfolio for researcher to discover many other aspects of red mud and its composite coatings. The study may be extended by future investigators to find its distinct application areas.

Keywords: Red mud; fly ash; aluminium; carbon; plasma coating; bond strength; thermal stability; sliding wear; wear mechanism.

LIST OF FIGURES

Figure No	Title of the Figure
2.1	Essential Features of wire FS
2.2	Entire set up of FS
2.3	Process setup for powder FS
2.4	Basic elements of detonation Gun spray
2.5	Arrangement of HVOF
2.6	Electric arc wire spray process
2.7	Plasma Arc spraying process
2.8	Compact outline of pin on disc tribometer
4.1	Outline of APS set up
4.2	Comprehensive outline of Pin on Disc Machine (a) Pin on disc set up, (b) Data acquisition system, (c) Model showing rotational direction of disc
5.1	Wear rate in cumulative mass loss of the prepared coatings made at (a) 6 kW, (b) 9 kW, (c) 12 kW and (d) 15 kW operating power levels.
5.2	Wear rate comparisons at different operating power level for (a) Red mud, (b) Red mud + 10 % fly ash, (c) red mud + 20 % fly ash, (d) red mud + 50 % fly ash, (e) red mud + 20 % aluminium and (f) red mud + 20 % carbon coatings
5.3	Variation of Frictional forces for all coating types up to 54 minute of sliding time made at 6 kW operating power level
5.4	Comparisons of Frictional forces with power for red mud + 20 % Carbon coating up to 54 minute sliding time
5.5	Effect of power on coefficient of friction for red mud+20 % Al coatings slid up to break in phase
5.6	Fluctuation of Coefficient of friction of red mud, red mud+20% fly ash and red mud+20% aluminium with time (up to break in phase) made at 6 kW operating power
5.7	Worn surfaces for red mud + 10% fly ash coatings for 6 kW operating power level.; (a) 3, (b) 6, (c) 12 and (d) 15 minutes time interval
5.8	Worn surfaces for red mud + 20% Al coatings for 12 kW operating power Level.; (a) 15, (b) 30, (c) 45 ,(d) 60, (e) 75 and (f) 81 minutes time intervals

5.9	Wear images for Red Mud + 20 % Carbon coating for 9 kW operating power level; considering (a) 27, (b) 51, (c) 78, (d) 96, (e) 111 and (f) 117 minutes time interval
5.10	(a) SEM and (b) EDS analysis of red mud
5.11	(a) SEM and (b) EDS analysis of fly ash
5.12	(a) SEM and (b) EDS analysis of activated Carbon
5.13	EDS records for (a) RM + 10% FA and (b) RM + 50% FA coatings made at 12 Kw
5.14	EDS analysis of RM+20% FA composite coating at 9 kW
5.15	EDS record of RM+ 20 % Al Composite coating at 6 kW
5.16	Surface responses for (a) red mud, (b) RM + 10 % FA, (c) RM + 20 % FA and (d) RM + 50 % FA coated at 12 kW operating power
5.17	Morphology of RM + 20 % FA coatings made at (a) 6 kW, (b) 9 kW, (c) 12 kW and (d) 15 kW
5.18	Coating Morphology for RM + 10 % FA; (a) 6 kW, (b) 9 kW, (c) 12 kW (d) 15 kW
5.19	Coating Morphology for RM + 20 % Al; (a) 6 kW, (b) 9 kW, (c) 12 kW (d) 15 kW
5.20	Morphology of RM + 20% C coatings made at (a) 6 kW, (b) 9 kW,(c) 12 kW and (d) 15 kW
5.21	Section Microstructure of RM + 20 % FA Coatings at (a) 6 kW, (b) 9 kW, (c) 12 kW and (d) 15 kW
5.22	Action of operating power on thickness
5.23	XRD of Red Mud Powder Collected from NALCO
5.24	XRD of Activated Carbon
5.25	XRD of RM + 10 % FA Coatings; (a) 6 kW, (b) 12 kW
5.26	X-Ray diffractogram of RM + 50 % FA Coatings at (a) 6 kW, (b) 9 kW, (c) 12 kW and (d) 15 kW operating power levels
5.27	XRD of Red Mud + 20 % Al Coatings, (a) 6 kW, (b) 9 kW, (c) 12 kW, (d) 15 kW
5.28	XRD of (a) RM + 20% C Powder, (b) RM + 20% C Coating at 9 kW
5.29	XRD of (a) RM + 20% FA Powder, (b) RM + 20% FA Coating at 9 kW
5.30	Effect of Plasma Torch Power on adhesion strengths of prepared coatings.

5.31	TG analyses of coatings
5.32	Originated DSC plots of coatings
5.33	Influence of temperature on adhesion strength.
5.34	Cracked surfaces of RM + 10% FA coatings at (a) 800°C, (b) 900°C and (c) 1000°C
5.35	Microstructures of RM + 20% Al coatings at (a) 500°C, (b) 600°C, (c) 700°C, (d)800°C, (e)900°C and (f) 1000°C
5.36	Standard linear graphs for L ₂₇ array
5.37	Effect of control factors on wear rate
5.38	Interaction graph between A×B×C for wear rate

LIST OF TABLES

Table No	Title of the Table
2.1	Various forms of surface modification technologies
2.2	Types of Thermal Spray Process
2.3	Compositions of red mud across different parts of world
4.1	Powders used for coating deposition
4.2	Operating parameters during coating deposition
5.1	Elemental analysis of red mud
5.2	Elemental analysis of RM+20% FA composite coated at 9 kW
5.3	Elemental analysis of RM+20% Al composite coated at 6 kW
5.4	Coating hardness for different operating power level
5.5	Coating porosity for different coating type
5.6	Effect of operating power on coating deposition efficiency
5.7	Levels of the variables used in the experiment.
5.8	Experimental design using L ₂₇ orthogonal array
5.9	Response table to wear
5.10	ANOVA table for wear rate
5.11	Results of the confirmation experiments

CONTENTS

CHAPTER/SECTION	PAGE NO
Certificate from Supervisor	i
Dedication	ii
Declaration of Originality	iii
Acknowledgement	iv
Abstract	v
List of Figures	vii
List of Tables	x
1.INTRODUCTION	1
2. LITERATURE REVIEW	7
2.1 Preparatory Statement	7
2.2 Surface Recasting	7
2.3 Procedure for Surface Recasting	9
a. Plating	9
b. Diffusion Process	10
c. Surface Hardening	11
d. Thin Film Coating	12
i. Physical Vapour Deposition	12
ii. Chemical Vapour Deposition	13
e. Hard Facing by Welding	13
f. Thermal Spraying	14
i. FS With Wire	15
ii. FS With Powder	16
iii. Detonation Gun Coating	17
iv. HVOF	18
v. Electric Arc Spraying	19
vi. PS	20

2.4 Anti Wear Coatings	26
a. Carbide Coatings	27
b. Oxide Coatings	28
i. Chromia (Cr ₂ O ₃) Coating	29
ii. Zirconia (ZrO ₂)Coating	30
iii. Titania (TiO ₂) Coating	30
iv. Alumina (Al ₂ O ₃) Coating	31
c. Metallic Coatings	33
d. Diamond Coatings	33
2.5 Sliding Wear Behaviour of Ceramic Coatings	35
2.6 Progress of Red Mud Utilisation	39
3. AIMS AND OBJECTIVES	49
4. MATERIALS AND METHODS	52
4.1 Introduction	53
4.2 Processing of Coatings	53
a. Preparation of Coating Powder	53
b. Preparation of Substrate	54
c. Plasma Spraying	54
4.3 Coating Characterisation	56
a. Dry Sliding Wear Behavior of Coatings	56
b. Coating Porosity	57
c. XRD Analysis	57
d. Morphology, Elemental and Thickness Analysis	57
e. Coating Hardness	57
f. Coating Deposition Efficiency	58
g. Thermal and Bond Strength Analysis	58
5. RESULTS AND DISCUSSION	59
5.1 Introduction	60
5.2 Study of Sliding Wear Behaviour	60
5.3 Elemental, Coating Morphology and Thickness Analysis	71
5.4 XRD Phase Composition Analysis	81
5.5 Coating Hardness	89
5.6 Coating Porosity	91

5.7 Coating Deposition Efficiency	92
5.8 Coating Adhesion Strength	94
5.9 TGA, DSC and Bond Strength at Elevated Temperatures	95
5.10 Design of Experiment By Taguchi Method	100
6. CONCLUSIONS AND SCOPE FOR FUTURE WORK	106
6.1 Conclusions	107
6.2 Scope For Future Work	108
7. REFERENCES	110
LIST OF PUBLICATIONS	125

CHAPTER-1

INTRODUCTION

Surface modification is a generic term that is now applied to a wide range of diverse technologies that can be gainfully used to enable industrial components in exhibiting increased reliability and enhanced performance. The incessant quest for higher efficiency and productivity across the entire spectrum of manufacturing and engineering industries has ensured the exposure of most modern-day components to increasingly harsher environments during routine operation. Therefore, critical industrial components are prone to more rapid degradation because the components fail to withstand the rigorous operating conditions. This fact has been taking a heavy toll on the industry's economy. In an overwhelmingly large number of cases, the accelerated deterioration of components and their eventual failure has been attributed to the material damage due to hostile environments and attributed to the high relative motion between mating surfaces, corrosive media, extreme temperatures, and cyclic stresses. Simultaneously, research efforts focussed on the development of new fabrication materials are beginning to yield diminishing returns. Moreover, it appears to be unlikely that any significant advances in terms of component performance and durability can be made only through the development of new alloys. Due to the above factors, the concept of incorporating engineered surfaces capable of combating the accompanying degradation phenomena such as wear, corrosion, and fatigue for improving component performance, reliability, and durability has gained increasing acceptance in recent years. The information that a vast majority of engineering components have failed catastrophically in their service due to surface related phenomena has further fuelled the concept and led to the development of a broad interdisciplinary area of surface modifications. A protective coating deposited to act as a barrier between the outer surfaces of the component and the aggressive environment that the component is exposed to during operation has now been globally acknowledged to be an attractive means for significantly reducing the damage to the actual component by acting as the first line of defence.

The increasing utility and industrial adoption of surface engineering is a consequence of the significant recent advances in the field. Highly rapid strides have been used in all fields of science, processing, control, modelling, application developments etc. Thus, the use of rapid strides has become an invaluable tool that is now being

increasingly considered as an integral part in component design. Currently, surface modification is best defined as “the design of the substrate and surface together as a system to give a cost-effective performance enhancement, of which neither is capable on its own.” The development of a suitable high-performance coating on a component fabricated using an appropriate high mechanical strength metal or alloy provides a promising method for meeting both the bulk and surface property requirements of virtually all imagined applications. The newer surfacing techniques and the traditional ones are eminently suited to modify a wide range of engineering properties. The properties that can be modified by adopting surface engineering include tribological, mechanical, thermo-mechanical, electrochemical, optical, electrical, electronic, magnetic, acoustic, and biocompatible properties.

The development of surface engineering has been dynamic mainly because it is a discipline of science and technology that has been increasingly relied on to meet all the key modern-day technological requirements, such as material conservation, enhanced efficiency, and environmental friendliness. The overall utility of surface engineering is further augmented due to the fact that modifications to the component surface can be metallurgical, mechanical, chemical, or physical. Simultaneously, the engineered surface can span at least five orders of magnitude in terms of thickness and three orders of magnitude in terms of hardness.

Driven by the technological need and fuelled by exciting possibilities, novel methods for applying coatings, improving existing methods, and obtaining new applications have proliferated in recent years. Surface modification technologies have improved rapidly in terms of deriving better solutions and in terms of the available number of technology variants a wide range of surface modification technologies offering different quality outputs and having different costs have been proposed. The significant increase in the availability of coating processes with a wide range of complexities that can deposit a plethora of coatings and handle components of diverse geometries ensures that components of all imaginable shapes and sizes can be coated economically.

The existing surface treatment processes lay under three broad categories:

Overlay Coatings: This category comprises a very wide variety of coating processes in which a material different from the bulk is deposited on the substrate. The coating is distinct from the substrate in the as coated condition, and there exists a clear boundary at the substrate coating interface. The adhesion of the coating to the substrate is a major problem.

Diffusion Coatings: This category comprises the chemical interaction between the coating element(s) and the substrate by diffusion. New elements are diffused into the substrate surface usually at elevated temperatures so that the composition and properties of the outer layers are different than those of the bulk layers.

Thermal Modifications of Surfaces: In this category, the existing metallurgy of the component surface is changed in the near surface region either by thermal or mechanical processes usually to increase its hardness. The type of coating to be used is based on the application. Many techniques are available for depositing the coatings, such as electroplating, vapour deposition, and thermal spraying. Among these techniques, thermal spraying is popular due to its wide range of applications, adhesion of the coating with the substrate and durability. Thermal spraying has gradually emerged as the most useful method in the industry for developing a variety of coatings to enhance the quality of new components and to reclaim worn components or incorrectly machined components. The type of thermal spraying is based on the type of heat source employed. Thus, techniques such as flame spraying (FS), high-velocity oxy-fuel spraying (HVOF), and plasma spraying (PS) are types of thermal spraying. PS utilises the exotic properties of a plasma medium to impart new functional properties to conventional and nonconventional materials and is considered as a highly versatile and technologically sophisticated thermal spraying technique. PS is widely used in the industry and has applications in corrosion, abrasion, and temperature resistant coatings and in the production of monolithic and near net shape castings [1]. The process can be applied to coat a variety of substrates of complicated shape and sizes by using metallic, ceramic, and polymeric consumables. The production rate obtained when using this process is very high and the coating adhesion

is also adequate. As the process is almost material independent, it has a very wide range of applications, such as for thermal barrier coating and wear-resistant coating. Thermal barrier coatings are provided to protect the base material, such as internal combustion engines and gas turbines, at elevated temperatures. Zirconia (ZrO_2) is a conventional thermal barrier coating material. As the name suggests, wear-resistant coatings are used to combat wear, especially in cylinder liners, pistons, valves, spindles, textile mill rollers, etc. Alumina (Al_2O_3), titania (TiO_2), and ZrO_2 are the some of the conventional wear-resistant coating materials [2].

A major limitation of the process is the relatively high price of the sprayable plasma consumables. The objective of this study is to evaluate the potential of red mud, an industrial waste such as plasma consumable. Red mud does not belong to the sprayable plasma category and is quite cheap as it is a waste. Another industrial waste considered in this study is fly ash. In this study, fly ash was pre-mixed with red mud in different proportions (10 wt.%, 20 wt.%, and 50 wt.%) to develop a series of plasma-sprayed coatings. Mixtures of red mud with aluminium powder (20 wt.%) and with carbon (20 wt.%) were deposited as coatings. Coatings were produced on mild steel by using all the aforementioned nonconventional coating materials. The performance of the coatings developed using all the mixtures was compared.

The coatings were characterised on the basis of their hardness, porosity, adhesion strength, and microstructure. The significant phase changes associated with the plasma processing during the coating deposition were studied. Moreover, the coating deposition efficiencies at various operating conditions were evaluated.

There are few studies on the resistance of ceramic coatings to sliding wear. This aspect was studied in the present study by causing the coatings to slide by using a pin on a disc tribometer. The capabilities of the coatings to sustain the sliding attack were assessed.

A qualitative analysis of the experimental results with respect to wear was optimised by using statistical techniques. The analysis was aimed at identifying the operating variables or factors that significantly influence the wear behaviour of red mud–fly ash

composite coatings on a metal such as mild steel. Factors were identified in accordance to their influence on the wear behaviour.

CHAPTER-2

LITERATURE REVIEW

2.1 PREPARATORY STATEMENT

This chapter presents the literature survey of the development of surface modification technology for tribological applications, a broad topic of interest. This treatise presents various coating techniques with a special reference to PS, the coating materials, and the characteristics of the materials. The performance of wear-resistant coatings under various conditions was reviewed critically with the corresponding failure mechanisms. The chapter also presents a review of the efforts that have been directed worldwide towards management problems pertaining to the utilisation, storage, and disposal of red mud, which is the material of interest in this study.

At the end of the chapter, a summary of the literature survey and the knowledge gap in the earlier investigations are presented.

2.2 SURFACE RECASTING

Surface recasting is a relatively new term that has emerged in the last two decades or so to describe interdisciplinary activities aimed at tailoring the surface properties of engineering materials. The objective of surface engineering is to upgrade the functional capabilities of surfaces with considering the economic factors [3,4]. Surface engineering is the name of the discipline, and surface modification is the philosophy behind this field of engineering. To elucidate the matter, an example is presented. Tungsten-carbide (WC)–cobalt composite is a very popular cutting tool material and is well known for its high hardness and wear resistance. If a thin coating of TiN is applied on the WC–Co insert, its capabilities increase considerably [5]. Actually, when a cutting tool is used, it is subjected to a high degree of abrasion. TiN is more capable of combating abrasion but is extremely brittle. However, the relatively tough core of the WC–Co composite protects it from fracture. Thus, by conducting a surface modification process, assembles two (or more) materials by using the appropriate method and exploited the qualities of both [4, 6, 7]. The surface modification process is a very versatile tool for technological development considering that it is applied judiciously with adhering to the following restrictions:

The technological value addition should justify the cost.

The selection of the technique must be technologically appropriate.

2.3 PROCEDURE OF SURFACE RECASTING

Currently, a large number of commercially available technologies are present in the industry, and [Table 2.1](#) represents some of them [4, 6]. An overview of such technologies is presented below.

a. Plating

Among all plating processes, electroplating is quite popular. The substrate (necessarily conducting) forms an electrode (cathode) and is submerged in an appropriate electrolyte [8]. When current passes through the electrolytic cell, ions of the plating material emerge from the electrolyte and deposit on the cathode (the substrate). In electroless plating, deposition occurs by catalytic reduction of the solute in the plating bath. Electrochemical conversion coating appears on the surface of the substrate (which acts as an electrode) because of a chemical reaction between the electrolyte and the surface. For example, in the presence of H_2SO_4 (electrolyte), the top layer of aluminium (electrode) is oxidised to form aluminium oxide [9]. Electroforming is the process of electro-depositing a material on a removable mandrel to ensure partial coating of a surface. Plating can be used for modification of physical, mechanical or corrosion properties [10]. There are different plating techniques that cater to a large number of materials. Composite coatings of non-conducting materials such as diamond can be obtained; polytetrafluoroethylene can also be plated. Plating caters to wear, corrosion, rebuilding, and electrical applications. Some of the plating processes can provide a uniform coating throughout the surface even in deep holes and re-entrant corners (electroless plating). Selective areas of a surface can also be plated [9,11,12].

However, electroplating is prone to metallurgical embrittlement and provides only moderate adhesion, and electroless plating is quite slow [4, 8, 13].

Table 2.1 Various forms of surface modification technologies

SURFACE MODIFICATION TECHNOLOGIES					
Plating	Diffusion Process	Surface Hardening	Thin Film Coating	Hardening By Welding	Thermal Spraying
Electro-deposition	Carburizing	Flame Hardening	PVD	SMAW	Flame Spraying
Electroless Deposition	Nitriding	Induction Hardening	CVD	GTAW	Electric Arc Spraying
Electro-chemical Conversion Coating	Carbonitridig	Electron beam Hardening		GMAW	Plasma Spraying
Electro-forming	Aluminising	Laser Beam Hardening		Submerged Arc Welding	D-gun Coating
	Silicnising	Ion Implanation		Plasma Welding	
	Chromising			Laser Beam Welding	
	Boronising		Electron Beam Welding		

b. Diffusion Processes

As the name suggests, this process involves the diffusion of an element into the substrate matrix [14]. The process is normally conducted at an elevated temperature to promote diffusion. The diffusing species create a layer on the substrate, and the properties of that layer are modified. The elements used as diffusing species are carbon, nitrogen, aluminium, chromium, silicon, boron, etc. The selection of the diffusing species is based on the application. However, carbon and nitrogen are the two most widely used elements and the processes are known as carburising and nitriding, respectively [15]. Both processes are normally conducted on steel substrates. The substrate is placed in an environment rich in carbon or nitrogen. At a high temperature, the elements slowly diffuse into the substrates due to the concentration gradient. Carburising enriches the carbon content of the substrate case, and the case layer hardens after quenching owing to the martensitic transformation. Nitriding also creates a very hard layer on the substrate surface. Here, hardening occurs owing to the solid solution strengthening. These two processes are mainly used for wear applications. Moreover, boronising and carbonitriding are also used. Conversely, chromising, siliconising, and aluminising are used for corrosion and oxidation resistance applications [16,17].

However, diffusion processes have certain limitations as well. They cannot cater to applications such as rebuilding. Some processes often create distortion (case carburising). Some of the processes are very slow, and the case depth obtained is limited (gas carburising). Some of the processes are used in aggressive environments (salt nitriding) with potential environmental hazard. The applications of these processes are limited only to metals.

c. Surface Hardening

This process involves heating a component surface (or part of it) beyond a critical temperature and quickly cooling it by quenching to induce martensitic transformation. The process is restricted to cast iron and steels. Here, a heat source is required to raise the temperature of the work piece. The process is named after the heat source used, and typical examples include flame hardening (oxy-acetylene flame), induction hardening (induction heating), laser hardening (laser beam), and electron beam

hardening (electron beam) [18]. The carbon content of the work piece must be at least 0.6%; otherwise, martensitic transformation may not occur. Except for the ion implantation process, these processes do not involve any material addition. In the ion implantation process, suitable materials are obtained in their ion form and are directed to the surface on which they have to be deposited. These processes are utilised to develop a hard case of low thickness while retaining the softness of the core [4, 19].

In this process, a small part of a big component can be hardened (flame hardening), and no material addition is required. Adhesion does not impose any restriction, because the hardened layer is an integral part of the original component. However, the process is restricted to ferrous materials. The process is sometimes prone to distortion. Some of the processes require highly skilled manpower (e.g., flame hardening). Except for flame hardening, the set-up cost is high for all other processes.

d. Thin Film Coating

In this process, a thin layer of a pure element or a compound can be deposited on a substrate [4, 6]. This technique can be broadly classified into two categories—physical and chemical vapour depositions.

(i) Physical Vapour Deposition (PVD)

This process is conducted in an evacuated chamber. The target (substrate) and the coating material are kept such that they face each other. The coating material is heated using a heat source, such as an electrical heater or electron beam under, a low pressure. The coating material evaporates directly from the solid state and deposits on the target. This is known as thermal evaporation [20]. Another process is known as sputter coating [21]. In this method, the target and coating materials are connected to two electrodes (anode and cathode, respectively) of a suitable power supply, and an inert gas is released in the space between them. The gas undergoes ionisation in the electric field. The positive ions rush towards the cathode (i.e., the coating material) and dislodge ions from it. These ions move towards the anode and deposit on the target. Ion plating is a combination of these two processes. In this method, the coating

material is heated, and plasma gas is created simultaneously to expedite the process [22].

By using this process, pure elements and compounds can be deposited. The process is quite simple, involves low cost equipment, and can be used for applications of many fields, such as electronic, electrical, and wearing component applications. This is a line of sight process; therefore, components with a complicated shape may not be coated. As the process is conducted in vacuum, large components cannot be coated [6].

(ii) Chemical Vapour Deposition (CVD)

The material to be coated is kept in an evacuated chamber equipped with the function of electrical heating. After the substrate is heated to the required temperature, appropriate gases are introduced into the reactor for chemical reaction by coming in contact with the hot substrate. One of the reaction products is a solid and deposits on the substrate surface. The residual gases are removed from the chamber [4, 23].

Intricate-shaped components can be coated using this technique. The rate of deposition of this process is higher than that of PVD. Moreover, certain items can be deposited using CVD only. However, as this process is conducted at a high temperature (700°C or above), thermal damages may come occur. The set-up of this method is more complicated than that of PVD [24].

e. Hard Facing by Welding

Conventionally, welding is a process of joining two metallic parts. Shield metal arc welding is the most common welding process. Here, the base metals are kept close to each other, and an electric arc is created between the base metal (near the junction) and the consumable electrode. As a result, both the consumable electrode (filler material) and the edge of the base metal melt. The filler material of the electrode transfers to the molten weld pool. Moreover, when this pool is frozen, a solid weld bead is formed. The strength of the weldment is supposed to be greater than that of the

base material [25]. In the case of hard facing, the filler material is deposited on the base material to form a metallurgically bonded second layer. Now, the first layer of the deposit is diluted by diffusing the base material constituents into the layer. Normally, a second layer is also deposited on the top of the first one. In welding, either similar or compatible filler material is normally used for the joining purpose. Alloyed electrodes with a tailored composition to suit particular situations of surfacing are also used [26]. There are many techniques of welding, as revealed in [Table 2.1](#). Each has its own application domain.

The strongest possible bonding is obtained using this process. All weldable metals and alloys can be used. The method can be conducted with low cost equipment. A thick layer can be built rapidly, and the process can be automated entirely. However, this technique is restricted to metallic materials. Products are vulnerable to residual stress-related distortion. The hard faced layer may undergo dilution due to diffusion of the base material constituents. Products may require a post-weld finishing operation in many applications [4, 25, 27].

f. Thermal Spraying

This is a generic category of material processing techniques that apply consumables in the form of finely divided molten or semi-molten droplets to produce a coating on the substrate placed in front of the impinging jet. The melting of the consumables may be accomplished in a number of ways, and the consumable can be introduced into the heat source in wire or powder form. Thermal spray consumables can be metallic, ceramic, or polymeric substances. Any material can be sprayed as long as the material can be melted by the heat source employed and does not undergo degradation during heating [25, 28]. The nature of bonding at the coating–substrate interface is not completely understood. It is normally assumed that bonding occurs by the mechanical interlocking. Under this circumstance, it is generally possible to ignore the metallurgical compatibility [6]. This is an extremely significant feature of thermal spraying. Another interesting aspect of thermal spraying is that the surface temperature seldom exceeds 200°C. Hard metal or ceramic coating can be applied to thermosetting plastics. Stress-related distortion problems are also not highly

significant. The spraying action is achieved using the rapid expansion of combustion gases (which transfer the momentum to the molten droplets) or using a separate supply of compressed air.

There are two basic ways of generating the heat required for melting the consumables [28, 29], combustion of a fuel gas and a high-energy electric arc. Table 2.2 shows the common thermal spray processes that can be categorised into the aforementioned categories. The aforementioned processes are discussed briefly in the following sections, but PS is discussed separately.

Table 2.2 Types of Thermal Spray Process

THERMAL SPRAY PROCESS	
❖ Gas Combustion Process	❖ Arc Process
✓ Oxy Fuel/Wire	✓ Electric Arc
✓ Oxy Fuel/Powder	✓ Plasma Arc
✓ Detonation Gun	
✓ HVOF	

(i) FS with Wire

The arrangement of this method is displayed in Figure 2.1 and Figure 2.2. The set-up comprises a spraying gun, a wire feeding arrangement, oxygen and acetylene gas cylinders, and an air compressor [4, 6, 31]. A proportional mixture of oxygen and acetylene is taken inside a chamber located in the gun itself, and the mixture is set ablaze. The flame comes out through the muzzle of the gun. The tip of the wire is fed to the flame; this causes the wire to melt quickly and form a droplet. A compressed air jet dislodges the molten droplet and carries it in atomised form to the target surface

placed in front of the gun. Moreover, the roller of the wire feeding arrangement rotates continuously at a fixed, preset speed to advance the wire to the flame [25, 28, 30, 32].

The set-up cost for FS is quite low. A thick metallic layer can be deposited easily; hence, it is quite useful for rebuilding. However, the method is only applicable to metallic materials [6].

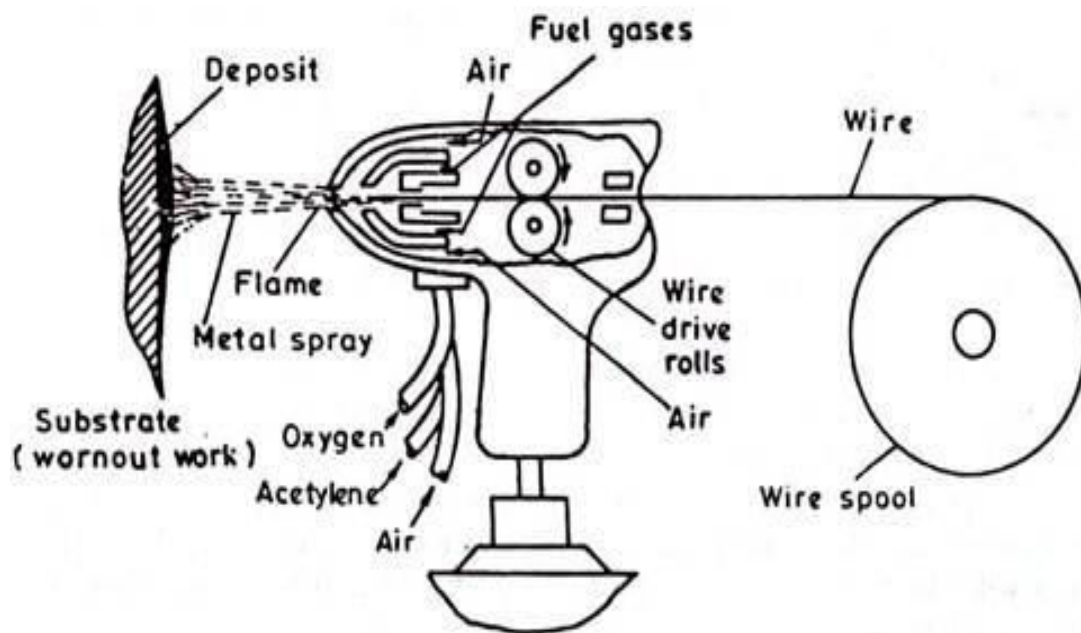


Figure 2.1 Essential Features of wire FS [4, 6, 31]

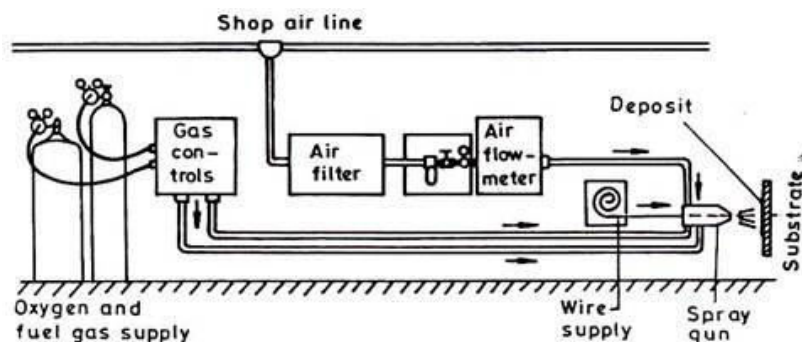


Figure 2.2 Entire set up of FS [31]

(ii) FS with Powder

The arrangement is illustrated in [Figure 2.3](#) [4, 31]. The process is conducted using a gun that is equipped with the functions of fuel gas (oxy-acetylene) injection and powder storage. The flame is kept at a convenient distance from the substrate. The consumable powders are placed inside the hopper integrated with the gun and can be released to the flame by using a trigger. The powder is gravity fed to the flame and then melts and deposits on the substrate to form a coating. In some cases, the flame is taken near the coating immediately after deposition for further melting. In this case, the achieved bond strength is higher, but the temperature of the substrate increases considerably [6, 28, 29].

The equipment cost of this method is low. A large number of alloys (even cermets) are available in powder form. However, ceramic materials cannot be deposited using this method. The deposition rate is very slow.

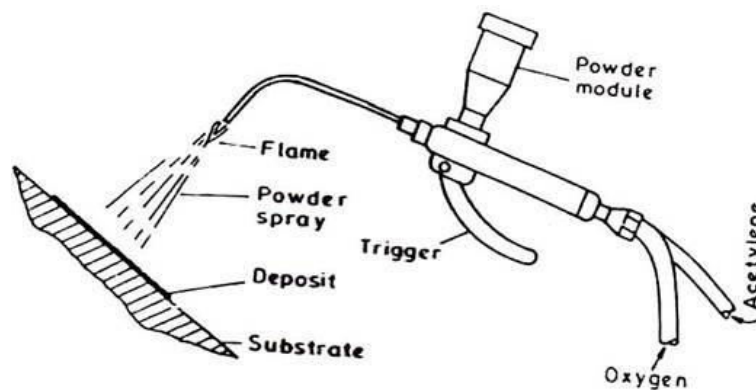


Figure 2.3 Process setup for powder FS [31]

(iii) Detonation Gun Coating

This is a proprietary coating process. The basic set-up is displayed in [Figure 2.4](#) [31]. Consumable powder is fed into the gun under a small gas pressure. Valves are opened to allow oxygen and acetylene to enter the combustion chamber of the gun. The mixture is then detonated by the sparks from spark plugs, and an explosion occurs immediately. The temperature of the detonation fuel is approximately 3800°C, and this is a sufficiently high temperature to melt most of the materials. Immediately after the detonation, hot particles (undergoing melting) rush towards the target at a very high velocity. This factor is very important for having a well-bonded, dense coating.

Detonation cycles are repeated four to eight times per second, and nitrogen gas is used to flush out the combustion products after each cycle. This process generates a very loud noise; therefore, spraying is conducted inside a sound proof room. The method also requires an elaborate arrangement for fuel and purge gas control, powder feeding, gun cooling, and spark plug operation [6, 28, 29]. By using this technique, metals, alloys, and ceramics can be melted, and a well-bonded, dense coating can be produced. However, the process is expensive, involves a very elaborate arrangement, and produces a loud noise.

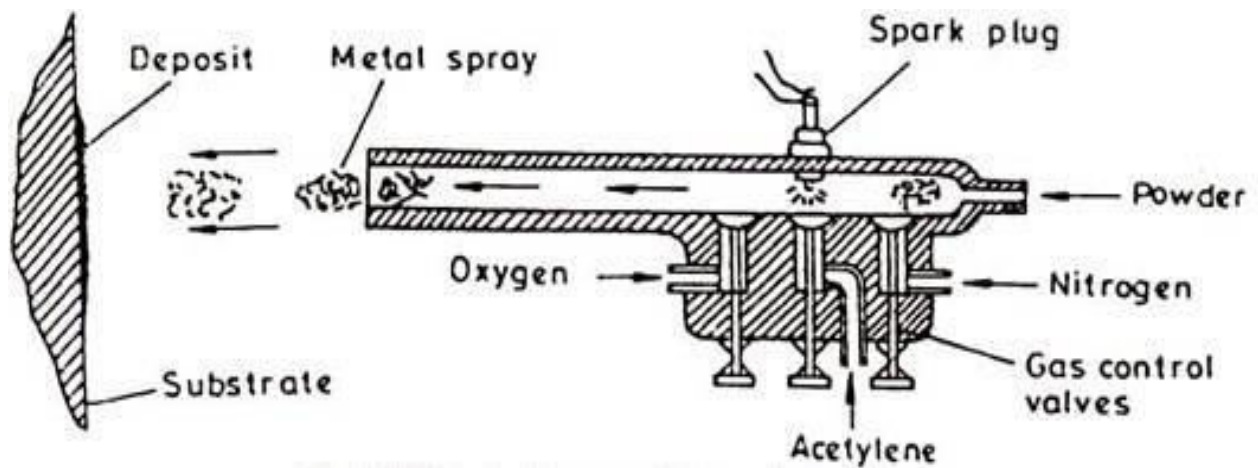


Figure 2.4 Basic elements of detonation Gun spray [31]

(iv) HVOF

The arrangement is shown in [Figure 2.5](#) [31]. The oxygen and fuel gas (propylene or hydrogen) mixture is introduced in the combustion chamber of the gun. The mixture lights into a flame when ignited, and the burnt gas acquires a very high temperature and escapes from the confinement of the small chamber at a high velocity in the expansion process. The flame is at a right angle with the muzzle of the gun. Powder is fed to the centre of the flame by a carrier gas from one end of the gun. The particles melt and are immediately carried to the target by the gas; thus, the particles escape at a very high velocity through the nozzle of the gun [33, 34, 35].

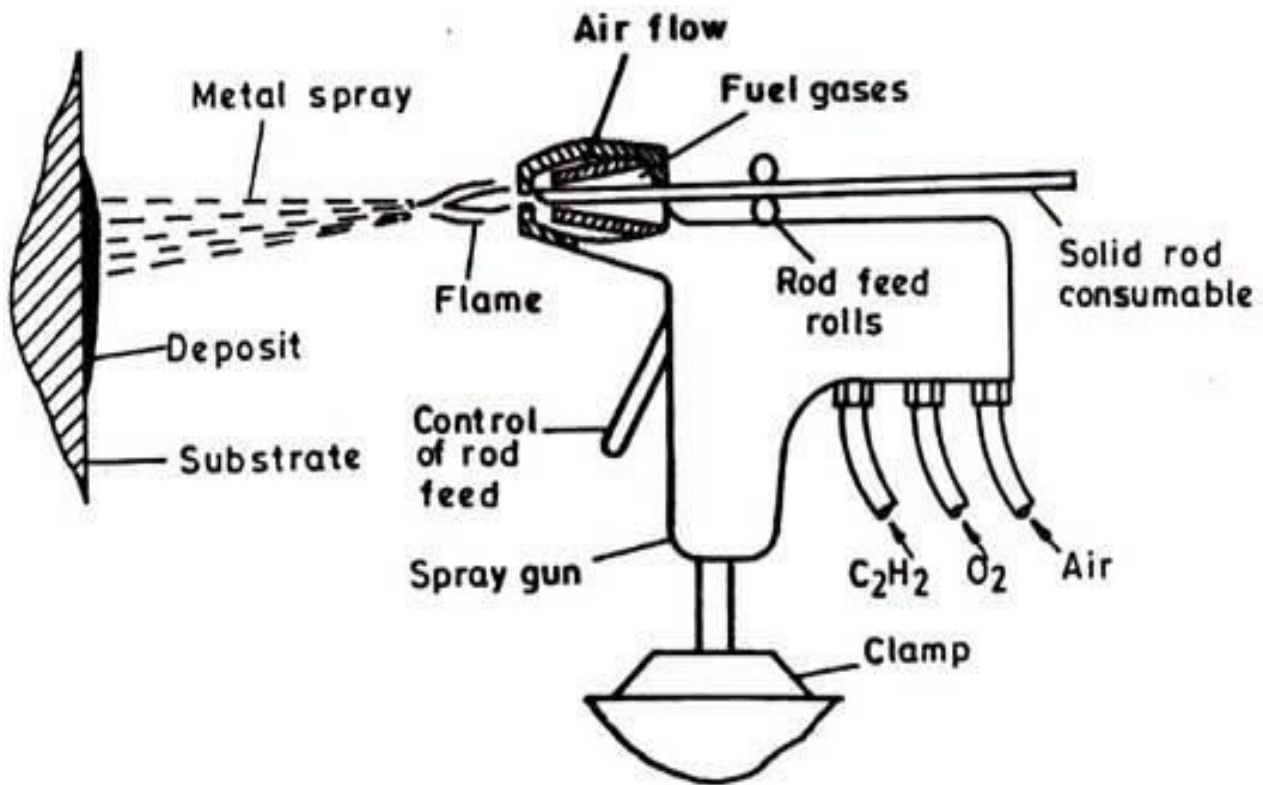


Figure 2.5 Arrangement of HVOF [31]

Advantages of this spraying technique include good substrate–coating adhesion and high coating density. The method can be applied to metals and ceramics and has a low set-up cost compared with that of PS or detonation gun.

(v) Electric Arc Spraying

The arrangement is shown in [Figure 2.6](#). An electric arc is created between the tips of two conducting wires. The heat produced melts the tips of the wire, and these molten tips are dislodged and directed to a target by using a compressed air jet. The wires are fed by an independent wire feeding mechanism. Electric power is supplied by a rugged welding power supply. The process is capable of spraying at a very high deposition rate [6, 36]. The set-up for electric arc spraying is simple and cheap; however, only conducting materials can be sprayed. The substrate–coating adhesion and density obtained using this method is not comparable to those obtained using PS or detonation gun.

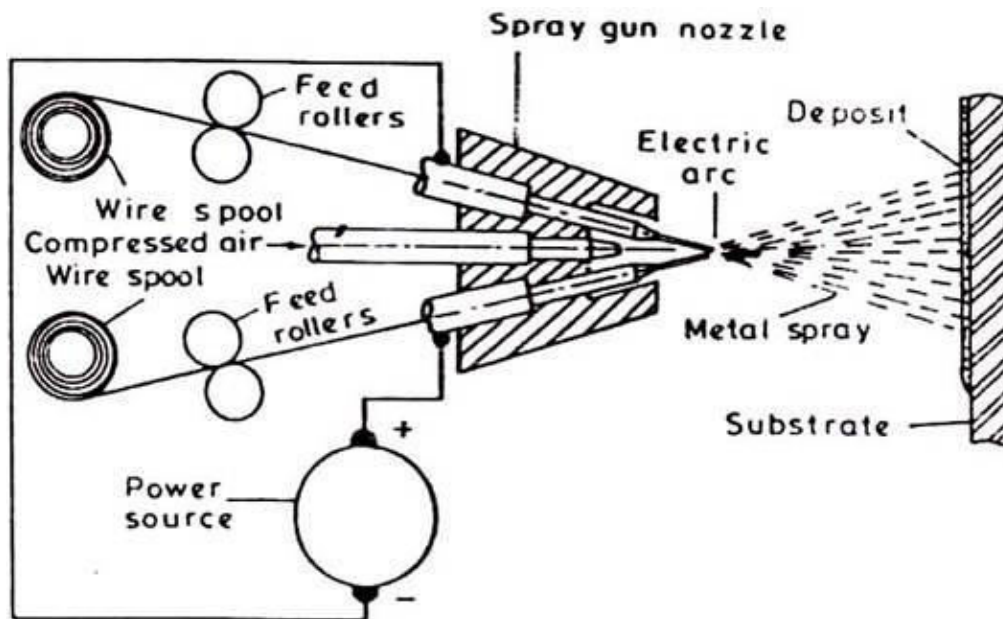


Figure 2.6 Electric arc wire spray process [4, 31]

(vi) PS

PS is the most versatile thermal spraying process, and the general arrangement is displayed in [Figure 2.7](#). An arc is created between the tungsten-tipped copper cathode and an annular copper anode (both water cooled). Plasma generating gas is forced to pass through the annular space between the electrodes. While passing through the arc, the gas undergoes ionisation in the high-temperature environment, thus generating plasma. Ionisation is achieved by collisions of the electrons of the arc with the neutral molecules of the gas. The plasma protrudes out of the electrode encasement in the form of a flame. The consumable material is poured into the flame in metered quantity in powdered form. The powders melt immediately, absorb the momentum of the expanding gas, and then rush towards the target to form a thin deposited layer. The next layer immediately deposits on the first, and thus, the coating is built layer by layer [3,6,25,32].

The temperature in the plasma arc can be as high as 10,000°C and is capable of melting anything. Elaborate cooling arrangement is required to protect the plasmatron

(i.e., the plasma generator) from excessive heating. The equipment comprises the following modules [37].

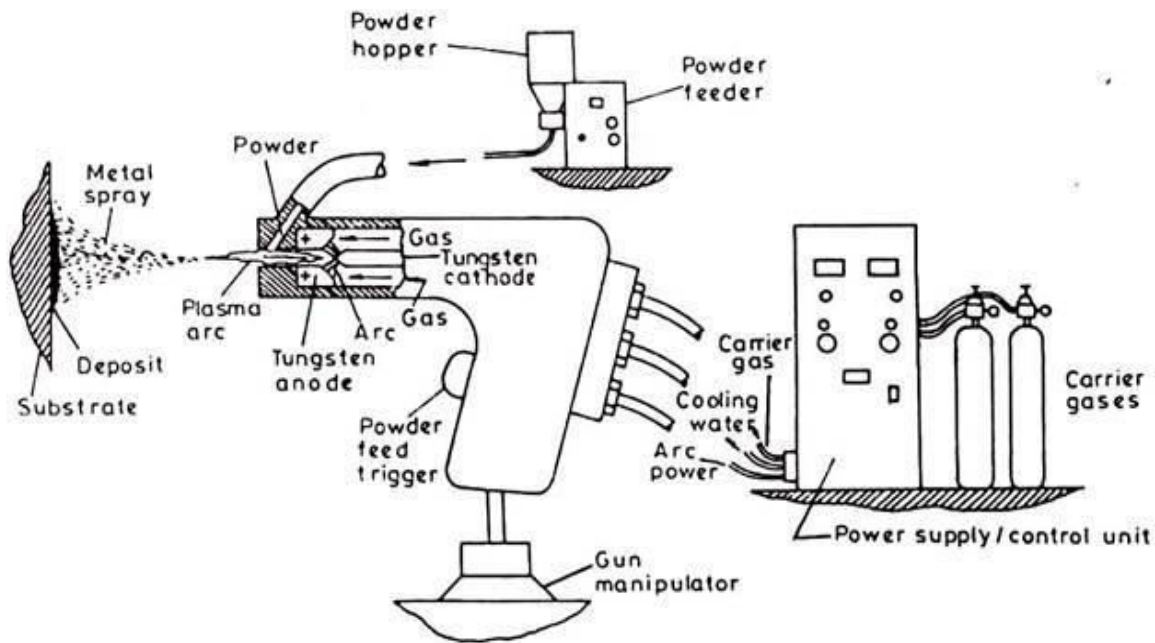


Figure 2.7 Plasma Arc spraying process [4, 31]

Plasmatron: This device houses the electrodes, and plasma reaction occurs in this device. The device has the shape of a gun and is connected to the water-cooled power supply cables, powder supply hose, and gas supply hose.

Power supply unit: Normally plasma arc works at a low voltage (40–70 V) and high current (300–1000 A) in DC ambient conditions. The available power (AC, three phase, 440 V) must be transformed and rectified to suit the reactor. The power supply unit performs this transformation and rectification functions.

Powder feeder: The powder is placed inside a hopper. A separate gas line directs the carrier gas that fluidises the powder and carries it to the plasma arc. The flow rate of the powder can be controlled precisely.

Coolant water supply unit: The unit circulates water into the plasmatron, the power supply unit, and the power cables. Units capable of supplying refrigerated water are also available.

Control unit: Important functions such as current control and gas flow rate control are performed by the control unit. The unit comprises relays, solenoid valves, and other interlocking arrangements that are essential for the equipment to operate safely. For example, the arc can only be started if the coolant supply is on and the water pressure and flow rate is adequate.

Requirements for PS:

Roughness of the substrate surface: A rough surface provides good coating adhesion and sufficient room for anchorage of the splats to facilitate bonding through mechanical interlocking. A rough surface is generally created by a shot blasting technique. The shots are kept inside a hopper, and compressed air is supplied at the bottom of the hopper. The shots are taken afloat by the compressed air stream into a hose and ultimately directed to an object placed in front of the exit nozzle of the hose. The shots used for this purpose are irregular in shape, highly angular in nature, and fabricated using a hard material such as alumina and silicon carbide. Upon impact, the shots create small craters on the surface by causing localised plastic deformation and finally yield a very rough and highly worked surface. The roughness obtained is determined by shot blasting parameters, such as shot size, shot shape, shot material, air pressure, standoff distance between the nozzle and the job, angle of impact, and substrate material [38]. The effect of shot blasting parameters on the adhesion of plasma-sprayed alumina has been studied [35, 39]. Mild steel serves as a substrate material. Adhesion increases proportionally with surface roughness, and the parameters listed above are crucial. A significant time lapse between shot blasting and PS causes a marked decrease in the bond strength [40].

Cleanliness of the substrates: The substrate to be sprayed on should be free from any dirt, grease, or any other material that might prevent appropriate contact of the splat and the substrate. Thus, the substrate must be thoroughly cleaned (ultrasonically, if possible) with a solvent before spraying. Spraying must be conducted immediately after shot blasting and cleaning. Otherwise, oxide layers tend to quickly grow on the nascent surfaces, and moisture may also affect the surface. These factors drastically deteriorate the coating quality owing to the large difference between the thermal

expansion coefficients (α) of the nascent surfaces and the oxide layers [40]. Ceramics have much lower α and thus undergo much less shrinkage than the metallic base while compressing a surface. If the compressive stress exceeds a certain limit, the coating peels off. To alleviate this problem, a suitable material, usually a metallic material with an intermediate value is plasma sprayed on the substrate, followed by PS on the ceramics. Bond coats may be useful for metallic top coats as well. Molybdenum is a classic example of a bond coat for metallic top coats. Molybdenum adheres very well to the steel substrate and develops a rough top surface that is ideal for top coat spraying. The selection of a bond coat is based on the type of application. For example, for a wear application, a combination of alumina and Ni–Al top and bond coats can be used [41]. For a thermal barrier application, CoCrAlY or Ni–Al bond coat [42] and zirconia top coat are popular. When subjected to hertzian loading, ceramic coatings deform elastically and metallic substrates deform plastically. During unloading, elastic recovery of the coating occurs. However, for the metallic substrate, a permanent set already occurs. Owing to this elastoplastic mismatch, the coating tends to spall off at the interface. A bond coat can reduce this mismatch as well [43]

Cooling water: Distilled water should be used for cooling whenever possible. Normally, a small volume of distilled water is recirculated into the gun and is cooled by an external water supply from a large tank. Sometimes, water from a large external tank is pumped directly into the gun [37].

Process parameters in PS:

In PS, one has to deal with many process parameters that determine the degree of particle melting, adhesion strength, and deposition efficiency of the powder [44]. Deposition efficiency is defined as the ratio of the amount of deposited powder to the amount of powder fed into the gun. An elaborate listing of these parameters and their effects are reported in the literature [45–48].

Some important parameters and their roles are listed below:

Arc power: This power represents the electrical power drawn by the arc. The power is injected in the plasma gas, which in turn heats the plasma stream. Part of the power is

dissipated as radiation and by the gun cooling water. The arc power determines the mass flow rate of a given powder that can be effectively melted by the arc. The deposition efficiency improves to a certain extent with increase in arc power, because the efficiency is associated with enhanced particle melting [40, 45, 49]. However, increasing the power beyond a certain limit may not cause a significant improvement. Conversely, once complete particle melting is achieved, a higher gas temperature may prove to be harmful. In the case of steel, vapourization may occur at some point, thus lowering the deposition efficiency.

Plasma gas: Normally, nitrogen or argon doped with approximately 10% of hydrogen or helium is used as plasma gas. The major constituents of the gas mixture form the primary gas, and the minor constituents form the secondary gas. The neutral molecules are subjected to electron bombardment, thus causing their ionisation. Temperature and enthalpy of the gas increase as the gas absorbs energy. As nitrogen and hydrogen are diatomic gases, they first undergo dissociation, followed by ionisation. Thus, they need higher energy input to enter the plasma state. This additional energy increases the enthalpy of the plasma. Conversely, the mono-atomic plasma gases—argon or helium—attain a much higher temperature in the normal enthalpy range. A good heating ability is expected from them for such a high temperature [50]. Moreover, hydrogen has a very high specific heat, followed by helium. Therefore, they are capable of acquiring very high enthalpies. When argon is doped with helium, the spray cone becomes quite narrow and then is especially useful for spraying on small targets.

Carrier gas: Normally, the primary gas itself is used as a carrier gas. The flow rate of the carrier gas is an important factor. A very low flow rate cannot transfer the powder effectively to the plasma jet. Moreover, if the flow rate is very high, then the powders might escape the hottest region of the jet. There is an optimum flow rate for each powder at which the fraction of unmelted powder is minimum; thus, the deposition efficiency is maximum [4, 45].

Mass flow rate of the powder: The ideal mass flow rate of each powder should be determined. Spraying with a lower mass flow rate by keeping all other conditions constant results in under-utilisation and slow coating build-up. Conversely, a very high mass flow rate may cause incomplete melting, thus resulting in a high amount of porosity in the coating. The unmelted powders may bounce off from the substrate surface as well because the deposition is efficiency low [44, 45].

Torch to base distance: This represents the distance between the tip of the gun and the substrate surface. A long distance may result in freezing of the melted particles before they reach the target, whereas a short standoff distance may not provide sufficient time for the particles in flight to melt [40,45]. The relationship between the coating properties and spray parameters while spraying alpha alumina was studied in detail [51]. It was found that the porosity increases and the thickness of the coating (hence deposition efficiency) decreases with an increase in the standoff distance. The usual alpha-phase to gamma-phase transformation during PS of alumina can be restricted by increasing this distance. A larger fraction of the unmelted particles enter the coating owing to an increase in the torch to base distance.

Spraying angle: This parameter is varied to accommodate the shape of the substrate. While coating alumina on a mild steel substrate, the coating porosity is found to increase as the spraying angle is increased from 30° to 60°. Beyond 60°, the porosity level remains unaffected by a further increase in the spraying angle [52]. The spraying angle also affects the adhesive strength of the coating [53, 54]. The influence of the spraying angle on the cohesive strength of chromia, 8-wt.%yttria-stabilised zirconia, and molybdenum has been investigated, and it has been found that the spraying angle does not have much influence on the cohesive strength of the coatings [55].

Substrate cooling: During continuous spraying, the substrate might get heated up and may develop thermal stress-related distortion accompanied by coating peeling. This is especially true in situations where thick deposits have to be applied. To harness the substrate temperature, the substrate is kept cool by an auxiliary air supply system. Moreover, the cooling air jet removes the unmelted particles from the coated surface and helps to reduce porosity [40].

Powder related variables: These variables include powder shape, size, size distribution, processing history, and phase composition. They constitute a set of extremely important parameters. For example, in a given situation, if the powder size is very small, it might get vaporized. Conversely, a very large particle may not melt substantially and thus will not deposit. The shape of the powder is also quite important. Spherical powder will not have the same characteristics as angular powder. Thus, both types of powders cannot be sprayed using the same set of parameters [4, 32, 56, 57].

Preheating of a substrate: A nascent shot blasted surface of a substrate absorbs water and oxygen immediately after shot blasting. Before spraying, the substrate should be preheated to remove moisture from the surface and for a sputter cleaning effect of the surface by the ions of the plasma [40].

Angle of powder injection: Powders can be injected into the plasma jet perpendicularly, coaxially, or obliquely. The residence time of the powders in the plasma jet varies with the angle of injection for a given carrier gas flow rate. The residence time in turn influences the degree of melting of a given powder. For example, a long residence time and thus oblique injection may prove to be useful for melting high melting point materials. The angle of injection influences the cohesive and adhesive strength of the coatings as well [4, 37].

2.4 ANTI WEAR COATINGS

Currently, a variety of materials, such as carbides, oxides, and metallic materials, belonging to the above category are available commercially. The wear-resistant coatings can be classified into the following categories: [3]

- (i) Carbides: WC, TiC, SiC, ZrC, Cr₂C₃, etc.

- (ii) Oxides: Al₂O₃, Cr₂O₃, TiO₂, ZrO₂, etc.

- (iii) Metallic materials: NiCrAlY, Triballoy, etc.

(iv) Diamond

The selection of a material is based on the application. However, ceramic coatings are very hard; hence, they offer more abrasion resistance on an average than their metallic counterparts.

a. Carbide Coatings

Among carbides, WC is very popular for wear and corrosion applications [58]. The WC powders are clad with a cobalt layer. The cobalt layer undergoes melting during spraying and forms a metallic matrix upon solidification in which the hard WC particles remain embedded. The spraying of WC–Co involves a close control of the process parameters such that only the cobalt phase melts without degrading the WC particles. Such degradation may occur in two ways: (a) Oxidation of WC leads to the formation of CoWO_4 and WC_2 [59], (b) Dissolution of WC in the cobalt matrix leads to the formation of brittle phases such as CoW_3C that embrittles the coating [60].

Increase in the spraying distance and an associated increase in the time in flight leads to loss of carbon and increase in oxygen. Thus, the hardness of the coating decreases [61]. Increase in the plasma gas flow rate reduces the dwell time and thus can control the oxidation to some extent. However, this increase enhances the possibility of cobalt dissolution in the matrix [62]. The other option to improve the quality of such a coating is to conduct the spraying procedure in vacuum [60].

Often carbides such as TiC, TaC, and NbC are provided with WC in the cermet to improve the oxidation resistance, hardness, and heating strength. Similarly, the binder phase is also modified by adding chromium and nickel with cobalt [3]. The wear mechanism of plasma-sprayed WC–Co coatings is based on a number of factors, such as mechanical properties, cobalt content, experimental conditions, and mating surfaces. The wear mode can be due to abrasion, [63, 64, 65] adhesion, or surface fatigue [66, 67]. The coefficient of friction of WC–Co (in a self-mated condition) increases with increase in the cobalt content [66]. When a WC–Co coating is tested at a temperature of 450°C , it exhibits signs of melting [68]. The wear resistance of these coatings is based on porosity [64]. Pores can act as source for crack growth. Thermal

diffusivity of the coatings is another important factor. In narrow contact regions, excessive heat generation may occur due to rubbing. If the thermal diffusivity of the coating is low, the heat cannot easily escape from a narrow region. Thus, the temperature rises, and failure occurs owing to thermal stress [64,68]. The wear mechanism of the WC–Co nanocomposite coating on mild steel substrates was studied in detail [69]. The wear rates of such coatings are found to be much higher than those of commercial WC–Co composite coatings presumably due to an enhanced decomposition of nanoparticles during spraying. Wear occurs due to the subsurface cracking along the preferred crack paths provided by the binder phase or failure at the inter-splat boundary. Coatings of TiC or TiC and TaC with a nickel cladding are alternative solutions for wear and corrosion problems. The high-temperature stability, low coefficient of thermal expansion, high hardness, and low specific gravity of these coatings may outperform those of other materials, especially in a steam environment [3,4]. Instead of nickel, nickel–chromium alloy can serve as the matrix material [70, 71]. The wear can be due to adhesion, abrasion, surface fatigue, or micro-fractures based on the operating conditions [67, 71].

A Cr_3C_2 coating (with Ni–Cr alloy cladding) is known for its excellent sliding wear resistance and superior oxidation and erosion resistances, although its hardness is lower than that of WC [3,4]. After spraying in air, Cr_3C_2 loses carbon and transforms to Cr_7C_3 . Such transformation generally improves the hardness and erosion resistances of the coating [70]. The sliding wear behaviour of the Cr_3C_2 –Ni–Cr composite has been studied by several authors against various metals and ceramics [64, 67, 73]. At lower loads, the wear is due to the detachment of splats from the surface. As the load increases, melting, plastic deformation, and shear failure occur.

b. Oxide Coatings

Metallic coatings and metal containing carbide coatings are sometime not suitable for use in high-temperature environments for both wear and corrosion applications. They often fail owing to oxidation or decarburisation. In such a case, the material of choice can be an oxide ceramic coating, such as Al_2O_3 . Cr_2O_3 , TiO_2 , ZrO_2 , and their combinations. However, the high wear resistance and chemical and thermal stabilities

of these materials are counterbalanced due to the small thermal expansion coefficient, low thermal conductivity, low mechanical strength, low fracture toughness, and weaker adhesion to the substrate material. The thickness of these coatings is also limited by the residual stress that increases with thickness. Therefore, to obtain a high-quality coating, it is essential to use an appropriate bond coat, spray parameters, and reinforcing additives [4].

i. Chromia (Cr_2O_3) Coating

Cr_2O_3 coatings are applied when corrosion resistance is required in addition to abrasion resistance. The coating adheres well to the substrate and exhibits an exceptionally high hardness of 2300 HV 0.5 kg [4]. Chromia coatings are also useful in ship and other diesel engines, water pumps, and printing rolls [3,4]. A Cr_2O_3 -40 wt.% TiO_2 coating provides a very high coefficient of friction (0.8) and thus can be used as a brake liner [4]. The wear mode of chromia coatings has been investigated under various conditions. Based on the experimental conditions, the wear can be due to abrasion [66], plastic deformation [67, 68, 74], micro-fractures [75], and a conglomerate of all of these factors [76]. This material has also been tested under lubricated conditions by using inorganic salt solutions (NaCl , NaNO_3 , and Na_3PO_4) as lubricants and also at a high temperature. The wear rate of self-mated chromia is found to increase considerably at 450°C , and the plastic deformation and surface fatigue are the predominant wear mechanisms [77]. Under a lubricated condition, the coatings exhibit tribochemical wear [78]. The coatings were also tested for erosion resistance [79].

ii. Zirconia (ZrO_2) Coating

Zirconia is widely used as a thermal barrier coating. However, it contains the essential qualities of a wear-resistant material, such as hardness and chemical inertness, and exhibits reasonably good wear behaviour. When hot-pressed zirconia is mated with high chromium-containing iron alloy (martensite, austenite, or pearlite), the iron transfers on to the ceramic surface while rubbing, and the austenitic material adheres well to the ceramic compared with the martensitic or pearlitic counterparts [80]. The

thick film improves the heat transfer from the contact area by maintaining the contact temperature reasonably low. Thus, the transformation of ZrO_2 is prevented. Conversely, the material transfer is limited when pearlitic or martensitic iron alloy is used. The contact temperature is sufficiently high to cause a phase transformation and related volume change in ZrO_2 by causing stress-induced spalling. In a similar experiment, the wear behaviour of sintered, partially stabilised zirconia (PSZ) with 8-wt.%yttria against PSZ and steels was tested at 200°C. When metals are used as the mating surface, a transferred layer soon forms on the ceramic surface (coated or sintered) [81]. In a ceramic–ceramic system, the contact wear is abrasive in nature. However, similar worn particles remain entrapped between the contact surfaces and induce a polishing wear. In the load range of 10 to 40 N, no transformation of ZrO_2 occurs [81, 82]. However, similar tests conducted at 800°C reveal a phase transformation from monoclinic ZrO_2 to tetragonal ZrO_2 [83]. The wear debris of ZrO_2 sometimes gets compacted during repeated loading and gets attached to the worn surface, thus forming a protective layer [84]. During rubbing, pre-existing or newly formed cracks may grow rapidly and eventually interconnect with each other, thus leading to a spallation of the coating [85]. The worn particles get entrapped between the mating surfaces and abrade the coating. The wear performance of ZrO_2 –12 mole% CeO_2 and ZrO_2 –12 mole% CeO_2 –10 mole% Al_2O_3 coatings against a bearing steel under various loads was studied [86]. The introduction of alumina as a dopant was found to significantly improve the wear performance of ceramics. Here, plastic deformation is the main wear mode. The wear performance of zirconia at 400°C and 600°C was reported in the literature [87]. At these temperatures, the adhesive mode of wear serves a major role.

iii. Titania (TiO_2) Coating

Titania coating is known for its high hardness, density, and adhesion strength [64, 67]. The coating has been used to combat abrasive, erosive, and fretting wear either in its pure form or in association with other compounds [88, 89]. The mechanism of wear of TiO_2 at 450°C under both lubricated and dry contact conditions has been studied [67, 68]. TiO_2 undergoes plastic smearing under lubricated contact and fails in this case

owing to the surface fatigue in the dry condition. TiO₂–stainless steel couples in various speed–load conditions were investigated in detail [90]. At a relatively low load, the failure occurs due to surface fatigue and adhesive wear. However, at a high load, the failure is attributed to the abrasion and delamination associated to a back and forth movement [91]. At a low speed, the transferred layer of steel oxidises to form Fe₂O₃, and the wear progresses by adhesion and surface fatigue. At a high speed, Fe₃O₄ forms instead of Fe₂O₃ [92]. The TiO₂ top layer also softens and melts owing to a steep rise in temperature, which helps in reducing the temperature subsequently [4, 93]. The performance of plasma-sprayed pure TiO₂ has been compared with those of Al₂O₃–40 wt. % TiO₂ and pure Al₂O₃ under both dry and lubricated contact conditions [94]. TiO₂ exhibits the best results. Due to its relatively high porosity, TiO₂ can provide good anchorage to the transferred film and can hold the lubricants effectively [95].

iv. Alumina (Al₂O₃) Coatings

Alumina is obtained from a mineral known as bauxite, which exists in nature as a number of hydrated phases, such as boehmite (γ -Al₂O₃, H₂O), hydrogillate, and diaspre (α -Al₂O₃, 3H₂O). Alumina also exists in several other metastable forms such as β , δ , θ , η , κ , and X [96]. α -Al₂O₃ is known to be a stable phase and is available in nature in the form of corundum. Moreover, α -Al₂O₃ can be extracted from the raw materials by fusing them. The phase transformation while freezing the plasma-sprayed alumina droplets has been studied in detail [97, 98]. Based on the molten particles, γ -Al₂O₃ tends to nucleate, because the liquid to γ transformation involves a low interfacial energy. The phase finally formed upon cooling is based on the particle diameter. For a particle diameter less than 10 μm , the metastable form is retained (γ , δ , β , or θ). PS of alumina particles with a mean diameter of 9 μm results in the development of the gamma phase in the coating after cooling [99]. The α form is found in particles with a large diameter. In fact, larger the diameter, the greater is the fraction of α -Al₂O₃ in the cooled solid. This form is desirable for its superior wear properties. In addition to the cooling rate, another method to achieve the finally formed phase is to vary the temperature of the substrate. If the substrate temperature is

maintained at 900°C, then the δ phase is formed. Here, α -Al₂O₃ can be formed by increasing the temperature of the substrate to 1100°C, thus resulting in slow cooling. During freezing, the latent heat of solidification is absorbed in the still molten pool. If this heat generation is balanced by the heat transfer to the substrate, columnar crystals grow. Conversely, if the aforementioned heat transfer is faster than the heat injection rate during solidification, equi-axed crystals are supposed to form. However, in reality, columnar crystals are generally found.

There are several advantages of alumina as a structural material, such as high availability, hardness, melting point, and resistance to wear and tear. Alumina bonds well with the metallic substrates when applied as a coating on them. Alumina is used in bearings, valves, pump seals, plungers, engine components, rocket nozzles, shields for guided missiles, vacuum tube envelopes, integrated circuits, etc. Plasma-sprayed alumina-coated railroad components are currently used in Japan [100].

Properties of alumina can be further complemented by the particulate (TiO₂, TiC) or whisker (SiC) reinforcement [101]. TiC reinforcement limits grain growth, improves strength and hardness, and retards crack propagation through the alumina matrix [102]. The sliding wear behaviour of both monolithic and SiC whisker-reinforced alumina was studied [4,103]. The whisker-reinforced composite was found to have good wear resistance. Monolithic alumina has a brittle response to sliding wear, whereas the worn surface of the composite reveals signs of plastic deformation with fractures. The whiskers also undergo pullout or fracture. TiO₂ is a commonly used additive in plasma-sprayable alumina powder [104,105]. TiO₂ has a relatively low melting point and effectively binds alumina grains. However, a successful Al₂O₃-TiO₂ coating is based on a judicious selection of the arc current, which can melt the powders effectively. An appropriate selection results in a good coating adhesion with high wear resistance [49]. The wear performance of Al₂O₃ and Al₂O₃-50 wt. % TiO₂ was reported in the literature [94]. In dry sand abrasion testing, alumina outperformed other materials presumably owing to its high hardness [106]. During dry sliding at a low velocity range, the tribocouple (ceramic and hardened stainless steel) exhibits a stick-slip phenomenon [107]. At a relatively high speed range, the coefficient of

friction reduces owing to the thermal softening of the interface [93]. The wear of alumina is found to increase appreciably beyond a critical speed and a critical load. Alumina has been found to fail due to plastic deformation and shear and grain pullout. During dry and lubricated sliding, mixed ceramic is found to perform better than pure alumina. A coating of Al_2O_3 –50 wt. % TiO_2 is quite porous and thus is quite capable of holding the transferred metallic layer that protects the surface [95]. The wear performance of such coatings can be further improved by sealing the pores by using polymeric substances [41]. A low thermal diffusivity of the alumina coatings results in a high localised thermal stress on the surface. The mode of wear of alumina is mainly abrasive. The pore size and pore size distribution serve a vital role in determining the wear properties. The Al_2O_3 – TiO_2 coating has a high thermal diffusivity and thus is less prone to wear.

The sliding wear behaviour of plasma-sprayed alumina against AISI-D2 steel under different speed–load conditions was reported [108]. Within the load range used (45N–133N), the wear versus load plot presents a maxima. In the initial phase, the wear volume increases with the load for a given number of sliding cycles. Beyond a certain load, a major plastic flow occurs on the coating surface due to load and frictional heating. The plastic flow leads to an increase in the real area of contact and a corresponding reduction in the normal stress, although the normal load increases [109]. Thus, the wear decreases with an increase in the load beyond the critical normal load. Conversely, the wear versus sliding speed plot displays a maximum within the speed range of 0.31 to 8 m/s. At a low speed range, the asperities move against each other and deform each other in the process. As the speed is increased, the asperities are subjected to heavy impacts and tend to fracture due to the root that produces a higher volume of debris. At a very high velocity, the friction-related temperature increases and becomes sufficiently high to soften the asperities, thereby protecting them from fracture. The wear rate is low under such circumstances. Therefore, the plastic deformation and brittle fracture form the failure mechanisms.

c. Metallic Coatings

Metallic coatings can be easily applied using FS or welding techniques, thus making the process very economical. Moreover, plasma-sprayable metallic consumables are also available in an abundant quantity. Metallic wear-resistant materials are classified into three categories—Cobalt-, nickel-, iron-based alloys.

The common alloying elements in a cobalt-based alloy are Cr, Mo, W, and Si. The microstructure comprises dispersed carbides of M_7C_3 type in a cobalt-rich FCC matrix. The carbides provide the necessary abrasion and corrosion resistances. Hardness at elevated temperatures is retained by the matrix [110,111]. Sometimes, a closed packed intermetallic compound is formed in the matrix, which is known as the Laves phase. This phase is relatively soft but offers a significant wear resistance [112]. The primary alloying elements in Ni-based alloys are Si, B, C, and Cr. Abrasion resistance can be attributed to the formation of extremely hard chromium borides. In addition to carbides, the Laves phase is also present in the matrix [110].

Iron-based alloys are classified into pearlitic steels, austenitic steels, martensitic steels, and high alloy irons. The primary alloying elements used are Mo, Ni, Cr, and C. The softer materials, such as ferritic, are used for rebuilding purpose. The harder materials, such as martensitic, provide wear resistance. Such alloys do not possess much corrosion, oxidation, or creep resistance [110,113,114]. Nickel aluminide is another example of a coating material that is used for wear application. When the pre-alloyed Ni–Al powders are sprayed, they react exothermically to form nickel aluminide. This reaction improves the adhesion of the coating and substrate. In addition to wear applications, nickel aluminide is also used as a bond coat for ceramic materials [42].

NiCoCrAlY is an example of plasma-sprayable superalloy and displays an excellent high-temperature corrosion resistance. Thus, it finds application in gas turbine blades. The compositional flexibility of such coatings permits the tailoring of such coating compositions for both property improvement and coating–substrate compatibility. Moreover, it serves as a bond coat for zirconia-based thermal barrier coatings [4,115].

d. Diamond Coatings

Thin diamond films used for industrial applications are commonly produced by CVD, plasma-assisted CVD, ion-beam deposition, and laser ablation techniques [116,117]. Such coatings are used for electronic devices and ultra wear-resistant overlays. The limitation of the aforementioned methods is their slow deposition rates. The DIA-JET process involves DC Ar–H₂ plasma with methane gas supplied at the plasma jet that is capable of depositing diamond films at a high rate [118]. However, the process is extremely sensitive to process parameters. The deposition of a diamond film is also possible by using an oxy-acetylene torch [119].

One significant limitation of the diamond coating is that it cannot be rubbed against ferrous materials owing to the phase transformation that leads to the formation of other carbon allotropes [120]. Diamond films are tested in terms of the sliding wear against abrasive papers, in which wear progresses by micro-fracturing of the protruding diamond grits. The process continues until the surface becomes flat; thereafter, wear progresses by an interfacial spalling. Therefore, the life of the coating is limited by its thickness [121].

2.5 SLIDING WEAR BEHAVIOR OF CERAMIC COATINGS

Sliding wear is defined according to the ASM/TSS Thermal Spray Terminology and Company Origins document as “The motion of two moving bodies in which these surface velocities, at the point of contact, are different with regard to magnitude and/or direction.” Key components of sliding wear are mechanical loading, types of loads, chemical media, temperature, and type and amount of lubricant. Materials need to be tribologically compatible to each other. Examples of sliding wear are in reciprocating and rotating machinery. More specifically, sliding wear is common in automotive and heavy duty piston ring applications, synchronizer rings and transmission systems, automotive and large cylinder bores for gas transmission applications, hydraulic rods for earth-moving equipment, and landing gears for mainframe aerospace applications that replace hard chrome plating [122]. Common

sliding wear tests are conducted by pin on disc tribometer as per ASTM G-99 standards. A model of pin on disc tribometer is shown in [Figure 2.8](#).

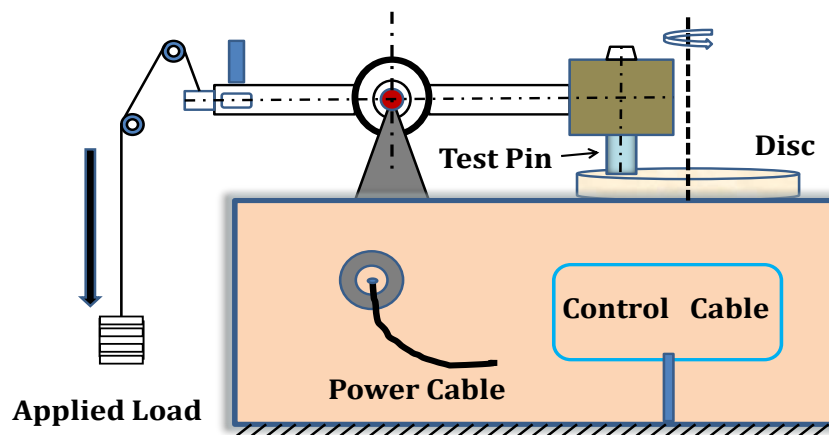


Figure 2.8 Compact outline of pin on disc tribometer

Coating technologies have already gained a promising momentum for the creation of emerging materials in the last few decades. Coatings with advanced wear properties claim frequent use in tribological applications. In the present scenario coating technologies manifest a promising momentum for emerging materials. Wear resistive coatings are claimed to be better tribological applications [123]. Plasma spray is one of the most widely used techniques involved in surface modification by improvement of wear resistance, which may affirm the great versatility and its application to a wide spectrum of materials. Surface modification by improving wear resistance is most widely adopted by plasma spraying technique, which could affirm a great versatility and its application to a wide spectrum of materials [123]. The coatings with a considerable amount of hardness can protect against a wear mediums. Several factors may influence the tribological behavior of a coated surface ramified such as the geometry of the contact including macrogeometry and macrotopography of the surfaces; the material characteristics; basic mechanical properties and the microstructure; and finally the operating parameters controlling the coating deposition [124]. Dry Sliding Wear Behaviour of Plasma Sprayed Flyash- Al_2O_3 and Flyash-SiC Coatings on the Al6061 Aluminum Alloy was studied by Umanath et al. [125]. Wear resistant coatings are fabricated from some common conventional materials like nickel, iron, cobalt and molybdenum based alloys [126-128]. Generally for thermal

resistant coatings, the thermal expansion should match the substrate to maintain structural integrity during heating and cooling [129]. The tribological properties of traditional manganese phosphate coatings and hBN composite coatings composed of nano hexagonal boron nitride (hBN) in layered manganese phosphate crystals on AISI 1040 steel were studied in [130].

Studies are also available regarding the wear behaviour of WC with 12% Co coatings produced by Air Plasma Spraying method [131]. Examinations of the wear behaviour of Mo and Mo+NiCrBSi thermally sprayed coatings were performed for the application as next-generation ring face coatings [132]. Now-a-days Plasma sprayed coatings are used as thermal barriers and abrasion, erosion or corrosion resistant coatings in a wide variety of applications owing to their high hardness and high temperature performance [133]. Almost all plasma sprayed ceramic coatings featured favourable tribological performance in linear contact at high temperatures: high anti-wear resistance and easy to be lubricated owing to the oil storage of pores in coatings [134-136]. But needful to say, plasma sprayed ceramic coatings exhibit some failure mechanisms during sliding such as plastic deformation, brittle fracture and polishing effects [137], which in turn demands a few additives, which could reduce the friction and wear of plasma sprayed ceramic coatings [138].

Several factors may influence the tribological behaviour of a coated surface such as: the geometry of the contact including macro geometry and topography of the surfaces; the material characteristics; basic mechanical properties as well the microstructure and finally the operating parameters controlling the coating deposition [139]. Plasma spraying process is a thermal spraying technique, which is a relatively specialized high temperature industrial process that utilizes electrically generated plasma to heat and melt the feedstock material. The process is capital intensive and requires significant electrical power. It offers a method of depositing a feedstock material over an underlying target material as a solid coating layer [133].

Red mud as an industrial waste material is considered to be the material of choice for coating applications. It is behoved to mention here that, red mud in the present decade should be considered as an alternative for replacing some conventional expensive coating materials. Utilisation of red mud and its implications is available in the literature [140] in great details. Few results on the wear behaviour of red mud were reported by some researchers. Fly ash is a most divided powder generated as a solid waste in quantities during power generation in coal – based power plants [126]. It can be a cost effective substitute for conventional extenders in high performance industrial protective coatings [141-143]. Characteristics of plasma sprayed pure red mud coatings were reported in [144]. Red mud as filling material is also found to be the wear enhancing agent for metals [145]. Tribological design of thermally sprayed red mud-fly ash and red mud-Al coatings on mild steel were reported [146-149]. Data pertaining to the sliding wear behaviour of fly ash based red mud composite coatings are not abundant and need to be addressed. According to recent investigations composite fly-ash coatings can obtain high corrosion resistant, in addition to increased wear resistance [133].

Interfaces that are usually exposed to elevated temperatures are of various moving assemblies in the aerospace industry, power generation and metal working processes [150]. Metallic or metallic alloy coatings when exposed to above 200°C; most of them lose their initial properties and soften appreciably [151]. So such coatings are limited to low temperature applications. To offset, it is needful to design a coating that can pass the high temperature climate. Deposition efficiency is an important factor that determines the techno economics of the process which is evaluated for the deposited coatings. The performances of wear resistant coatings under various conditions have been reviewed critically along with the corresponding failure mechanisms [152]. History reveals Ni-Cr alloy as a widely used coating material on mild steel. But the outlook of Ni-Cr alloy is dark due to its increasing demand. To replace Ni-Cr alloys, a project was undertaken by United States National Bureau of Standards by ceramic coated steel in number of applications [153]. The Bureau considered several factors specially importance for coatings suitability to high temperature such as high bond

strength, low thickness, no re-boil, protection of steel against oxidation and high resistance to thermal shock.

Development of ceramic coatings is resuming a promising momentum towards high temperature applications areas, owing to its greater refractoriness and bond strength. The adhesive (bond) strength of coating sprayed onto a metal substrate is usually considered due to mechanical anchoring, chemical (metallurgical) bonding, and van der Waals forces [154]. The roughness of the substrate is a major influencing factor on adhesive strength [155]. The roughened surface enhances mechanical anchoring of the coating, and the clean surface can also be expected to strengthen metallurgical bonding and physical bonding between the coating and the substrate [156]. Literature reveals bond strength of Al–Si coating on mild steel by kinetic spraying deposition technique [157]. Thermal spraying is the application of a material (consumable) to a substrate by melting into droplets and impinging the softened or molten droplets on a substrate to form a continuous/ pulsed coating [158]. Results of adhesion measurements for different systems of steel sheet-phosphate inter layer ceramic coating are described [159-160]. The development of new coating technological methods is still in progress. New coating technologies and advanced techniques in conformal coating have been described by Szuch et al. [161]. Relatively simple and low-cost manufacturing technique of thermal barrier coatings has been developed, which is called the slurry spray technique [162]. A broad description of physics of different coatings and their application are reported [163]. Fly ash/quartz/illmenite composite coatings developed by means of plasma spraying technique on copper metal are revealed [164].

2.6 PROGRESS OF RED MUD UTILISATION:

Aluminium metal is commercially produced from bauxite ore through two main process steps. In the first step, alumina is obtained using the Bayer's process [165] and in the second step the alumina is electrolysed in a Hall-Heroult cell [166] to yield aluminium metal. The production of alumina from bauxite by the Bayer's process is associated with the generation of red mud as the major waste material. Based on the

quality of bauxite, the quantity of the generated red mud varies from 55%–65% of the bauxite processed. The enormous quantity of red mud discharged by industries producing alumina poses environmental and economic problems. The treatment and disposal of this residue is a major task in an alumina plant.

Red mud, as the name suggests, is brick red in colour and is slimy with an average particle size of approximately 80 μm . It comprises the iron, titanium, and silica constituents of the parent ore with other minor constituents. Red mud is alkaline, thixotropic, and possesses a high surface area in the range of 13–16 m^2/g with a true density of 3.30 g/cc . The leaching chemistry of bauxite suggests that the physical and chemical properties of red mud are based on the bauxite used and the manner in which the bauxite is processed. Residues from different bauxites have a wide range of compositions: Fe_2O_3 : 20%–60%, Al_2O_3 : 10%–30%, SiO_2 : 2%–20%, Na_2O : 2%–10%, CaO : 2%–8%, and TiO_2 traces: 28%. Detailed characterisation of red mud generated from the NALCO aluminium refinery at Damanjodi, India, was reported by Mohapatra *et al.* [167] and of some other sources by various authors [168-170]. The important parameters that are crucial for the further handling, disposal, and use of red mud include moisture content, rheology, surface area, particle size, mineralogy, contents of valuable metals, presence of rare earth metals, and presence of toxic substances. The composition of red mud samples from some randomly selected locations is presented in [Table 2.3](#) [4,171].

To date, almost all over the world, red mud is disposed at a plant site in two main ways based on the facilities available and the surroundings. In countries such as France, England, Germany, and Japan in which less land is available for dumping and the sea is nearby, the mud is discharged into the sea. Where free land is available nearby, the mud is pumped into pools and ponds constructed for this purpose.

Probably, the easiest use of the mud is to conduct some sort of useful landfilling instead of just dumping the mud. Some attempts in this direction are include filling material for mined or quarrying areas, landfill cover, road-bed and levee material, alternative to natural marsh sediment, agricultural land soil neutralisation, and composting domestic waste. In many of these areas, some sort of neutralisation or red

mud amendment becomes necessary. A brief description of these uses is presented below.

Table 2.3 Compositions of red mud across different parts of world [4]

Country		Prominent constituents, wt %				
		Fe ₂ O ₃	Al ₂ O ₃	TiO ₂	SiO ₂	Na ₂ O
INDIA	Al. Corprn.	20.26	19.60	28.00	6.74	8.09
	MALCO	45.17	27.00	5.12	5.70	3.64
	HINDALCO	35.46	23.00	17.20	5.00	4.85
	BALCO	33.80	15.58	22.50	6.84	5.20
	NALCO	52.39	14.73	3.30	8.44	4.00
HUNGARY		38.45	15.20	4.60	10.15	8.12
JAMAICA		50.9	14.20	6.87	3.40	3.18
SURINAM		24.81	19.00	12.15	11.90	9.29
USA	Sherwon	50.54	11.13	Traces	2.56	9.00
	Arkansas	55.60	12.15	4.50	4.50	1.50
	Alcoa Mobile	30.40	16.20	10.11	11.14	2.00
FRG BAUDART		38.75	20.00	5.50	13.00	8.16
TAIWAN		41.30	20.21	2.90	17.93	3.80
AUSTRALIA		40.50	27.70	3.50	19.90	1.20

Bauxite mines or other quarries are being filled with red mud. Thus, the slurry should be neutralised, and high solid pipeline transportation is necessary. Considerable progress has been made on the latter aspect. For neutralisation, lime, gypsum, sea water, or other materials with similar neutralisation properties are mixed with red mud. In Australia and Hungary, neutralisation is conducted by adding gypsum to red mud. After this addition, red mud is known as red mud amended with gypsum [172]. Recently, Galarraga *et al.* [173] successfully pilot tested the neutralisation of red mud

pulp from 12.20 to 7.60 pH by using carbon dioxide. Mine filling is a good use of red mud, although the values of metals in red mud are left to be recovered in future. Good progress has been reported by Kirkpatrick and Brown [174] and Kirkpatrick [175] in this regard. After caustic neutralisation, red mud and local clay mixtures have been successfully used as land covers.

Brown and Kirkpatrick [174] again reported use of red mud as road-bed and levee material. Due to its compactibility, disced red mud was stacked and then compressed by heavy equipment to form hard road surfaces on the mud lake. The road surfaces are extensively used to support the large trucks carrying the landfill cover and to move equipment around the lake. A study at Tulane University by Goldstein and Reimers [176] revealed that over 25 square miles of Louisiana wetlands are lost per year due to sediment starvation, coastal erosion, and subsidence. The dredged sediments are quite often found to be polluted and unsuitable for filling in wetlands. Red mud, in this case, has been proposed to be a suitable alternative.

Considerable efforts have been focussed on finding the suitable uses of red mud so that the alumina industry may contain no residue at all. For complete utilisation of red mud, Kovalenko [177] proposed the following avenues:

- Used in building material production as an additive to cement.
- Production of colouring agent for paint works for ground floors of industrial and other buildings.
- Production of toned paper in the wood–pulp and paper industry.
- Production of iron ore sinter and pellets in ferrous metallurgy.
- Used in agriculture for improving the soil structure and as a micro-fertiliser and neutraliser of pesticides.

Attempts have been made over the years to find a use of red mud, and studies have been conducted for determining the use of red mud as a partial substitute for clay in ceramic products such as bricks and tiles [178] and as an additive for mortar and concrete [179]. The use of red mud in agricultural applications, such as in acidic soils or as a treatment for iron deficient soils, was reported [180]. Numerous other uses for

red mud have been reported in the literature, which are well documented in the book by Thakur and Das [171].

The uses range from making various building materials, adsorbents, and colouring agents to even preparing exotic ceramic glass materials. Smirnov *et al.* [181] proposed a technology of sulphuric acid processing that uses deactivated red mud with coagulation and the granulation of Fe–Al coagulants, followed by burdening, forming, and heat treatment to produce building materials. Red mud can be used as an adsorbent and a colouring agent. Martinent-Catalot *et al.* [182] reported the suitability of red mud as an arsenic fixation on co-disposal projects and as colouring material for various materials. Liu [183] conducted a study to use red mud to remove toxic materials from wastewater. The results indicated that only 0.5 mg/litre of red mud was sufficient for a near complete removal of all the metals except selenium at an initial water pH of 8.0 and at retention time of as low as 1 min. Other authors [184,185] reported the use of red mud to adsorb nickel.

Red mud has some applications in ceramic industries as well. Yalcin and Sevinc [186] experimented with the red mud obtained from the Seydischir Aluminium Plant, Turkey, and attempted to use it in making ceramic glazes such as porcelain, vitreous (sanitary ware glazes), tile, and electro-porcelain glazes in the ceramic industry. The results revealed that the addition of up to 37 wt.% of red mud waste was possible in the production of these glazes. Recently, Balasubramanian *et al.* [187] used specific mixtures of red mud, fly ash, and spent pot liner to prepare glass–ceramic products that exhibited excellent properties and aesthetic appearance for possible applications as decorative tiles in the building industry.

A recent experimental study by Mahata *et al.* [188] confirmed the formation of aluminium titanate–mullite composite from red mud rich in titanium. This formation was achieved by preferentially removing Fe₂O₃ from red mud by conducting dilute HCl acid leaching, thus leaving a residue rich in Al₂O₃, TiO₂, and SiO₂. Then, pure Al₂O₃ powder was added to obtain the required molar ratios. Thus, a composite material comprising aluminium titanate (Al₂TiO₅)–iron titanate (Fe₂TiO₅) solid solution and mullite (3Al₂O₃·2SiO₂) phases after final reaction synthesis was

obtained. This material has potential uses as liquid metal flow regulators, risers, thermocouple sleeves, burner nozzles, ceramic filters, etc.

There can be many such uses of red mud. However, these applications use only a small fraction of the waste material. For bulk use, application such as metal extraction processes and land filling may be considered.

The analysis presented in [Table 2.3](#) presents that iron is the major constituent of red mud, followed by Al_2O_3 , Na_2O , SiO_2 , and TiO_2 . Among these constituents, the recovery of silica is not significant. Titania has the highest potential application value. Moreover, if titania is successfully recovered, iron can be obtained as a value added product. However, alumina and alkali can be recycled in the Bayer's process stream. Based on their amount in red mud, economic extraction of other metals can also be significant. As iron is the major constituent of red mud, much attention has been directed towards its recovery. Studies on this aspect were initiated as early as the nineteen fifties. A large number of processes of iron recovery from red mud were reported either exclusively or in combination with other metals, and many of these processes have been patented.

Chlorination of red mud was reported by Laszlo and Lozsef [189] on a sample containing approximately 66% of Fe_2O_3 , 13.30% Al_2O_3 , and 6.1% TiO_2 . At 800°C , most of the Fe_2O_3 content could be separated as vapour but the residual Fe_2O_3 content contaminated the TiO_2 content, thus hampering its whiteness. Chlorination at 900°C converts Al_2O_3 , Fe_2O_3 , TiO_2 , and SiO_2 into chlorides. SiO_2 can be separated from the mixture of chlorides by adding Al_2O_3 with the formation of equivalent amounts of AlCl_3 . On treatment with TiO_2 , Al_2O_3 precipitated with the formation of TiCl_4 . The remaining gaseous mixture of TiCl_4 and FeCl_3 was further treated with Fe_2O_3 to obtain TiO_2 and FeCl_3 . FeCl_3 was finally converted to Fe_2O_3 . Heck [190] suggested a method for preparing Fe powder from red mud by charging red mud from the top of a vertical kiln and reducing gas (H_2 , NH_3 , and fuel gas) from the bottom. The iron powder particles collected from the bottom were less than $10\ \mu\text{m}$ in size. A method reported by Marvin [191] for the recovery of Fe, TiO_2 , and Al_2O_3 from red mud employed an electric arc furnace with a charge of coke and red mud for the reduction

of Fe_2O_3 . A reaction at 1600°C – 1700°C resulted in a 90% recovery of Fe, Al_2O_3 , TiO_2 , and the residual Fe remaining in the slag. A scheme for the recovery of iron, alumina, titania, and alkali was presented by Ni [192]. The scheme involved electro-smelting to produce pig iron of low titania content. The treatment of the slag with concentrated NaOH in the presence of lime under pressure recovered more than 90% of Al_2O_3 . The remaining mud was leached with dilute alkali, followed by water. After filtration, the titania from the residue was recovered by chlorination.

Watanabe and Yuki [193] patented a method to obtain pure Fe powder from red mud. The Fe content of red mud was reduced using hydrogen or carbon monoxide or town gas at 300°C – 400°C . Powder iron was separated by magnetic separation. Braithwait [194] suggested the separation of iron from red mud in a slurry form by applying high-intensity magnetic separation. The resulting magnetic product may be an ingredient for iron making or for preparing pigment in the pottery industry. However, the recovery of iron is low. Another investigation [195] reports the reduction of iron with chlorocarbons before magnetic separation and uses of the resulting magnetic portion as feed for iron making.

A study by Mozharenko and Noskov [196] suggested the possibility of using red mud in blast furnaces and steel making after compaction to a fraction in range of 3–10 mm with preparation of granules and lumping into briquettes. Based on the experiments conducted on charge materials sintered with the addition of granulated red mud, it was found that the compacted red mud in the sinter composition could be implemented as the metal and flux-containing additive in blast furnaces, steel making, and electro-metallurgy. Red mud is a promising binder for different metallurgical wastes.

Some of the more recent studies reported on iron recovery are as follows: A study by Xiang *et al.* [197] employed low-temperature ($<350^\circ\text{C}$) reduction of red mud, followed by magnetic separation. Moreover, a study by Mishra *et al.* [198] employed a relatively high-temperature (650°C – 1050°C) reduction, followed by magnetic separation. Liu *et al.* [199] used high gradient magnetic separation to remove the hematite from the dried and milled red mud. As the hematite particles in the bauxite are assumed to be reasonably well-liberated, magnetic separation seems to be feasible

in theory. However, experimental results revealed contradicting results. However, this technology offers the advantages of low energy and enrichment of the titania content of the mud.

Studies related to the recovery of aluminium and titanium from red mud are mostly part of a scheme for recovery of iron and these two metals. After removing iron, the residue is subjected to various treatments for aluminium and titanium recovery. Thus, most of the studies reported in literature provide schemes for the recovery of these three metals. Dubos *et al.* [200] added 8% of CaO to red mud and sintered the product by adding coke. More than 90% of iron from the sinter was separated by magnetic separation, and the nonmagnetic slag was further treated with lime and soda and leached to recover 85%–90% of Na₂O and 75%–80% of Al₂O₃. Tathavadkaret *al.* [201] develop a novel route for extracting alumina from red mud or bauxite. The process involves roasting of red mud or bauxite with an alkali carbonate in air at temperatures above 777°C, digestion of the reaction product in water, and filtration. Al(OH)₃ is precipitated from the filtrate containing water-soluble alkali aluminate by adjusting the solution pH and calcined to yield pure alumina with an extraction efficiency of more than 98%. Alkali carbonates can be recovered by evaporating the filtrate obtained after removing the Al(OH)₃ precipitate. Based on the alkali-roasting technique, a zero-waste technology for alumina extraction can be devised.

Kasliwal and Sai [202] described a process for the enrichment of titanium dioxide in red mud. The method involves leaching the red mud with hydrochloric acid, followed by roasting the leached residue with sodium carbonate. In this process, TiO₂ increased from 18% to 36% in the first step and further increased to 76% after the second step. Sayan and Bayramoglu [203] studied sulphuric acid leaching for treating red mud for TiO₂ recovery.

The recovery of metals other than iron, aluminium, and titanium from red mud is not significant, that is, no constituent is present in an appreciable concentration. This fact justifies its recovery. However, based on the bauxite composition, certain constituents may be present in red mud in larger amounts and can be considered for recovery.

Reports have indicated a general strategy to utilise red mud. Rayzman and Filipovich [204] suggested an integrated method in which coal combustion and red mud sintering are conducted simultaneously in an alumina refinery. After soda and alumina recovery, the residue can be utilised by metallurgical or chemical technology. Mishra *et al.* [205] suggested a similar approach that involves the removal of aluminium and soda by conducting the sintering and alkali washing stages, followed by pyrometallurgy of the residue to obtain pig iron and a slag rich in titanium. The slag can further be leached with sulphuric acid to recover titanium.

Due to the increase in environmental threats, it has become necessary to determine alternative uses of such industrial wastes and to develop value added products. Although substantial development is observed in the area of disposal and utilisation of red mud, no report on its use as a potential coating material is published. Although a large number of investigations have been conducted during last decade in the field of ceramic coating on the processing of a variety of plasma spray ceramic coatings, not much effort has been focussed on using low-grade materials for this purpose. In 2000, Mishra and Ananthapadmanabhan [206] made the first successful attempt to develop coatings of fly ash and fly ash pre-mixed with aluminium on metal substrates by conducting PS. Ramakrishna *et al.* [207] reported the possibility of coating fly ash on steel substrates by using detonation spraying. However, the studies on the development of thermal spray coatings by using low-grade mineral and/or industrial waste is still scarce. As industrial wastes such as red mud and fly ash are rich in metal oxides, they have tremendous potential to be used as coating materials. This aspect should be explored mainly because many of the conventional coating materials are relatively expensive to the extent that the cost of spray grade powders only can account for even 50%–60% of the cost of operating a plasma spray unit. Conversely, industrial wastes such as red mud or fly ash are not only free of cost but also are available abundantly.

Against this background, the present study has been undertaken with an objective to explore the coating potential of red mud. Red mud does not belong to the plasma-sprayable category and is cheap because it is a waste. Attempts have been made in this

study to deposit red mud coatings on metal substrates at various operating conditions of plasma and to establish their suitability for some typical tribological applications.

The future possesses challenges for the scientists, technologists, and engineers in terms of the sound management when the disposal and deposition technologies of industrial wastes such as red mud and fly ash are used. This subject will continue to be an important area of concern in the coming years. The present investigation is a step in this direction.

CHAPTER-3

AIMS AND OBJECTIVES

- 1) The present study primarily aims to explore the coating potential and feasibility of red mud – RM (the waste generated during the production of alumina from bauxite) and its composites (e.g. with Fly Ash- FA) as coatings on mild steel substrate using plasma spraying (PS) technique. RM would be pre-mixed with 20 % Al and 20 % activated charcoal. RM + FA composites shall be examined at different FA content, viz. 10 %, 20% and 50 %. Towards this end, the **micro-structural characteristics**, **mechanical characteristics**, **thermal behaviour** and **wear behaviour** of the obtained coatings must be studied experimentally using different operating power of PS viz. 6, 9, 12 and 15kW.

- 2) **Micro-structural** characteristics of the coatings; such as surface morphology and coating thickness shall be investigated by using SEM and FESEM. Occurrence of phase transformations during spraying is to be examined by XRD and elemental analysis.

- 3) Different **mechanical characteristics** such as micro-hardness, coating deposition efficiency, porosity and interface bond strength (adhesion strength) would also be evaluated to ensure the robustness of the coatings by using pertinent experimental techniques.

- 4) **Thermal behaviour** of the coatings may be determined by performing DSC and TGA experiments at elevated temperatures. The compatibility of these coatings at high temperature up to 1000°C shall be checked by evaluating their adhesion strengths. In order to understand the effect of heat treatment on the surface topography of the coatings, SEM and FESEM shall be employed after exposing coatings to high temperature atmosphere.

- 5) **Wear behaviour** of the prepared coatings is to be evaluated with particular reference to sliding wear under a fixed unlubricated condition with track diameter of 100 mm and at a sliding speed of 100 rpm (0.523 m/s); applying a normal load of 10 N. Mass loss and coefficient of friction would be predicted with respect to time in dry sliding wear tests and the data subsequently compared for each coating

type with respect to PS operating power. Morphology of the coatings by means of SEM and FESEM is to be observed after sliding wear tests at different sliding times to evaluate the sliding mechanisms from the analysis of wear morphologies.

- 6) Finally it is aimed to analyze the experimental results by Taguchi Optimization technique to identify the significant factors or interactions that influence the wear rate.

CHAPTER-4

MATERIALS AND METHODS

4.1 INTRODUCTION

In this chapter a detailed explanation of the raw materials used for coating and the methods used to study their characteristics is written. The coating procedure itself requires some basic preparation, i.e., shot blasting and cleaning. After plasma spraying, the coatings are subjected to series of tests like XRD phase transformation, coating thickness, coating morphology, sliding wear test, wear morphology, wear mechanism, co-efficient of friction, deposition efficiency, coating hardness, coating porosity, thermal behaviour etc. The details are described below.

4.2 PROCESSING OF COATINGS

a. Preparation of Coating Powder

The present experimental work included the preparation of coating powder from the raw materials as red mud, fly ash, carbon and aluminium powders. The powder mixture of red mud composites was prepared using V-shaped drum mixer. Pure red mud powder was also used as coating material for the comparison. Coating of the various combinations of mixed powders was conducted on mild steel substrate. Data in [Table 4.1](#) shows the different mixtures chosen for plasma spraying. Red mud, as the primary raw material was collected in powder form from National Aluminium Company (NALCO) located at Damonjodi in the state of Odisha, India. Carbon (activated charcoal) used in this work is prepared by activating (heating) common wood charcoal at approximately 900°C in the absence of oxygen. This treatment removes residual non-carbon elements and produces a porous internal microstructure having an extremely high surface area. Activated charcoal or activated carbon is an amorphous form of carbon. Common charcoal contains other organic residues, is much less porous and has a lower surface area. Aluminium powder is purchased from Rourkela market. The as-received powder was sieved to obtain particles in the required size range of 80-100 µm. Raw fly ash was collected from the captive power plant of Rourkela steel plant, India and sieved to maintain same size range as that of

other powder. Powders having different weight ratios of red mud, fly ash, carbon and aluminum (Table 4.1) were prepared by mixing thoroughly.

Table 4.1 Powders used for coating deposition

Sl. no.	Coating material	Mixture composition (by weight %)
1	Red mud (RM)	100
2	Red mud + fly ash (FA)	90 + 10
3	Red mud + fly ash	80 + 20
4	Red mud + fly ash	50 + 50
5	Red mud + Aluminium(AL)	80 + 20
6	Red mud + Carbon(C)	80 + 20

b. Preparation of Substrates

The commercially available mild steel rod was used as a source for substrate preparation. The rod was cut to pieces having one particular dimension ($l = 40$ mm and $\text{Ø} = 12$ mm) each. The specimens were grit blasted from one side cross section (initial roughness 0.03 mm) at a pressure of 3 kg/cm^2 using alumina grits of grit size 60. The stand-off distance in the shot blasting was kept between 120-150 mm. Then the average roughness of the substrate was $6.8 \text{ }\mu\text{m}$. The grit blasted specimens were used for plasma spraying after cleaning in an ultrasonic cleaning unit. In order to measure the adhesion strength, mild steel substrates of rectangular shape ($100 \times 90 \times 10$ mm) are produced and coated with no part left out. For the convenience of DSC and TGA experiments, mild steel substrates of circular shape, $\text{Ø} = 5$ mm and thickness 2 mm are designed and fully coated.

c. Plasma Spraying

The spraying process was performed at the Laser and Plasma technology division of Bhabha Atomic Research Centre, Mumbai, India by adopting conventional atmospheric plasma spraying (APS) set up. A typical image of APS set up is shown in Figure 4.1. The plasma input power was varied from 6 to 15 kW by controlling the gas

flow rate, voltage and arc current. The powder feed rate was maintained constant at 10 gm/min by using a turntable type volumetric powder feeder. Plasma generation used argon as primary and nitrogen as a secondary gas agent. The mixtures of powders were deposited at a spraying angle of 90° by maintaining the powder feeding external to the gun. The operating parameters of the coating deposition process are shown in Table 4.2.

Table 4.2 Operating parameters during coating deposition

Operating parameters	Values
Plasma arc current (Ampere)	200,225,250,300
Arc voltage (Volt)	30,40,48,50
Torch input power (kW)	6,9,12,15
Plasma gas(argon), (litre/min)	20
Secondary gas(nitrogen),(litre/min)	2
Career gas(argon) flow rate (litre/min)	7
Powder feed rate (gm/min)	10
Torch to base distance (mm)	110
Arc length range (mm)	2,3,6,8,11

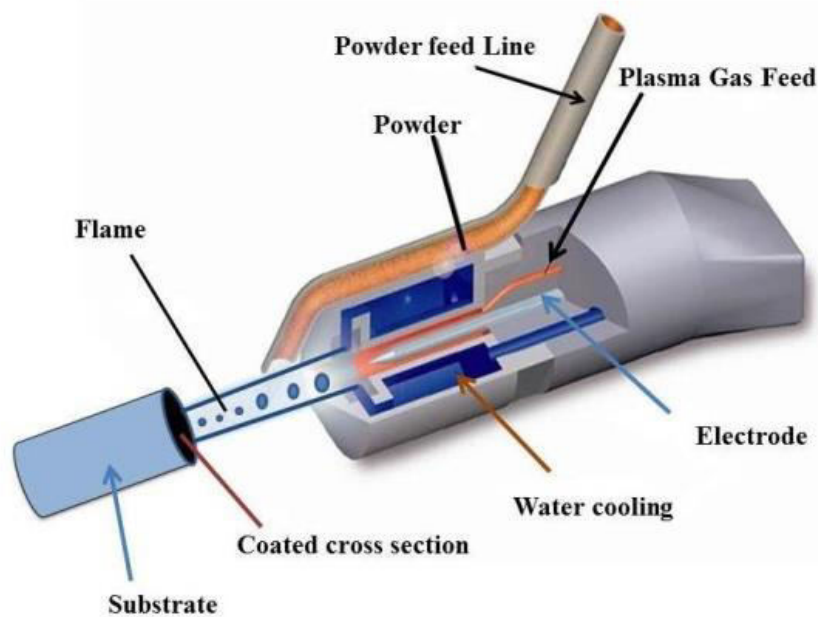


Figure-4.1 Outline of APS set up

4.3 COATING CHARACTERISATION:

a. Dry Sliding wear behaviour of Coatings

The experiments were conducted using a pin on disc type friction and wear monitor allotted by MAGNUM Engineers, Bangalore, India. The detailed experimental set up is materialized in [Figure.4.2\(a\)](#). The tool possesses a data acquisition system ([Figure 4.2 \(b\)](#)). The concerned machine was used to evaluate the wear behavior of the coatings against hardened ground steel disc (En-32) having hardness of 65 HRC and surface roughness (Ra) 0.5 μm . The gadget is designed so as to study the wear behavior both at lubricated and un-lubricated sliding condition, which occurs between a stationary pin and a rotating disc.



Figure 4.2 Comprehensive outline of Pin on Disc Machine (a) Pin on disc set up, (b) Data acquisition system, (c) Model showing rotational direction of disc

D.C motor is implicated for rotating the disc with range of speed from 0-250 rpm with wear track diameter 0-150 mm; yielding a sliding speed of 0-15 m/s. Dead weight was applied on the pin by means of pulley and string arrangement. The system has a maximum loading capacity of 400 N. The device is fabricated to keep the pin specimen stationary and perpendicular to disc, while the circular disc spins anti clockwise as shown in [Figure 4.2\(c\)](#). The wear tests were carried out as per ASTM G-99 standard under unlubricated condition at standard atmospheric temperature and pressure under a constant normal force of 10 N and a fixed speed of 100 rpm. The track diameter of the equipment was kept at 100 mm.

b. Coating Porosity

Image analysis technique was adopted for the measurement of porosity of coating materials. The polished surfaces of various coatings were kept under a microscope (Neomate) equipped with a charge-coupled-device (CCD) camera (JVC, TK 870E). The volume of interest (VOIS) image analysis software played an important role in the determination of porosity. The software can measure accurately the total area captured by the objective of the microscope. Hence the total area and the area covered by the pores are separately measured to report porosity.

c. XRD Analysis

The coatings are examined for the identification of the (crystalline) phases with a Philips X Ray Diffractometer. The X-ray diffractograms are taken using Cu K α radiation. All coated samples have been studied. Experiments are also done to know the different phases occurring in the precursor powder and compared with the coatings after plasma spraying.

d. Morphology, Elemental and Thickness Analysis

The morphology, EDS (Energy dispersive spectroscopy) and the thickness of the coatings involved taking microstructures by the help of scanning electron microscope (SEM, JEOL; JSM-6480 LV) and field emission scanning electron microscope (FESEM, Nova Nano SEM-450). Coating microstructures are studied both before and after sliding. Thickness of the coatings is measured on the polished cross-sections of the samples. Five readings are taken on each specimen and the average value is reported as the mean coating thickness.

e. Coating Hardness

The polished sections of the coatings were put under the optical microscope for the microscopic observations, which revealed the presence of three distinguishable different phases namely dull, white and spotted. The three different distinct phases

were subject to micro indenting to record micro hardness data with the help of Leitz micro hardness tester using 40 Pa (0.393 N) for 25 seconds on all samples and reported in HV.

f. Coating Deposition Efficiency

Deposition efficiency (η) is defined as the ratio of the weight of coating deposited on the substrate to the weight of the expended feedstock. Weighing method is implemented to measure this. Specimens are weighed before and after coating deposition. Weight of coating deposited (G_c) on the substrate is measured. From the powder feed rate and time of deposition the weight of expended feed stock (G_p) is determined. Weighing of samples is done using a precision electronic balance with + 0.1 mg accuracy. The deposition efficiency (η) is then calculated using the following equation [183].

$$\left(\eta = \frac{G_c}{G_p} \times 100 \right) \%$$

g. Thermal and bond strength analysis

The first two thermal analysis techniques used were thermogravimetric analysis (TGA) as per ASTM E-2008 standards and differential scanning calorimeter (DSC) applying Setaram DSC 131 analyser. The temperature parameters for the DSC experiments are fixed from room temperature to 1000°C at a heating rate of 10°C/min in oxidative environment, with air flow rate 10 ml/min. Finally adhesion strength of coatings is measured at normal atmospheric temperature (35°C) and pressure in laboratory for all coatings. Adhesion strength at elevated temperature is also evaluated at an interval of 100°C up to 1000°C placing in a muffle furnace. Coated specimens are kept at the each desired temperature in furnace for 2 hour. Specimens are allowed to cool under normal atmosphere to reach air temperature. Adhesion strength is measured using a Caltech BGD 1520 digital pull off adhesion tester with 10 mm dolly as per ASTM D4541 standards. Both resin and hardener mixed in equal proportion and used as adhesive. Adhesion strengths are reported corresponding to adhesive failure of coatings.

CHAPTER-5

RESULTS AND DISCUSSION

5.1 INTRODUCTION

Plasma sprayed coatings of red mud , red mud + fly ash , red mud + aluminium and red mud + carbon and were developed on mild steel substrate using a 50 kW atmospheric plasma spray system supplied by M/s Ion Arc Machines (Mumbai, India) Pvt. Ltd. at the Laser and Plasma Technology Division, Bhabha Atomic Research Centre, Mumbai. Spraying was done at different input power level namely 6, 9, 12 and 15 kW to the dc plasma torch. Characterization of the coatings was done with respect to their quality and tribological performance. The results of various tests are presented and discussed in this chapter.

5.2 STUDY OF SLIDING WEAR BEHAVIOR

Prior to starting the wear testing experiment, the pin and the disc surface of the concerned equipment were polished perfectly with emery papers for better ensuring of smooth contact with the coating samples. Hereafter the surface roughness was reduced to 0.1 μm . The wear tests were carried out as per ASTM G- 99 standard under an unlubricated condition in a normal laboratory ambience having a relative humidity of 40-55% and the temperature range of 20-25°C. The weight of the specimens before and after the wear experiment was recorded by using an electronic weighing machine having an accuracy of (0.01 mg) for monitoring the mass loss occurrence in the coating samples. Specimens were periodically cleaned with a woollen cloth to avoid entrapment of wear debris and to maintain uniformity in each set of experiments. The test pieces were cleaned with tetrachloroethylene solution before and after each test. Wear rate is expressed in terms of cumulative mass loss estimated by measuring the mass loss (Δm) of the specimen after each test.

The frictional force (F) was measured directly from the apparatus in ‘N’ at each time interval.

The wear experiment was carried out at a normal atmospheric temperature under a constant normal force of 10 N and a fixed speed of 100 rpm. The track diameter of the

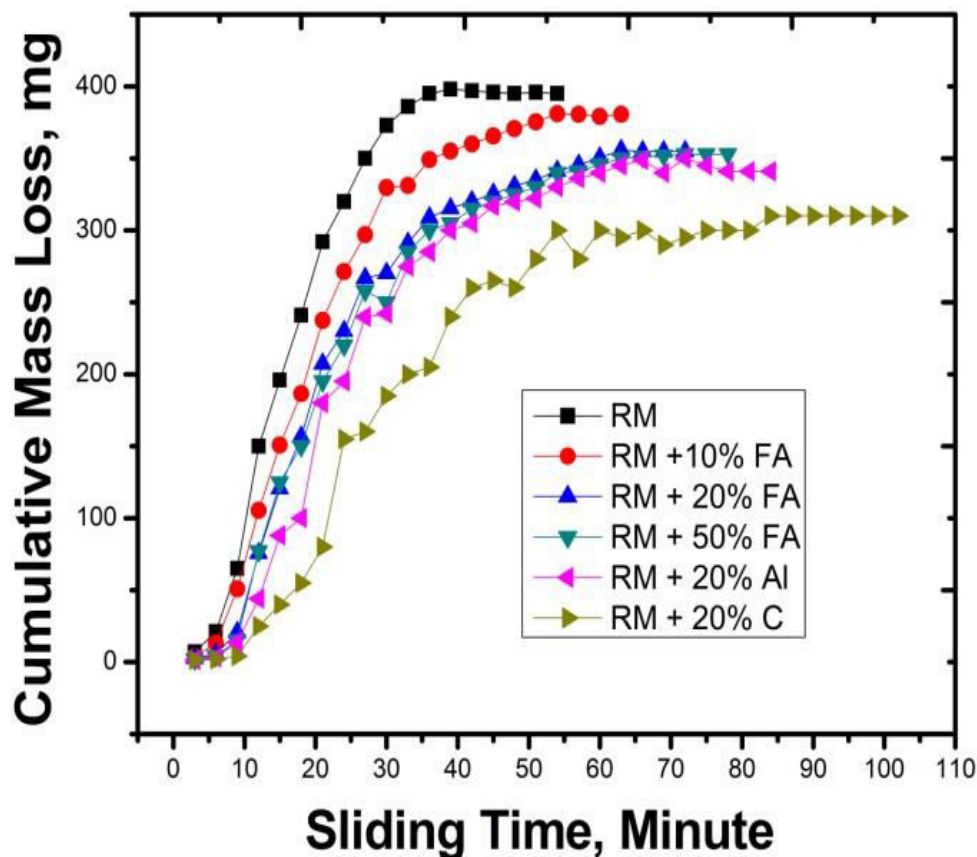
equipment was kept at 100 mm. The coated samples are slid up to the survival of coating on the substrate. Samples are weighed at a time intervals of 3 minutes each. Each sample was allowed for sliding for the distinct (existence of coating) time interval.

Initially, the experiment was performed with red mud coated samples and then continued for fly ash, aluminium and carbon based red mud coating composites. [Figure 5.1](#) illustrates the variation of wear rates with sliding distance for different operating power levels.

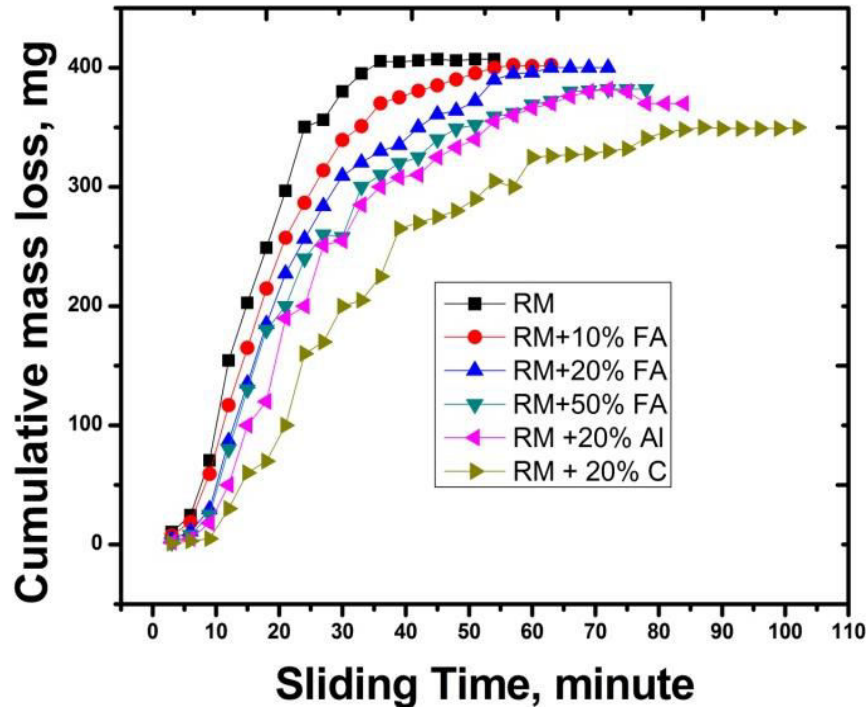
The wear results for pure red mud coating operated at 6 kW operating power is visible in [Figure.5.1 \(a\)](#). It discloses the variation of wear rate with a minimum value of 10.33 mg to a maximum value of 407 mg. The wear rate value was found to increase from 10.33 mg to 70.60 mg for the first 9 minutes of sliding. After a drastic increase from 9 to 12 minutes of duration, the wear rate plot assumed a plateau after 36 minutes of sliding. The evolution of wear rate value may be attributed to the variation of coating layer property. This fact indicates hardness of denser surface of top layer than that of bulk layer.

The wear rate was reduced for fly ash (10%, 20% and 50%), 20 % aluminium and 20% carbon composite coatings, as illustrated in [Figure. 5.1](#). The wear rate trend for composite coatings is quite similar to those of pure red mud coating. The initial slow increase up to about 12 minute in wear rate for the composite coatings was visible followed by a drastic increase and then the wear rate was roughly constant (stabilisation phase) for all composite coating type. The plots in [Figure.5.2](#) represent the variation of wear rates of each coating type with that of sliding distance for different operating power level. The coatings are distinguished in terms of survival of the coating layer with respect to sliding time. It is termed here as break in phase. The operating power has no effect on break in phase. On the other hand the break in phase is different for all coatings. The pure red mud coating survives up to sliding time of 54 minute and is minimum among all the coatings prepared. The break in phase time

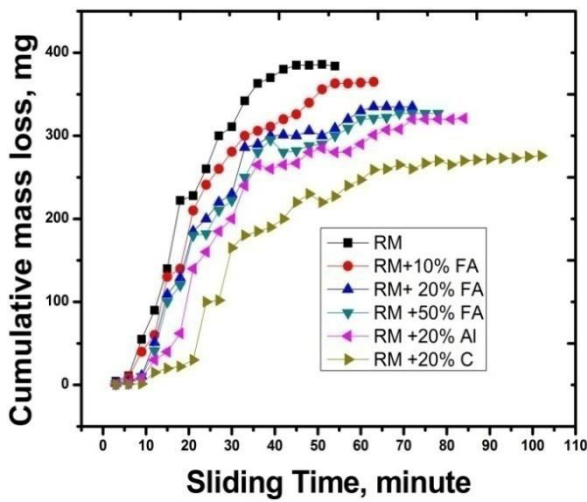
increases with adding fly ash, aluminium and carbon to red mud. The red mud + 20 % carbon coating exists up to a sliding time of 120 minute and is maximum among all the coatings. The break in phase time for red mud + 10 % fly ash, red mud + 20 % fly ash, red mud + 50 % fly ash and red mud + 20 % aluminium coatings are 63, 72, 78 and 84 minutes respectively. The effect of operating power level on wear rate is quite interesting. The wear rate is affected by the porosity and hardness. The wear rate was found to decrease up to 12 kW and increase again slightly for 15 kW. The wear rate for 15 kW was found to lie between 9 and 12 kW. This might be due to the improper particle to particle bonding and poor stacking to the substrate, which in turn lowered the hardness as well as density due to poor interfacial bond strength.



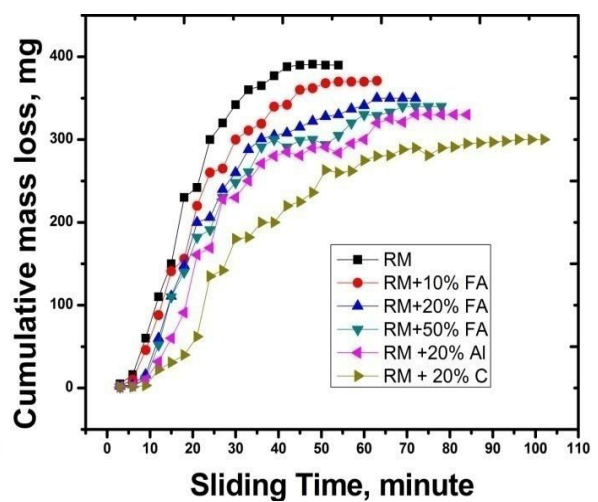
(a)



(b)



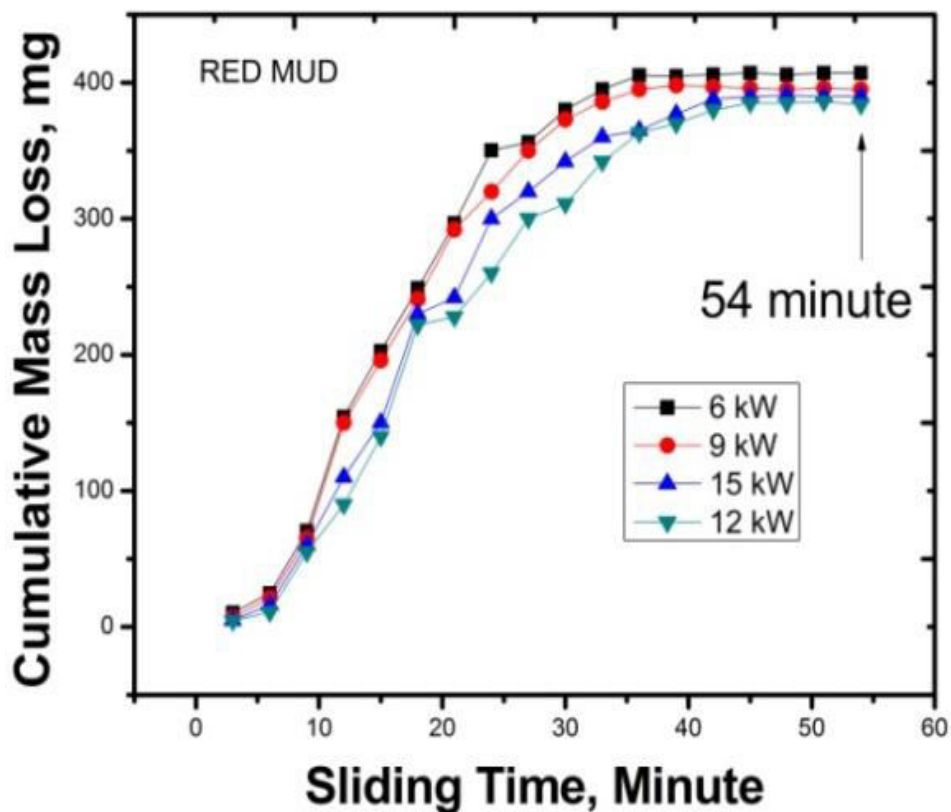
(c)



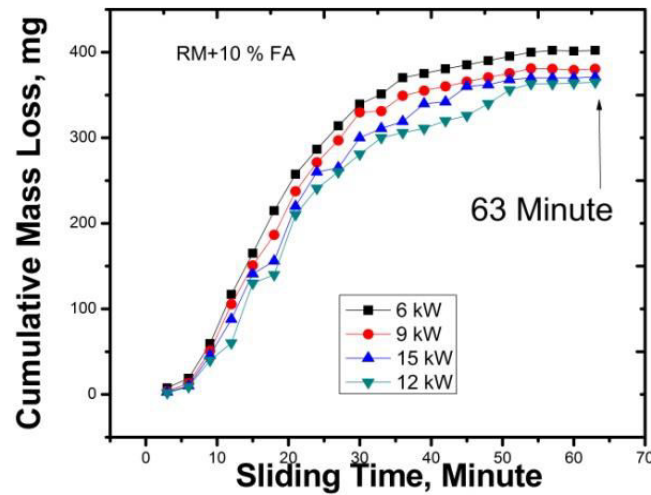
(d)

Figure 5.1 Wear rate in cumulative mass loss of the prepared coatings made at (a) 6 kW, (b) 9 kW, (c) 12 kW and (d) 15 kW operating power levels.

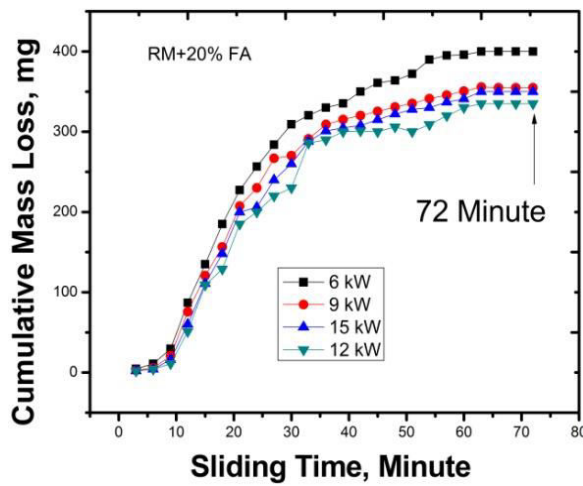
In the sliding wear behaviour the coefficient of friction (μ) has been also reported. The value of μ is found by the equation, $F=\mu R$. Where F is the frictional force in N. R is the normal load in N. The variation of frictional forces with sliding time is shown in [Figure 5.3](#), which includes the data for all coating materials made at 6 kW operating power level. As per the observations, the maximum frictional force is evidenced for pure red mud coating and decreases with the addition of fly ash, aluminium and carbon, akin to the results observed for the wear rate. An increase in frictional force up to a maximum value of 0.63 N for pure red mud coating at 12 minute sliding time is observed followed by a fluctuating wavy response (studied up to 54 minutes of sliding). [Figure.5.4](#) compares frictional forces for the red mud + 20 % carbon coatings with operating power. The frictional force is found to be maximum at 6 kW and minimum at 12 kW operating power. At 15 kW of operating power, the frictional force was found to be in the range of values for the power levels between 9 to 12 kW. These results are in accordance with the findings observed for wear rates.



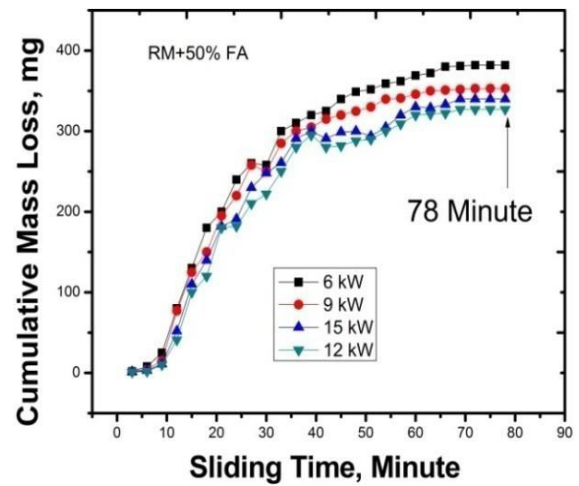
(a)



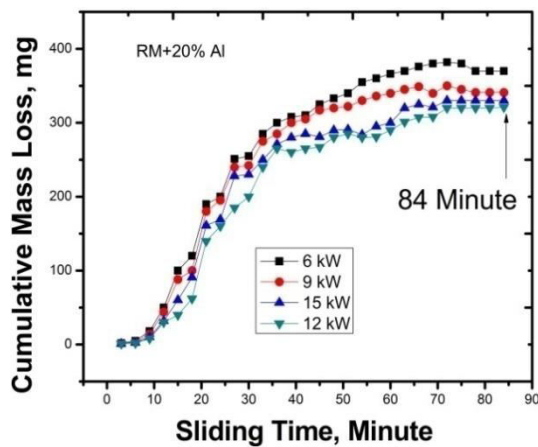
(b)



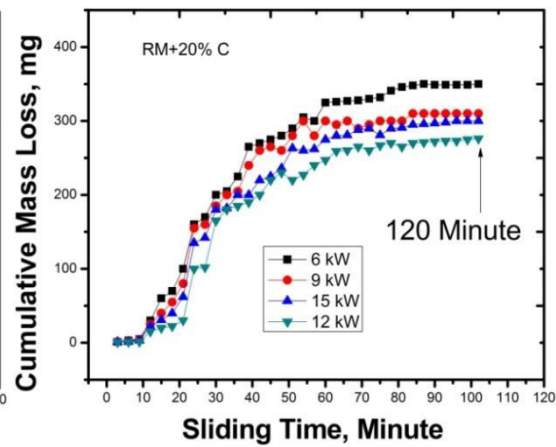
(c)



(d)



(e)



(f)

Figure 5.2 Wear rate comparisons at different operating power level for (a) Red mud, (b) Red mud + 10 % fly ash, (c) red mud + 20 % fly ash, (d) red mud + 50 % fly ash, (e) red mud + 20 % aluminium and (f) red mud + 20 % carbon coatings

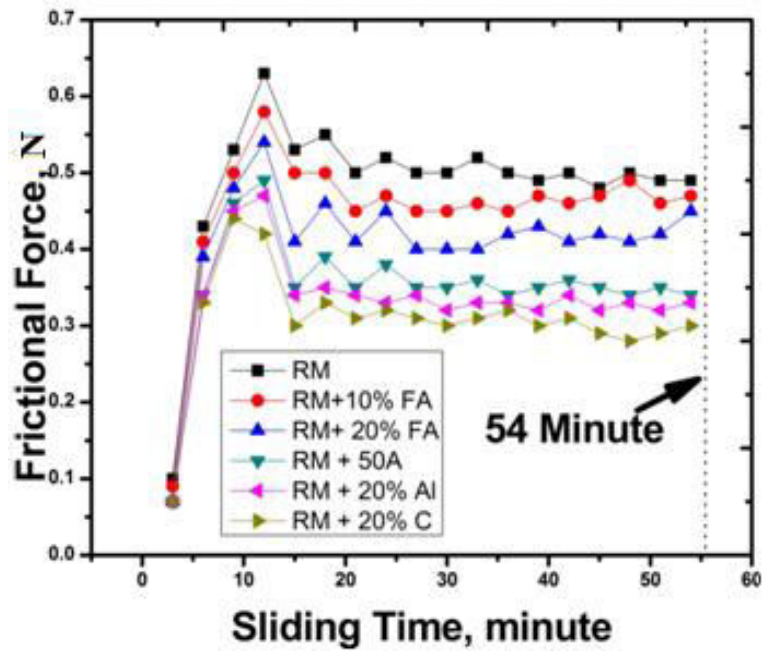


Figure 5.3 Variation of Frictional forces for all coating types up to 54 minute of sliding time made at 6 kW operating power level

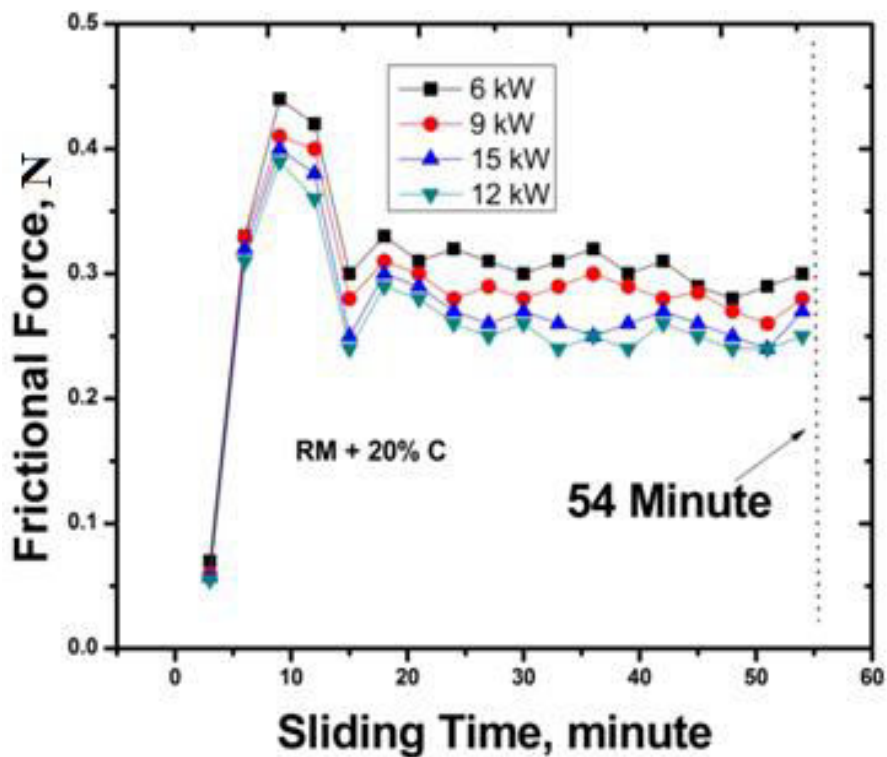


Figure 5.4 Comparisons of Frictional forces with power for red mud + 20 % Carbon coating up to 54 minute sliding time

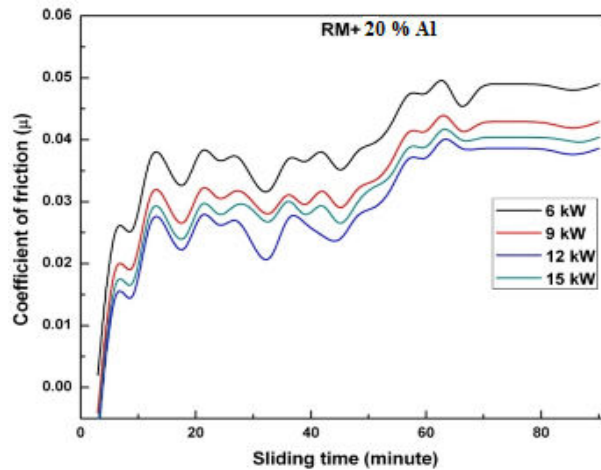


Figure 5.5 Effect of power on coefficient of friction for red mud+20 % Al coatings slid up to break in phase

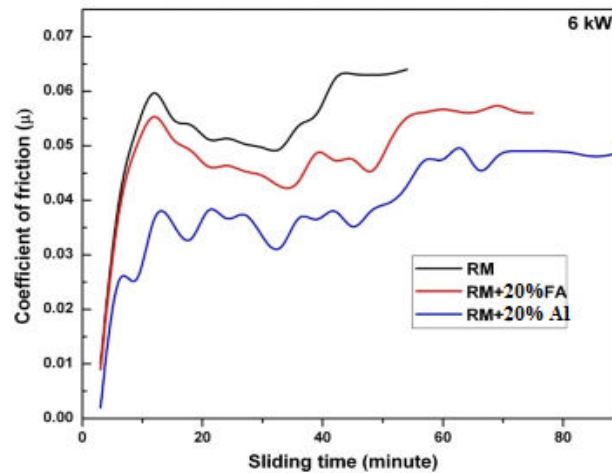


Figure 5.6 Fluctuation of Coefficient of friction of red mud, red mud+20% fly ash and red mud+20% aluminium with time (up to break in phase) made at 6 kW operating power

Figure 5.5 shows the results of the coefficient of friction for RM + 20 % Al coatings made at different operating power levels conducted up to a sliding time of 84 minutes. At incipient the value of μ increases up to 0.38 at sliding time of 15 minute. There after a wavy response is observable up to about 50 minute. Again the value of coefficient of friction increases up to 70 minute and thereafter almost stabilises. This trend is similar for all the operating power levels. For further understanding of the deviation of coefficient of friction with time (up to break in time) for RM, RM+20% FA and RM+20 % Al coatings are revealed in Figure 5.6.

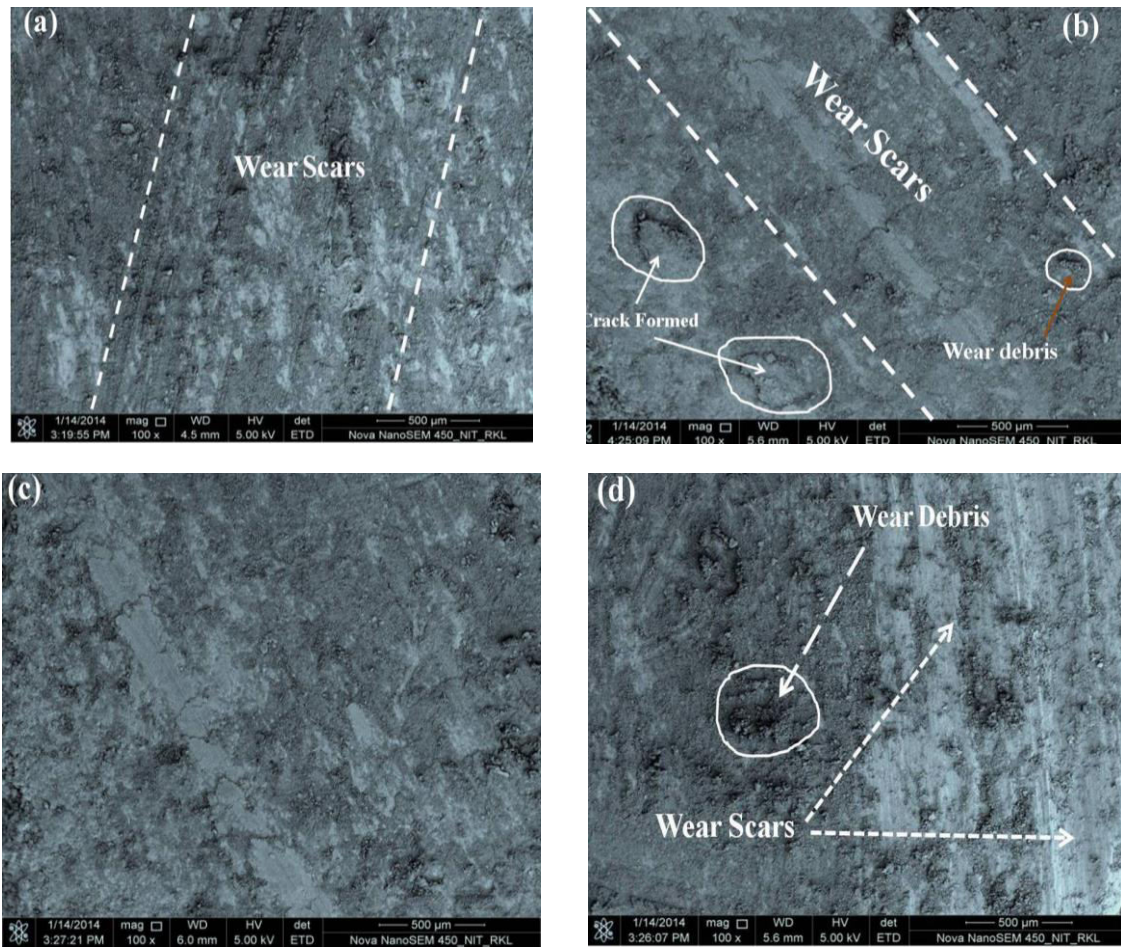
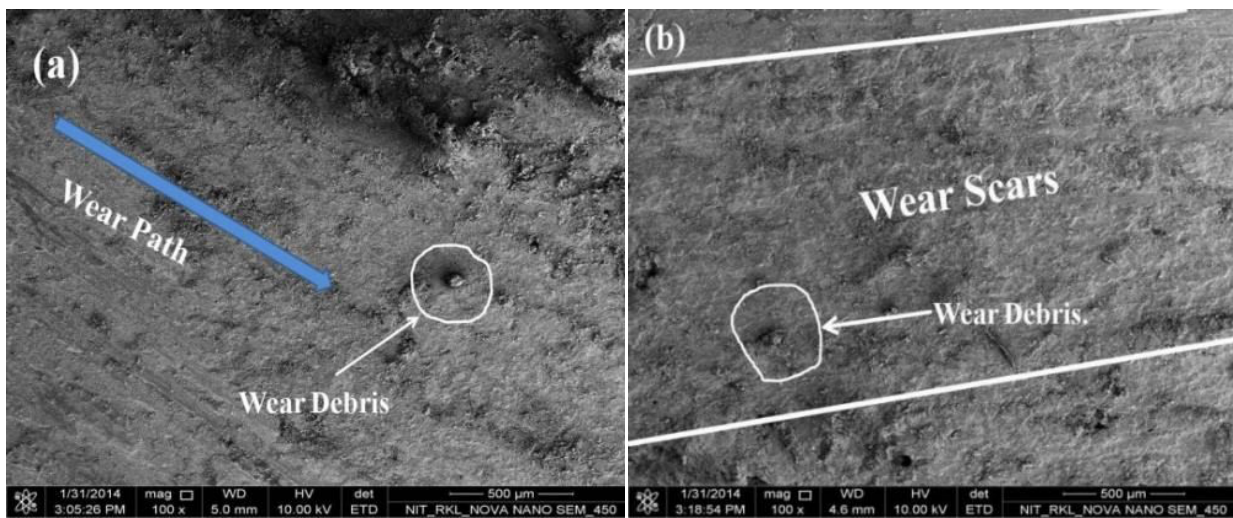


Figure 5.7 Worn surfaces for red mud + 10% fly ash coatings for 6 kW operating power level.; (a) 3, (b) 6, (c) 12 and (d) 15 minutes time interval



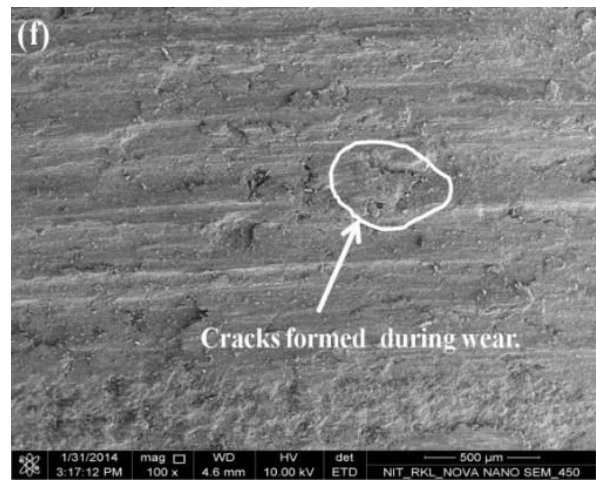
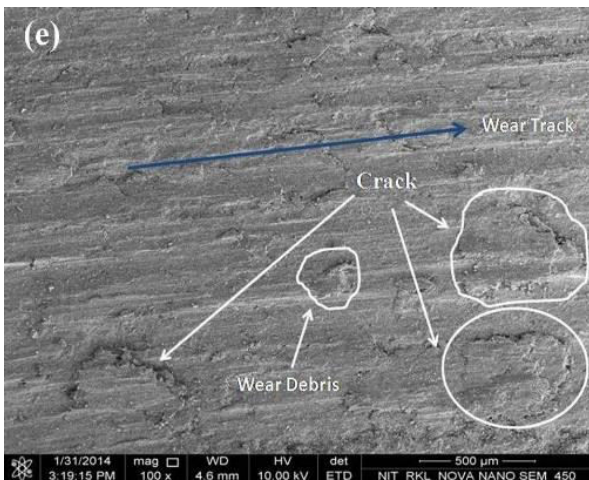
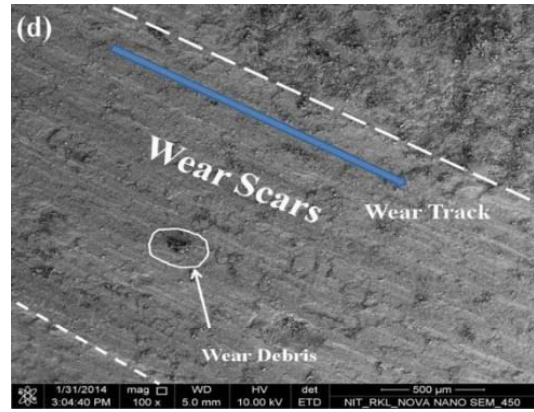
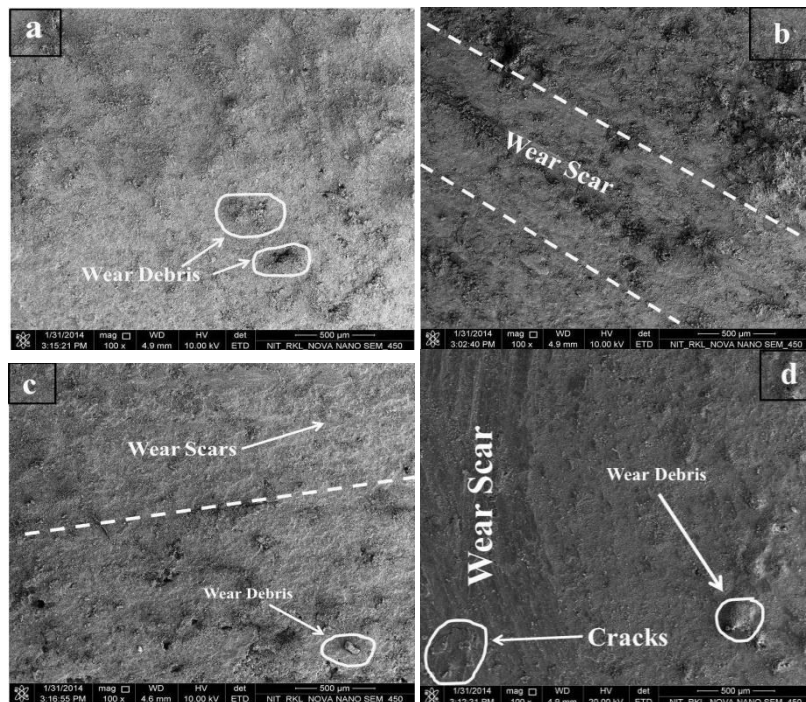


Figure 5.8 Worn surfaces for red mud + 20% Al coatings for 12 kW operating power Level.; (a) 15, (b) 30, (c) 45 ,(d) 60, (e) 75 and (f) 81 minutes time intervals



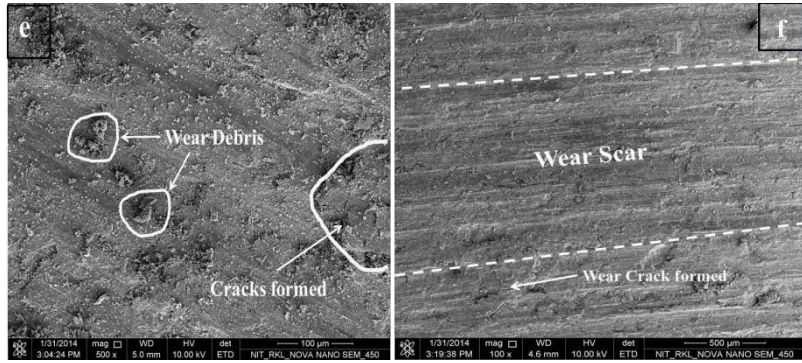


Figure 5.9 Wear images for Red Mud + 20 % Carbon coating for 9 kW operating power level; considering (a) 27, (b) 51, (c) 78, (d) 96, (e) 111 and (f) 117 minutes time interval

At the end of the wear behaviour study, the wear mechanisms are identified by wear morphology. Selected coating samples are highlighted in some images captured by FESEM and SEM. [Figure 5.7](#) represents the wear morphological images for red mud with 10% fly ash coating (prepared at 6 kW operating power) allowed for sliding for the time intervals of 3, 6, 12 and 15 minutes. Owing to continuous sliding of counter surfaces, wear debris formed ([Figure 5.7\(a\)](#)) which interlock within the sliding interfaces, causing pitting and eventually crack formation ([Figure 5.7\(b\)](#)). Wear scars, debris formed and cracked sections are clearly visible in [Figure 5.7\(c\)](#) and [Figure 5.7\(d\)](#) indicating a fatigue failure on the worn surface. [Figure 5.8](#) shows the worn surfaces for 20% Al based red mud coatings (prepared at 12 kW of operating power level) for the sliding intervals 15, 30, 45, 60, 75 and 81 minutes. Worn images for red mud + 20 % carbon coating for 9 kW operating power level; considering 27, 51, 78, 96, 111 and 117 minutes time interval are shown in [Figure 5.9](#).

The wear morphology changes with an increase in the sliding distance impacting change in surface roughness leading to the interruption of its contact mechanism. The change in wear characteristics may be attributed to the variation of the hardness of coating inter-layers with respect to the change in sliding distance. At incipient, a slow

increase in wear rate is observed and then attains a rapid increment and then the stabilisation situation. The further increase in sliding distance cannot change the contact area; causing a relatively steady wear rate. Hence, it can be concluded that the wear takes place by the phenomenon of adhesion and abrasive mechanism due to the development of shear stresses between the hard asperities of the two surfaces in contact. After the “stabilisation” phase, the trend of wear rate remains almost constant for coatings deposited at all power levels. The duration of this stage extends till the end of the test.

5.3 ELEMENTAL, COATING MORPHOLOGY AND THICKNESS ANALYSIS:

In this section the elemental analysis of the selected precursor powder and its coatings are focused. Coating microstructures are analysed for selected coating samples. Sectional microstructures (representing the thickness) are seen and analysis is done considering the effect of operating power. The microstructures and EDS analysis reports are collected by the help of scanning electron microscope (JEOL; JSM-6480 LV) and field emission scanning electron microscope (FESEM, Nova Nano SEM-450). SEM and EDS picture of red mud, fly ash and activated carbon powder is shown in [Figure 5.10](#), [Figure 5.11](#) and [Figure 5.12](#) respectively.

EDS experiment was performed by the above SEM with the required attached module. Data presented in [Table 5.1](#) indicates the weight as well the atomic percentage of elements comprising of pure red mud powder. The EDS analysis of red mud revealed the signature of elements like Fe, Al, Si, O and some other minor constituents. The prominent constituent of red mud was found to be iron with its oxides. Fly ash based coating elements are reviewed and recorded in [Figure 5.13](#) for 12 kW power supply. The elemental analysis is independent of operating power. [Figure 5.13 \(a\)](#) illustrates the elements available in RM + 10 % FA coating. Augmentation of FA to RM makes the coating more Si and Al enriched, corresponding to [Figure 5.13\(b\)](#).

Table 5.1 Elemental analysis of red mud

Element	Weight%	Atomic%
C K	27.59	33.29
O K	31.65	24.54
Al K	4.41	4.47
Si K	4.21	7.07
Fe K	32.14	30.62
Totals	100.00	

The EDS analysis of red mud with 20% fly ash coatings prepared at 9 kW of operating power is shown in Figure 5.14. Also, the analogous elements in % relating to Figure 5.14 are reported in Table 5.2, indicating the increase in silica and aluminium constituents in the composite coating. EDS record of RM + 20 % Al composite coating made at 6 kW operating power is pictured in Figure 5.15 and its elemental analysis is reported in Table 5.3.

Table 5.2 Elemental analysis of RM + 20% FA composite coated at 9 kW

Element	Weight %	Atomic %
Fe K	26.13	25.90
O K	21.74	42.61
Ti K	14.02	9.18
Si K	17.10	7.93
Al K	16.59	7.66
Cr K	2.14	1.29
C K	1.99	5.20
Ca K	0.29	0.22
Au K	0.00	0.00
Mg K	0.00	0.00
Totals	100 %	100

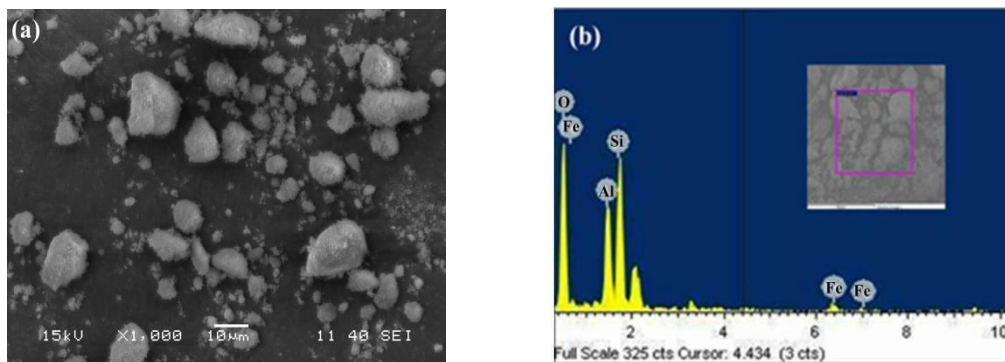
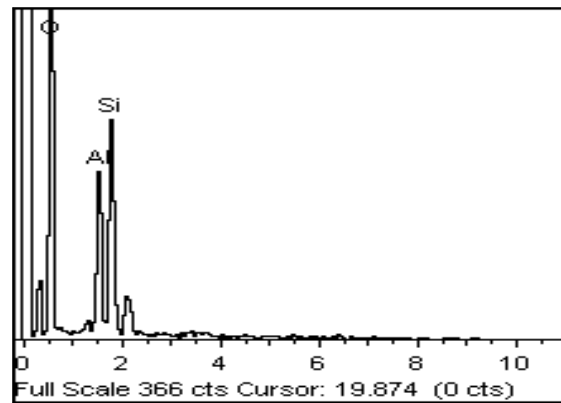
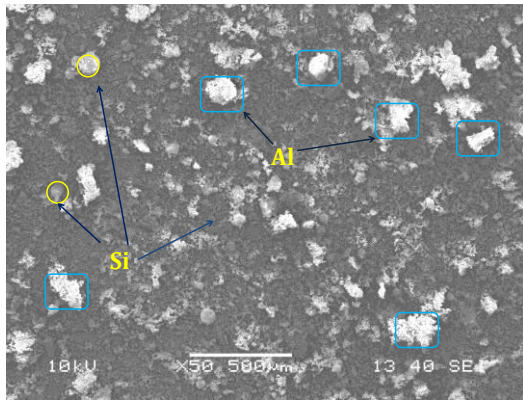


Figure 5.10 (a) SEM and (b) EDS analysis of red mud



(a)

(b)

Figure 5.11 (a) SEM and (b) EDS analysis of fly ash

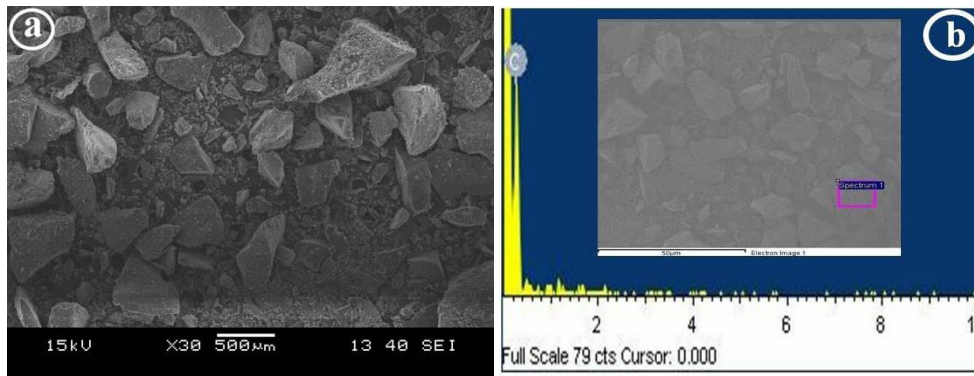
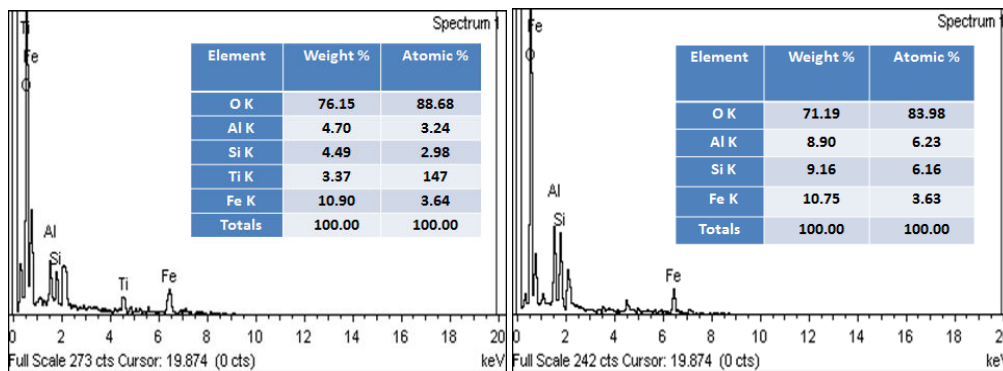


Figure 5.12 (a) SEM and (b) EDS analysis of activated Carbon



(a)

(b)

Figure 5.13. EDS records for (a) RM + 10% FA and (b) RM + 50% FA coatings made at 12 kW

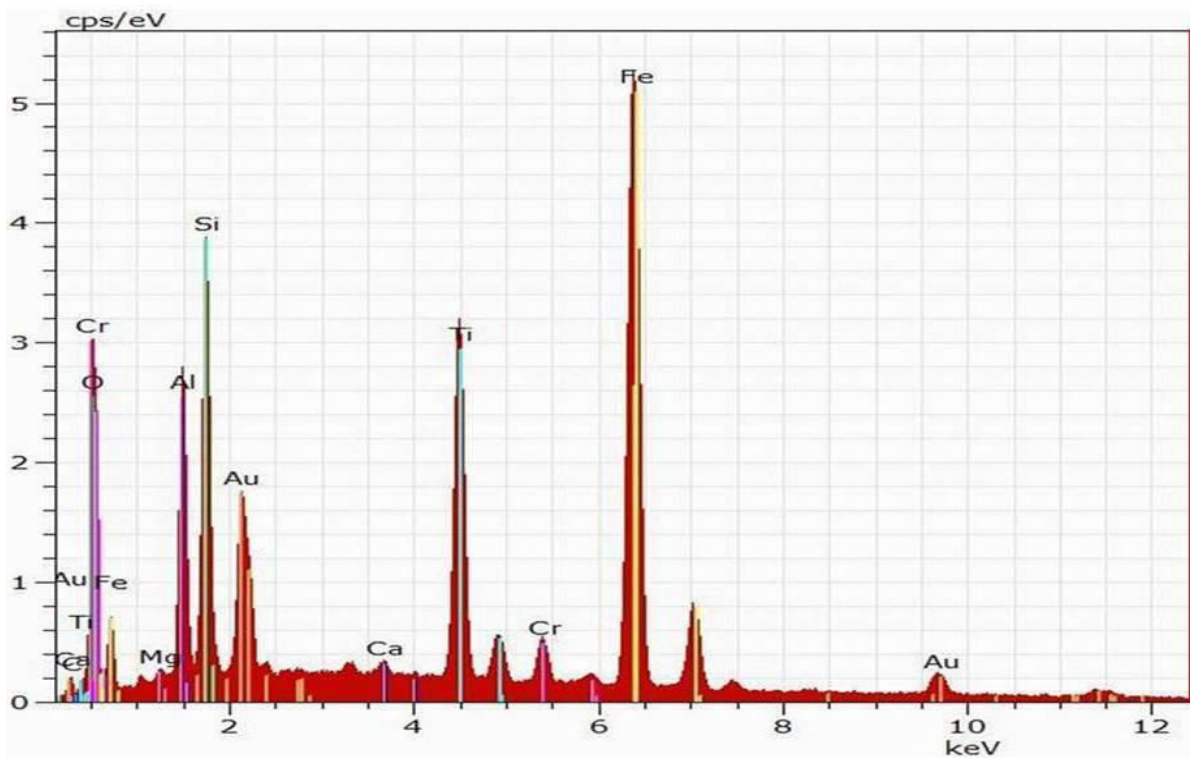


Figure 5.14 EDS analysis of RM+20% FA composite coating at 9 kW

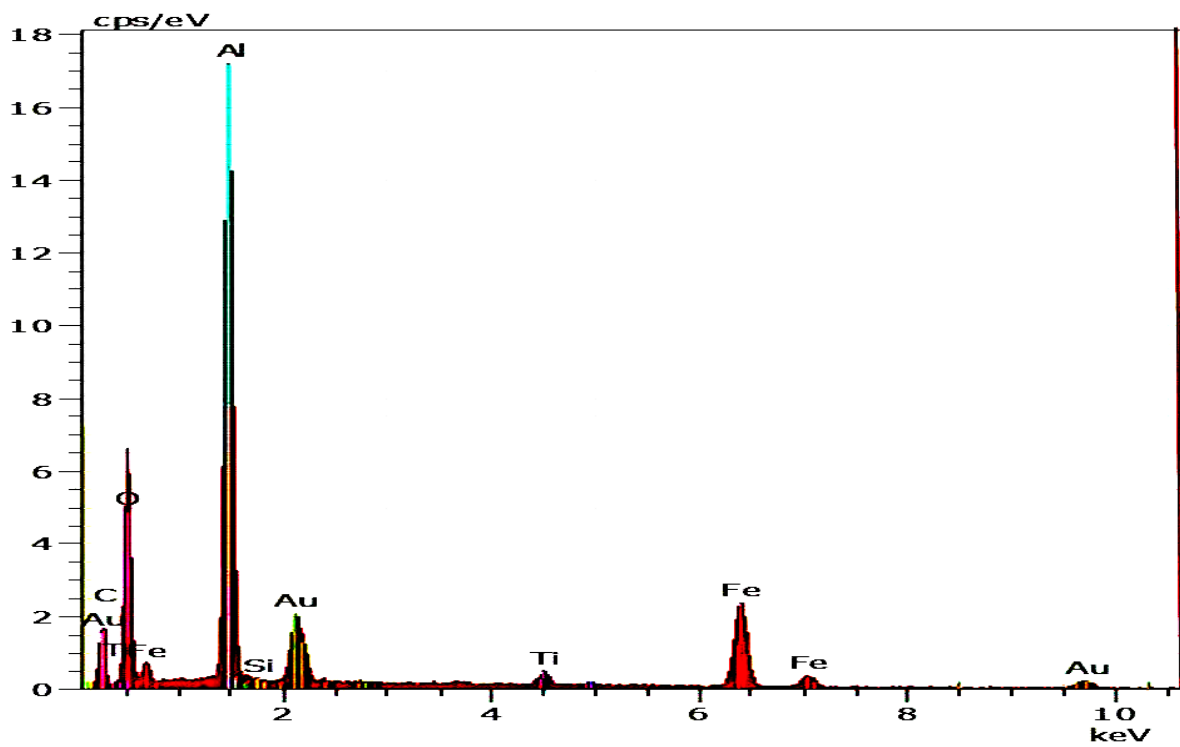


Figure 5.15 EDS record of RM+ 20 % Al Composite coating at 6 kW

Table 5.3.Elemental analysis of RM+20 % Al Composite coated at 6 kW

Element	Weight %	Atomic %
Fe K	39.13	26.89
O K	22.74	41.61
Ti K	9.00	9.18
Si K	14.10	7.93
Al K	11.61	5.46
Cr K	1.14	2.39
C K	1.99	5.20
Ca K	0.29	0.22
Au K	0.00	0.00
Mg K	0.00	0.00
Totals	100 %	100

Coating surface characteristics are controlled by inter particle bonding of powder materials during plasma melting. Adhesion strength of the coating layers to the metal substrate dominates the surface behaviour. The existing research focuses, how the plasma torch input power decides the coating floors. Is there any changes arise to coating layers, after fly ash augmentation? Electron microscopy images are exercised to reveal it. [Figure 5.16](#) reports the surface modifications for; (a) red mud, (b) red mud + 10 % FA, (c) red mud + 20 % FA and (d) red mud + 50 % FA at magnification $\times 30$ for 12 kW input. Particles are broadly distributed for pure red mud and seem to be even throughout.

The reinforcement of fly ash to red mud results in more agglomeration of particles leading to a lumpy, non-uniform and a coarser exterior. The coating morphology is extensively affected by plasma torch input power. As the power level increases the structural pattern changes.[Figure 5.17](#) and [Figure 5.18](#) reveal the outcomes. It is believed that the plasma flame temperature increases with input power, dominating the mechanism of coating. Rise of flame temperature, plays a significant role on surface chemistry of prevailing coatings. At 6 and 9 kW operating power, large spherical particles are seen, might be due to improper melting of coating precursor.

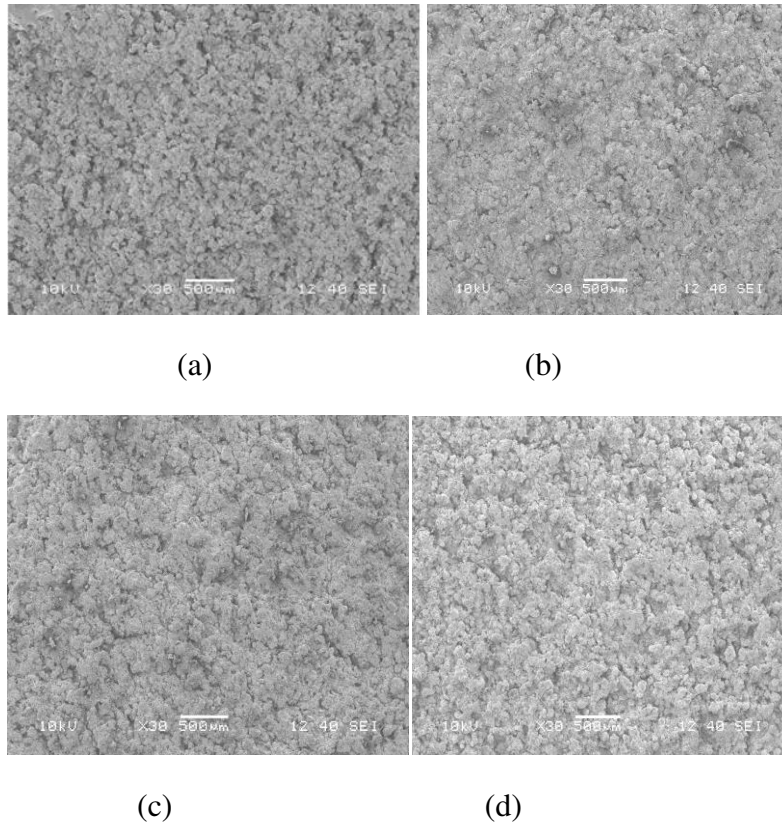


Figure 5.16 Surface responses for (a) red mud, (b) RM + 10 % FA, (c) RM + 20 % FA and (d) RM + 50 % FA coated at 12 kW operating power

Surface seems to be rougher with spotted cavities. As the input power increases, the surface topology modifies to a flatter, homogeneous film with less spotted cavities and pores. [Figure 5.17](#) shows surfaces of RM + 20 % FA coatings with different operating power. [Figure 5.19](#) and [Figure 5.20](#) reveal the morphology of RM + 20% Al and RM + 20% C coatings respectively. At 6 kW, most of the coated inter sections are porous. Air voids has occupied from metal-coating interface to the tip. Increase of plasma operating power (alternatively plasma temperature) promotes a better metallurgical union and agglomeration between the melted particles. So at higher temperature, it is believed that, molten particles get adhered to the substrate at sufficient strength. Minimum air voids are noticed with a smooth structure. This might be due to the proper particle to particle bonding and improved stacking rate to the substrate, which have been resulted in increased interfacial bond strength and more dense film at boundary. The coating morphology for red mud with 20 % aluminium is visible in [Figure 5.19](#). In this case the operating power has no significant effect on structural properties. For all operating power level small globular grains are seen and fused

together to form a splat area. Very few cavities are seen, might be originated at inter particle boundary regions. Addition of aluminium to red mud might have helped in joining of molten particles during in flight traverse as aluminium remains in molten state for longer time after leaving plasma jet.

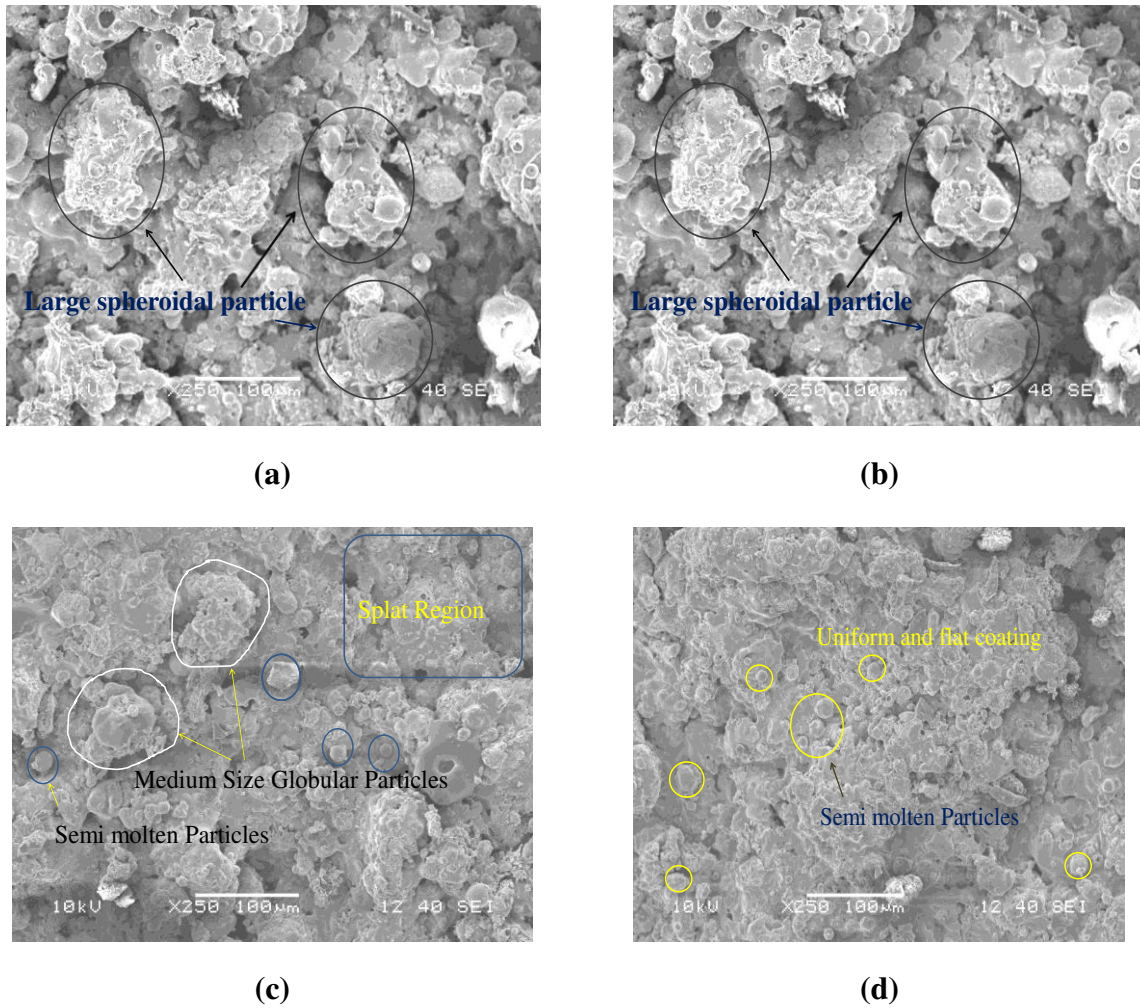
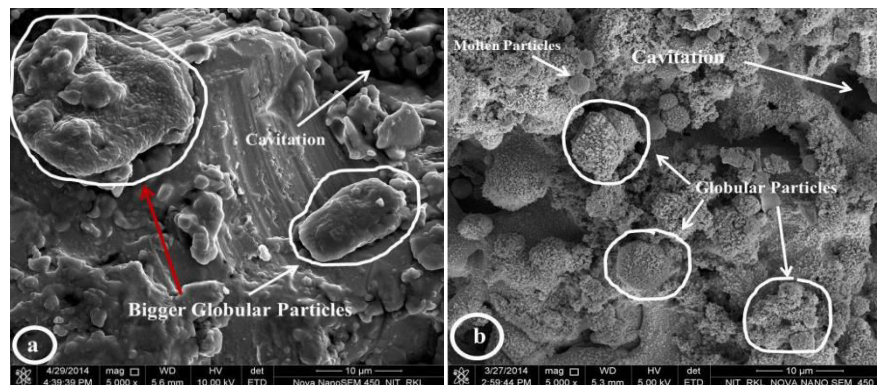


Figure 5.17 Morphology of RM + 20 % FA coatings made at (a) 6 kW, (b) 9 kW, (c) 12 kW and (d) 15 kW



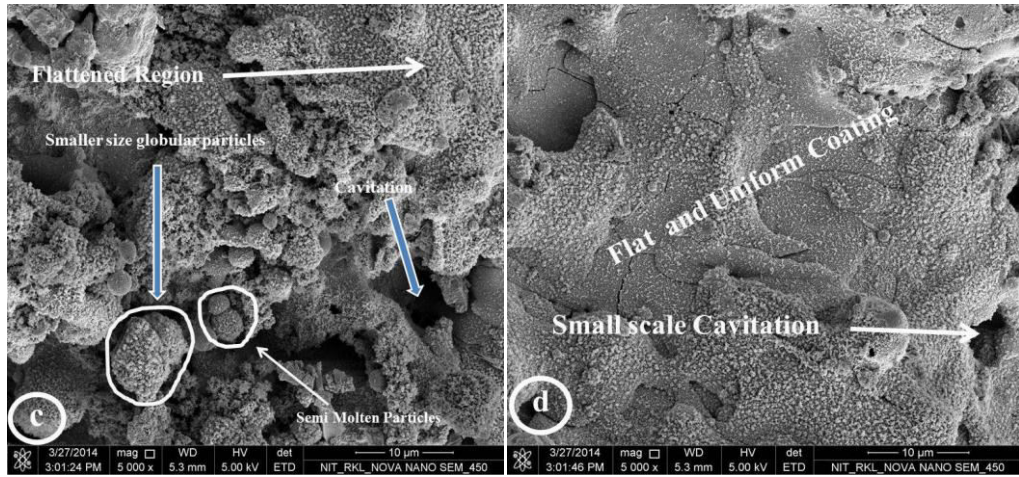


Figure 5.18 Coating Morphology for RM + 10 % FA; (a) 6 kW, (b) 9 kW, (c) 12 kW (d) 15 kW

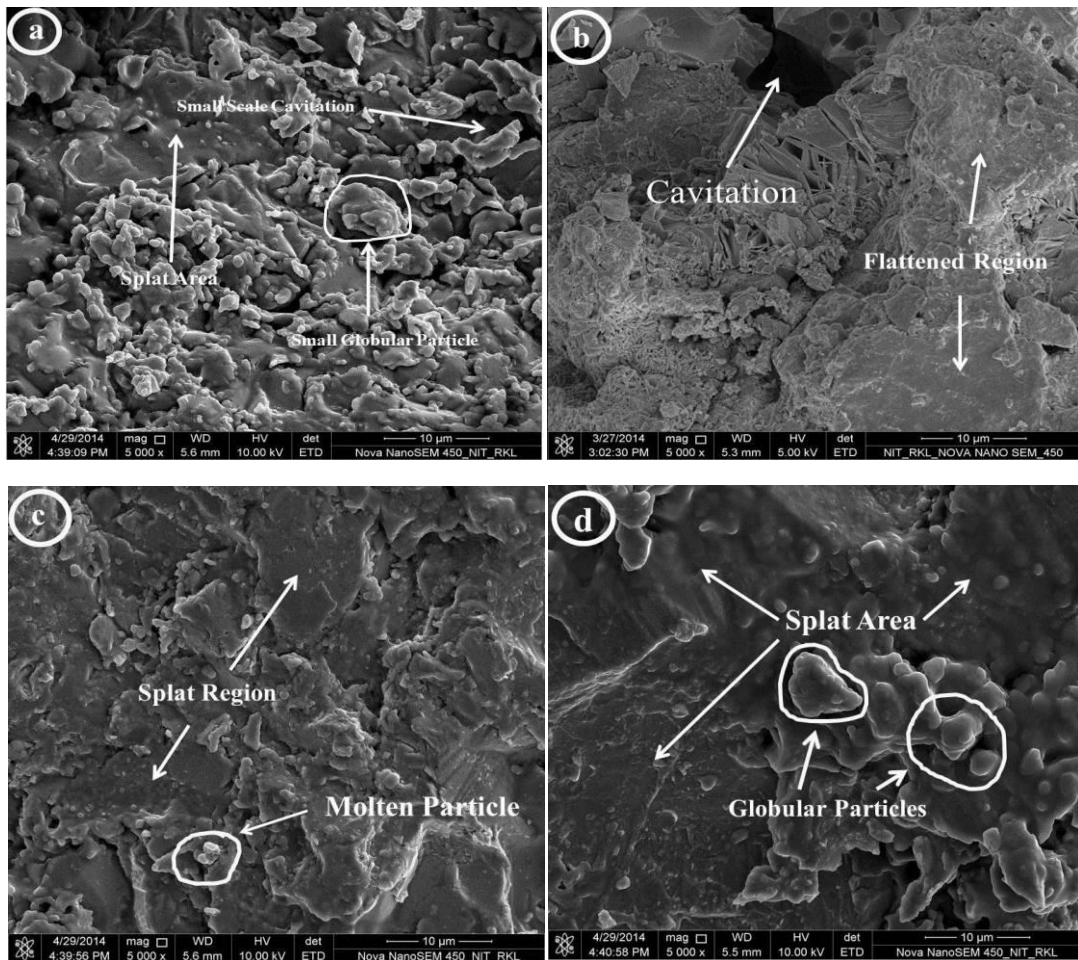


Figure 5.19 Coating Morphology for RM + 20 % Al; (a) 6 kW, (b) 9 kW, (c) 12 kW (d) 15 kW

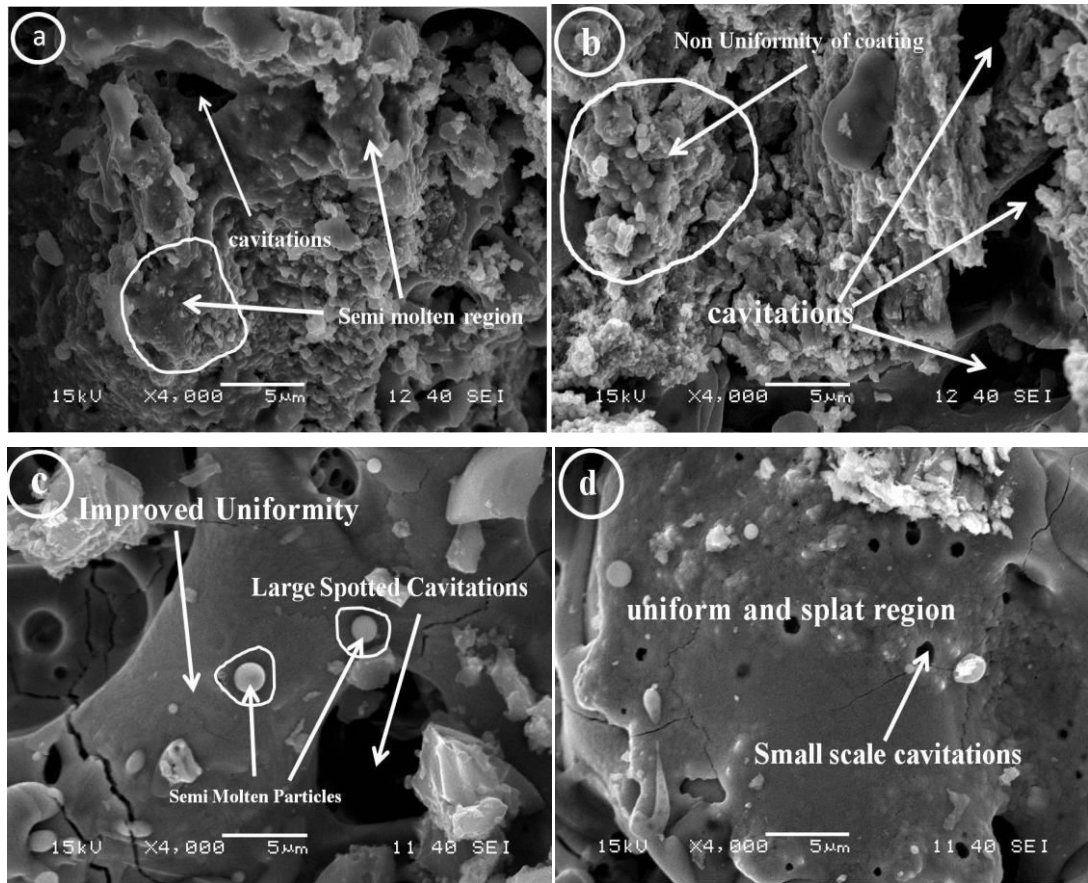
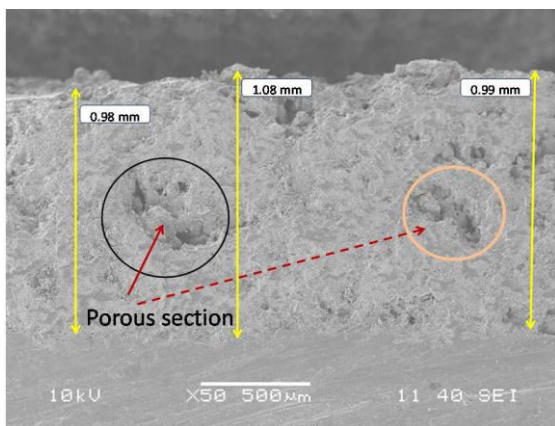
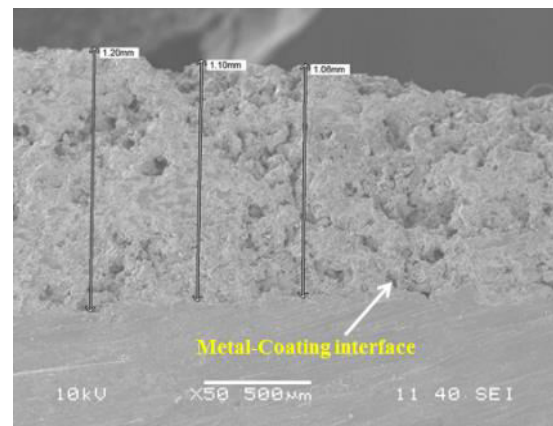


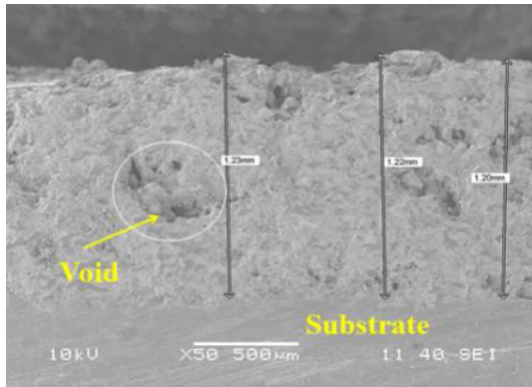
Figure 5.20 Morphology of RM + 20% C coatings made at (a) 6 kW, (b) 9 kW, (c) 12 kW and (d) 15 kW



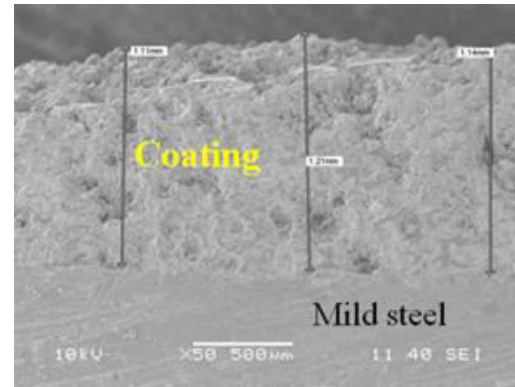
(a)



(b)



(c)



(d)

Figure 5.21 Section Microstructure of RM + 20 % FA Coatings at (a) 6 kW, (b) 9 kW, (c) 12 kW and (d) 15 kW

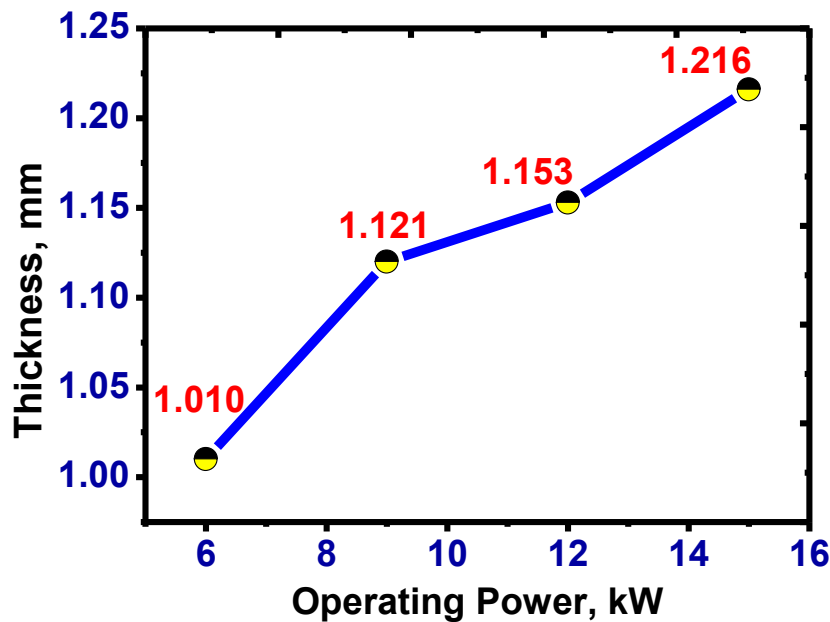


Figure 5.22 Action of operating power on thickness

In this section the analysis of coating thickness is focused considering red mud + 20% fly ash composite. SEM images are captured at magnification $\times 50$ to understand the effect of power on coating thickness. Sectional images are shown in Figure 5.21. Observations on thickness indicate a marginal change with power. The mean coating thickness is increased with operating power. Figure 5.22 manifests that, improvement of the coating thickness is relatively narrow with operating power. The average thickness for 6 kW is 1.01 mm and rises up to 1.216 mm for 15 kW. Three readings were taken on and the values are averaged. With increase in power level thermal flux

increases, this increases the enthalpy of the system. When feed material passes through plasma most of the precursor powder particles get melted and also some disintegrated which flies off. The molten particles which are at much higher temperature when strikes the substrate get saturated and deposition volume increases thereby causing the rise in coating thickness with power.

5.4 XRD PHASE COMPOSITION ANALYSIS:

To ascertain the phases present and phase changes taken place during plasma spraying, the X-ray diffractograms were captured for composite precursor powder and its coatings using a Philips X-ray diffractometer. Compositions of coatings are investigated with respect to operating power. The XRD result for red mud powder and activated carbon are shown in [Figure 5.23](#) and [Figure 5.24](#). The major phases of red mud powder such as Silicon dioxide (SiO_2), Calcium Aluminoferrite ($\text{Ca}_2\text{Fe}_{1.28}\text{Al}_{0.75}\text{O}_5$), Hematite (Fe_2O_3), Titanium dioxide (TiO_2) and Aluminide (AlFe_3) were noticed.

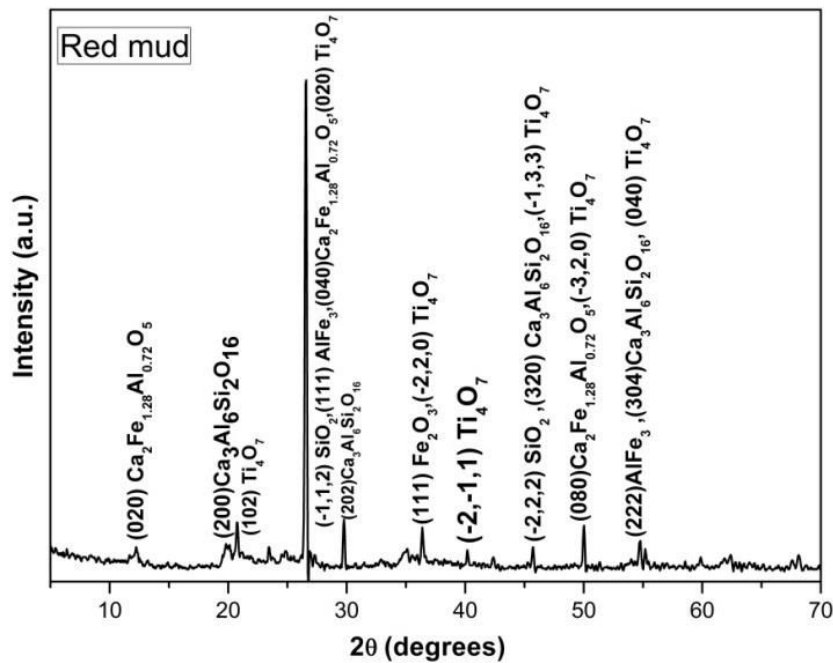


Figure 5.23 XRD of Red Mud Powder collected from NALCO

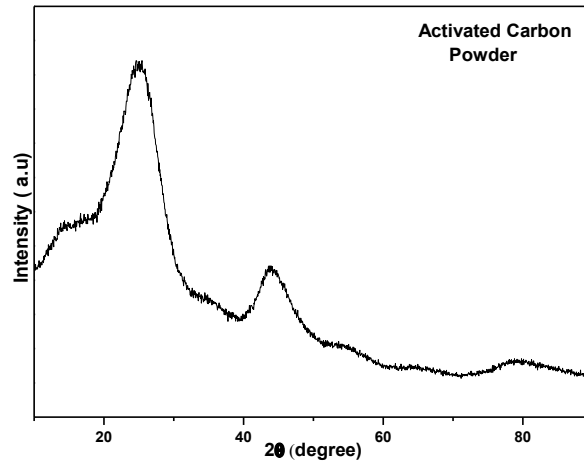
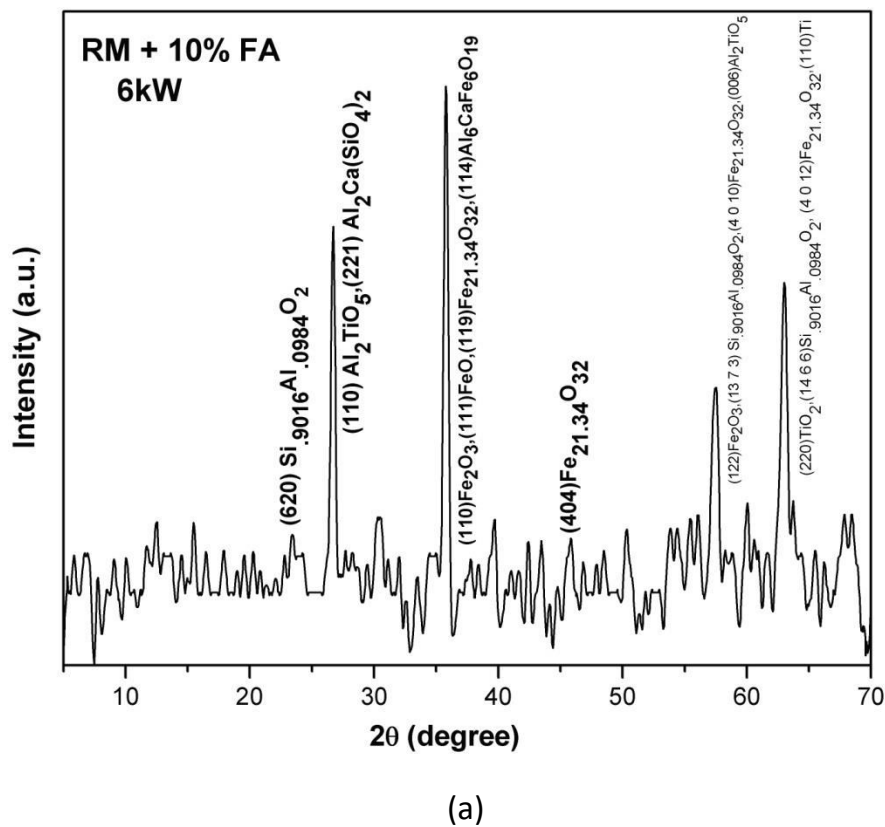
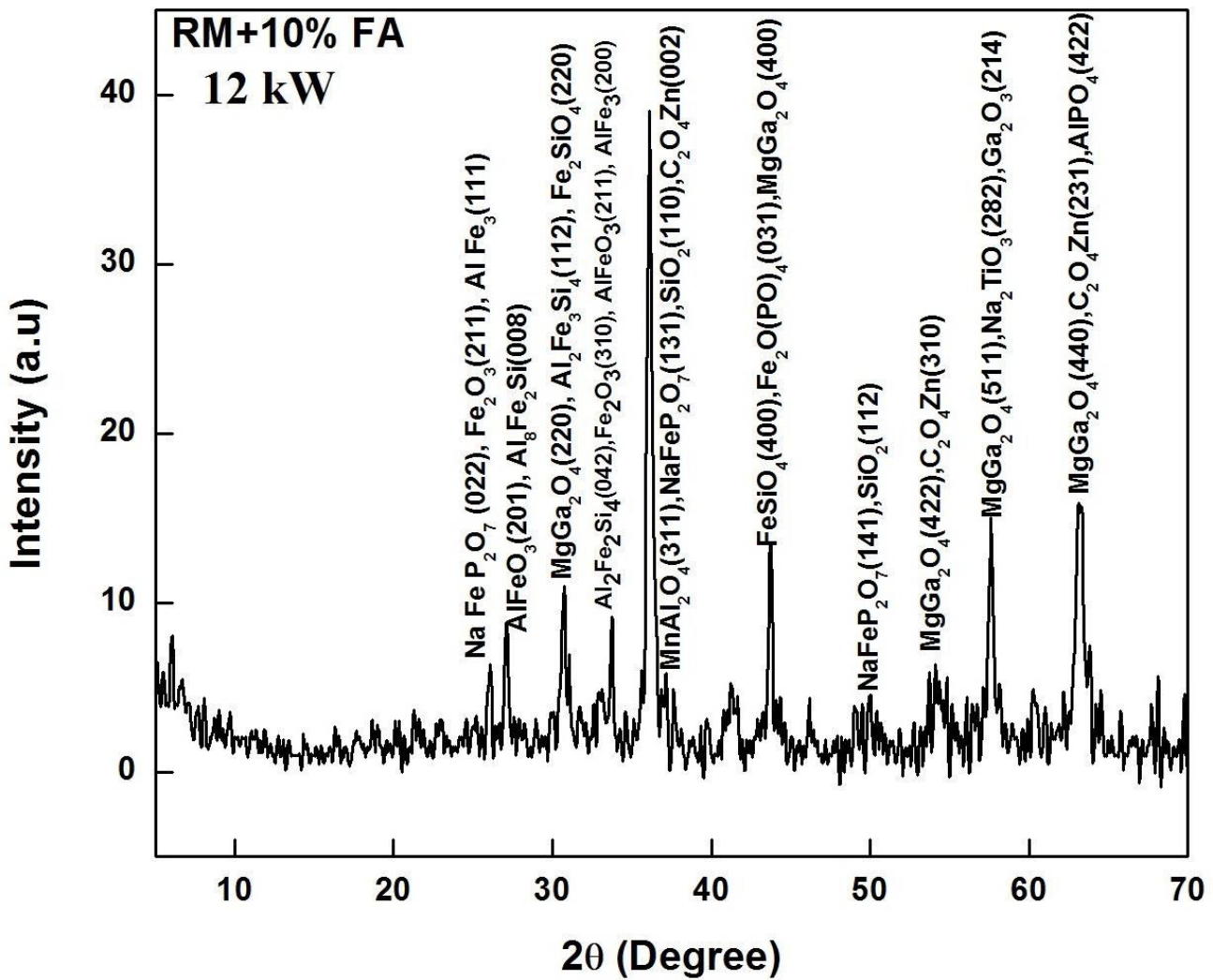


Figure 5.24 XRD of activated carbon

For red mud with 10 % fly ash coatings at 6 and 12 kW operating power level the XRD patterns are shown in Figure 5.25. For 6 kW power level (Figure 5.25.a) the major phases are silicon aluminium oxides ($\text{Si}_{0.9016}\text{Al}_{0.0984}\text{O}_2$), whereas for 12 kW power level (Figure 5.25.b) the major phase is changed to pyrophosphate (NaFeP_2O_7).

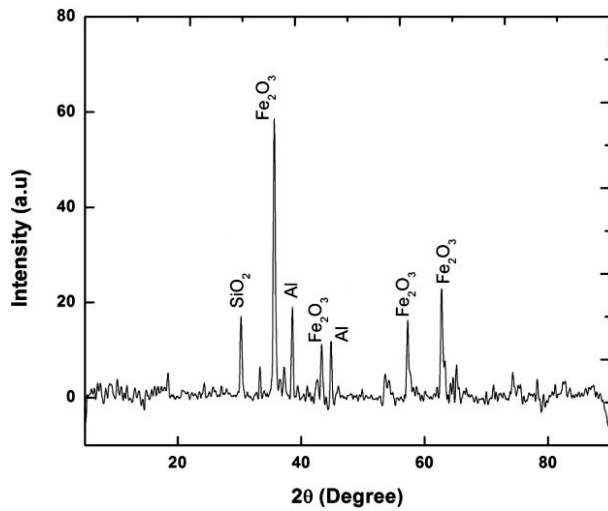




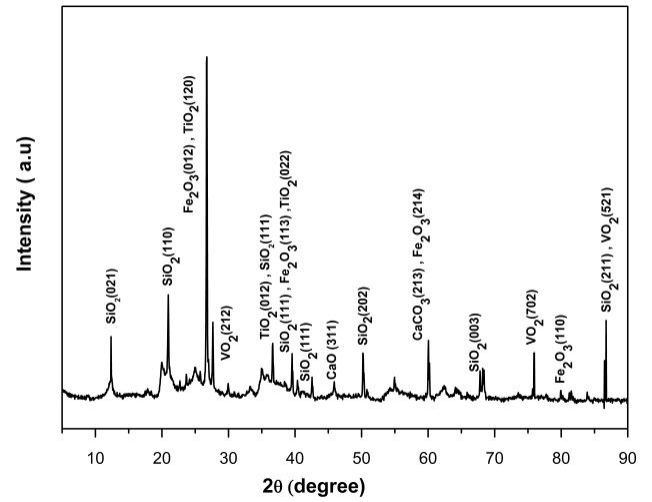
(b)

Figure 5.25 XRD of RM + 10 % FA Coatings; (a) 6 kW, (b) 12 kW

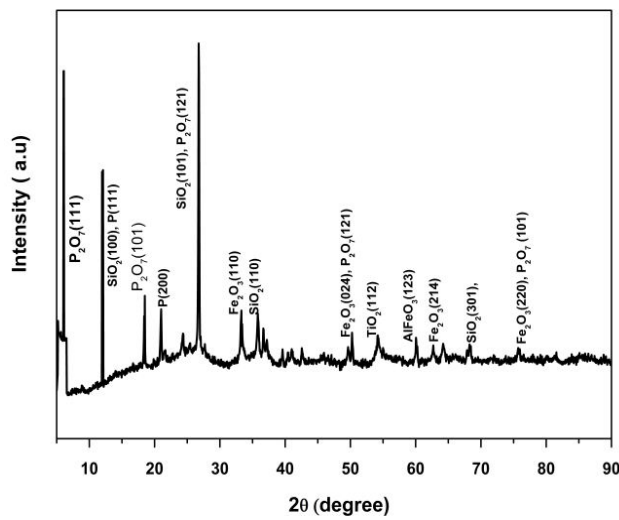
Figure 5.26 reports the XRD of RM + 50 % FA coatings. It is observed that the major phases are iron oxide (Fe_2O_3), Silicon dioxide (SiO_2) and minor phase like Titanium dioxides (TiO_2) are visible for 6 and 9 kW power level. But as the spraying power alters to 12 kW, the anatomy of coatings is rephrased. The major phases are reconstructed to Pyrophosphate (P_2O_7). At the other end, for 15 kW, more numbers of shortened peaks are observed. Majority of peaks confirms Calcite (CaCO_3) compound. XRD patterns differentiated for red mud with 20 % aluminium coating is shown in Figure 5.27.



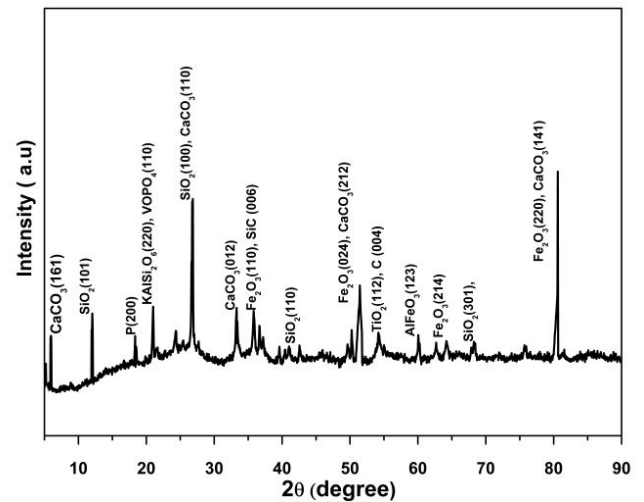
(a)



(b)



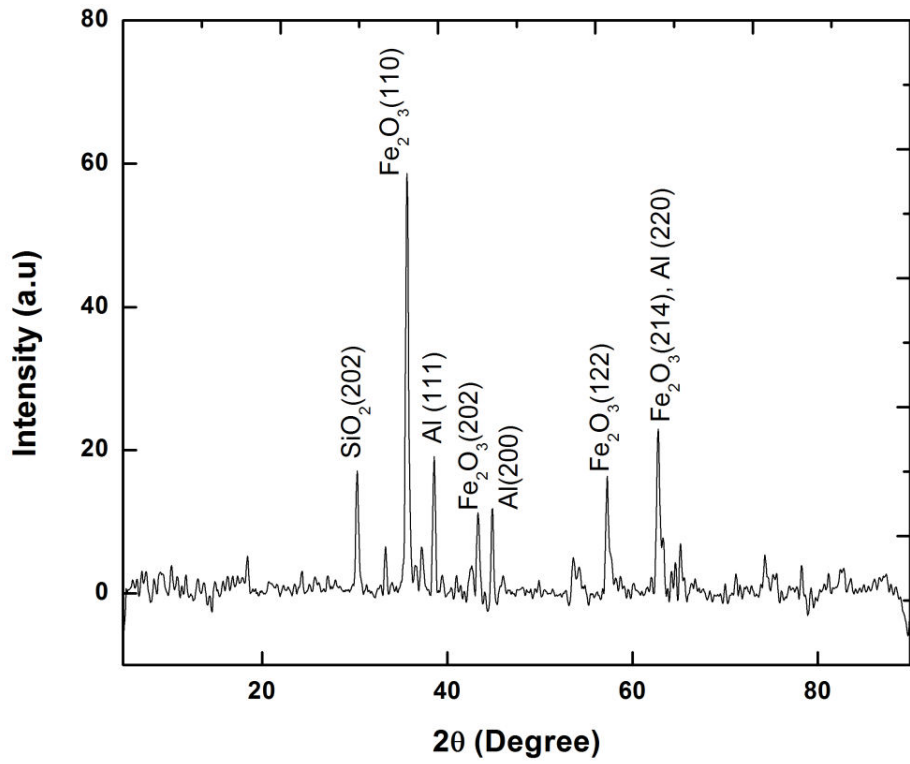
(c)



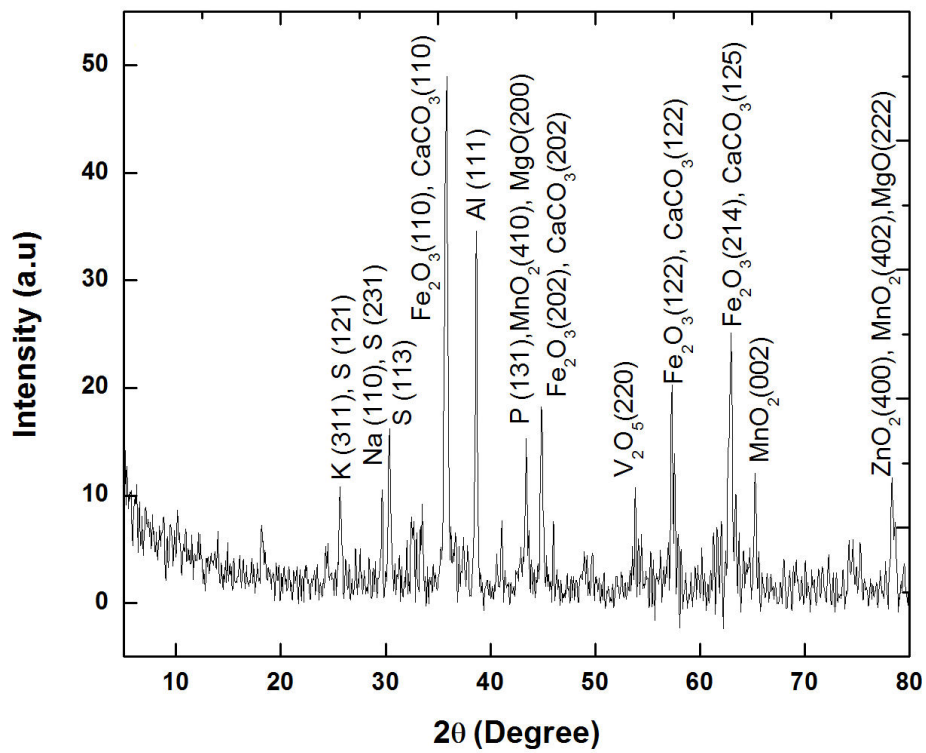
(d)

Figure 5.26. X-Ray diffractogram of RM + 50 % FA Coatings at (a) 6 kW, (b) 9 kW, (c) 12 kW and (d) 15 kW operating power levels

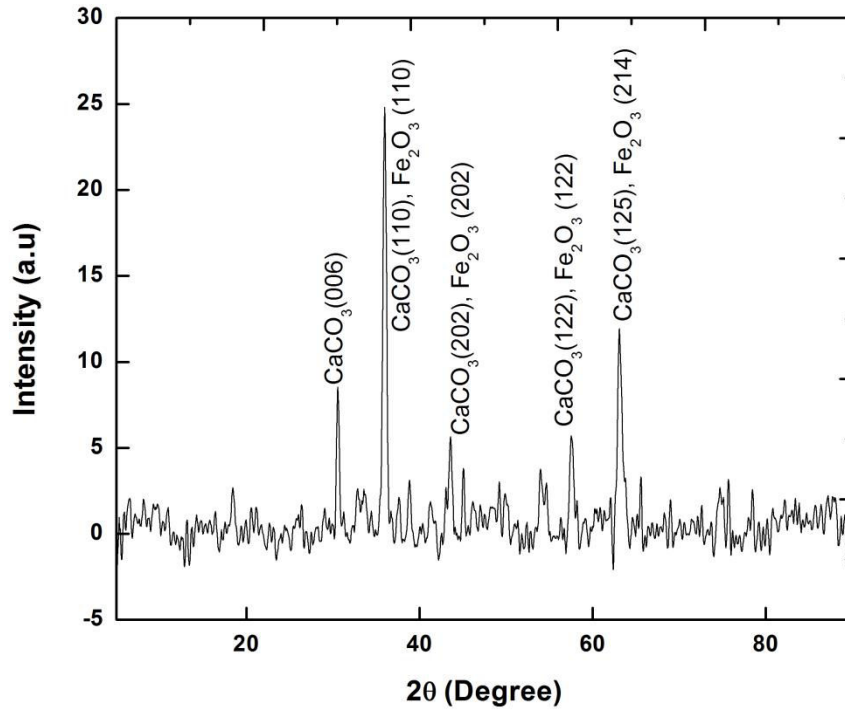
At 6 kW operating power level (Figure 5.27.(a)) the major phases are silicon dioxide (SiO_2), hematite and aluminium are observed, whereas for 9 kW (Figure 5.27.(b)) the major phases changed to calcium carbonate (CaCO_3), magnesium oxides (MgO), manganese oxides (MnO_2). Again for 12 kW power level (Figure 5.27. (c)) the major phases found are Calcium Carbonate and Hematite. Significant changes in phases are perceived for 15 kW operating power level. Most of the elements have formed oxides like aluminium iron oxides (AlFeO_3) and other elemental oxides as perceptible in Figure 5.27(d).



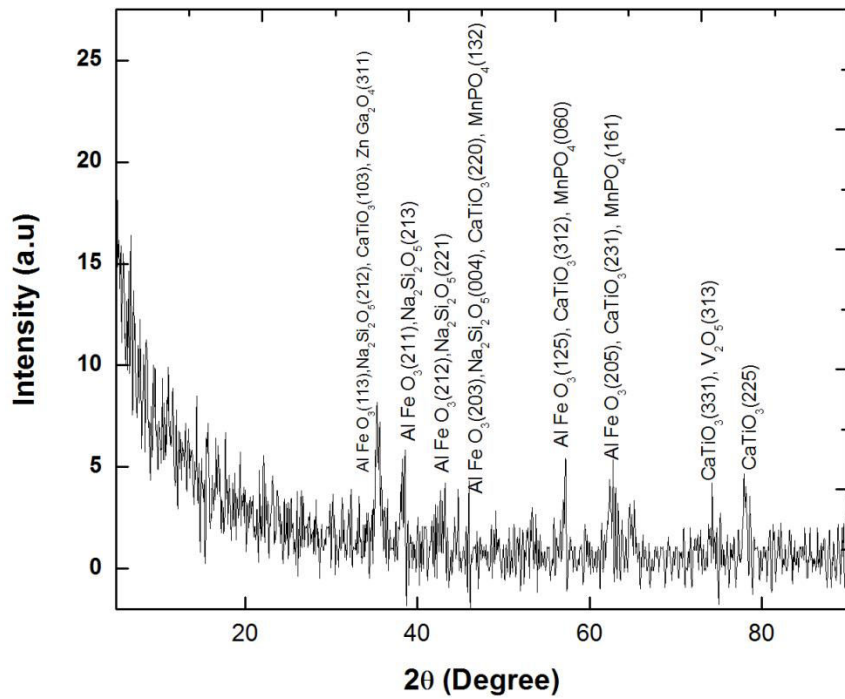
(a)



(b)

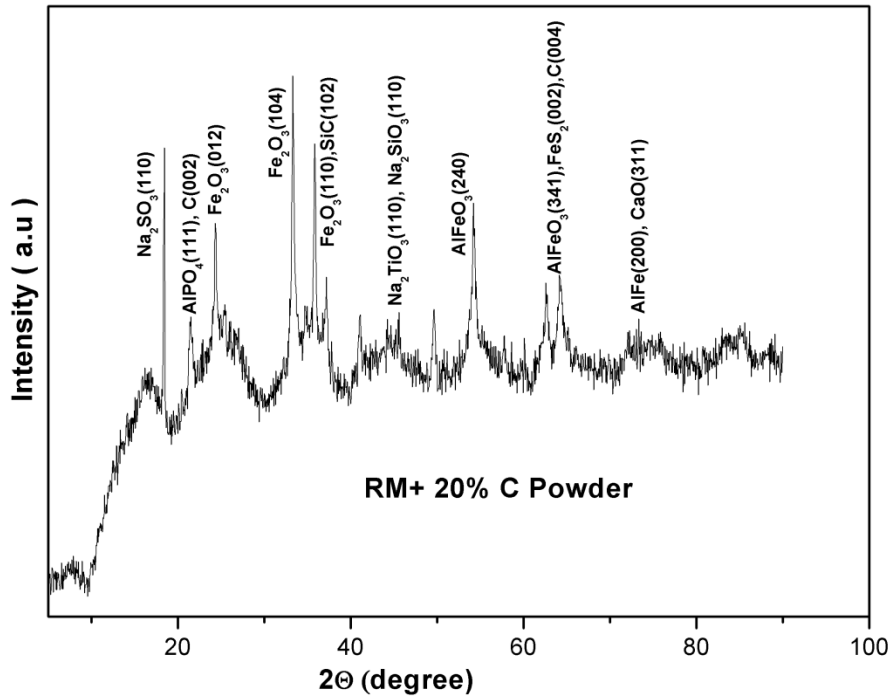


(c)

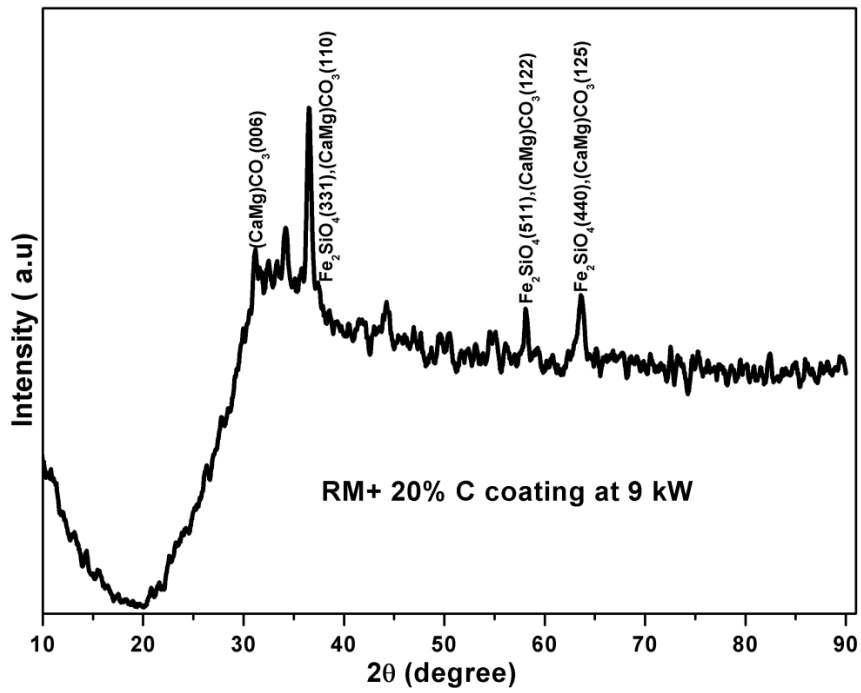


(d)

Figure 5.27 XRD of Red Mud + 20 % Al Coatings, (a) 6 kW, (b) 9 kW, (c) 12 kW, (d) 15 kW

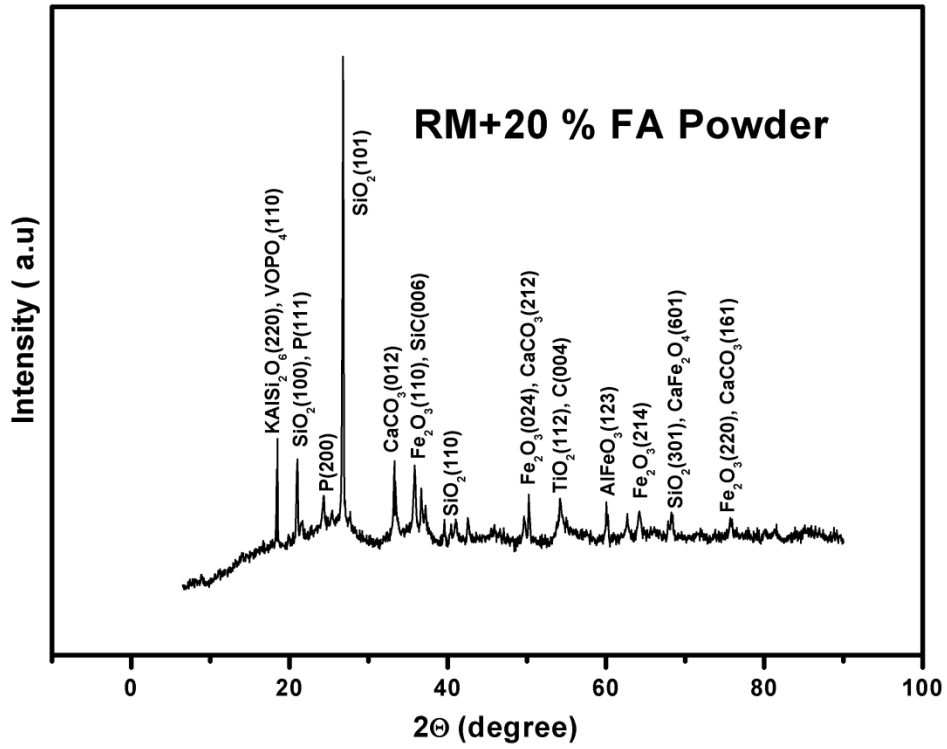


(a)

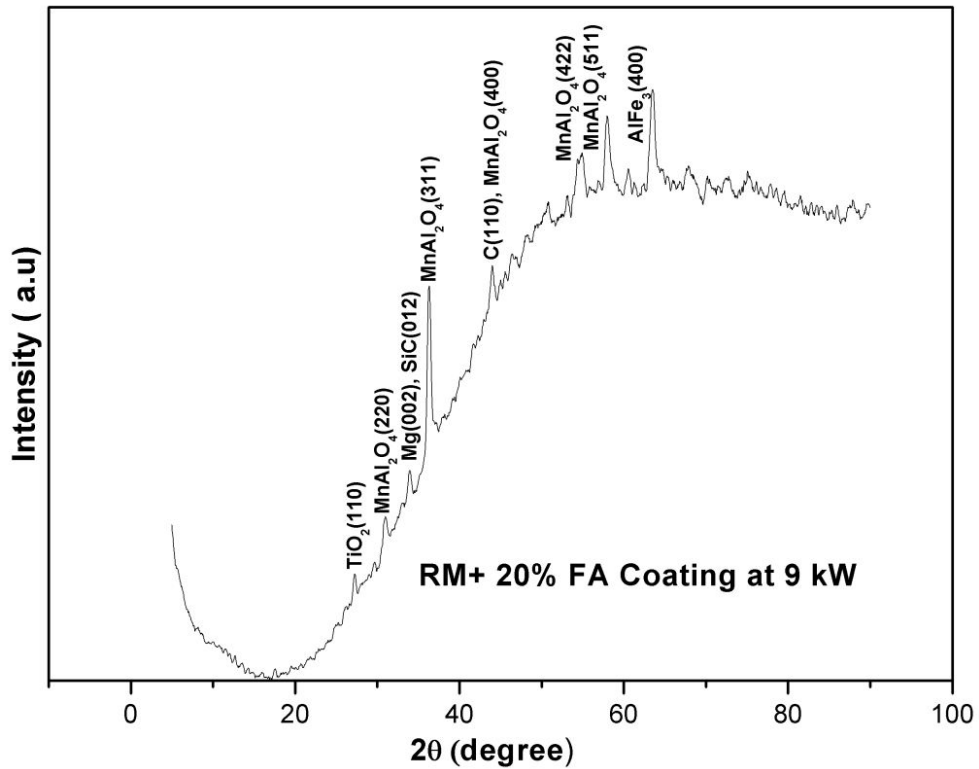


(b)

Figure 5.28 XRD of (a) RM + 20% C Powder, (b) RM + 20% C Coating at 9 kW



(a)



(b)

Figure 5.29 XRD of (a) RM + 20% FA Powder, (b) RM + 20% FA Coating at 9 kW

The XRD of RM + 20% C powder primarily contains Phases of sodium sulfite (Na_2SO_3), iron oxide (Fe_2O_3) and aluminium iron oxide (AlFeO_3). After plasma coating at 9 kW there is a major phase change to fayalite (Fe_2SiO_4) and dolomite as visible in [Figure 5.28](#). [Figure 5.29](#) shows the XRD diffractogram of (a) RM + 20% FA powder, (b) RM + 20% FA coating made at 9 kW. The chief XRD peaks for the powder are silicon dioxide (SiO_2), hematite (Fe_2O_3), limestone (CaCO_3) and titanium dioxide (TiO_2). After successful plasma coating the major phases reconstructed to manganese aluminate (MnAl_2O_4).

5.5 COATING HARDNESS

Study of coating microhardness has been conducted using a Leitz Micro-Harness tester at 40 Pa with 25 seconds indentation time. Polished sections are observed in the microscope to observe the three distinctly different regions/ phases namely dull, white and spotted/mixed. Micro-hardness measurement was done on these optically distinguishable phases. The experimental results are manifested in [Table 5.4](#). Three distinguishable structures are observed by the microscope for all coatings. The micro harness results are reported in HV. The results show the harness value is minimum (489 HV) for pure red mud coatings. The reinforcement of fly ash to red mud increases the hardness value as observable in [Table 5.4](#). Hardness is maximum for red mud + 20 % aluminium composite coatings. A highest value of 791HV is obtained for it. The results are attributing to the fact that, alumina (Al_2O_3) and inter oxide compounds are formed during the plasma spraying of red mud-aluminium particles. The hardness values for red mud-carbon coatings are moderate and fall between the values for red mud- fly ash and red mud-aluminium coatings. The primary reason for improvement in hardness in case of red mud + fly ash and red mud + aluminium mixtures are due to the increase in alumina and silicon dioxide content in the feedstock and its coatings. The secondary cause might be due to the formation of alumino-silicate (mullite phase) during spray deposition.

Table 5.4 Coating hardness for different operating power level

Coating Type	Operating Power (kW)	Micro hardness (HV)		
		Dull	White	Spotted
100% RM	6	542	489	494
	9	534	495	513
	12	588	511	500
	15	555	500	518
90% RM + 10% FA	6	640	630	621
	9	650	644	632
	12	662	640	621
	15	653	641	636
80% RM+ 20%FA	6	659	639	641
	9	670	642	652
	12	697	681	654
	15	680	683	658
50% RM + 50% FA	6	697	671	662
	9	679	630	678
	12	724	709	669
	15	711	669	675
80% RM+ 20%A1	6	749	762	781
	9	753	759	742
	12	752	787	735
	15	761	791	697
80% RM+ 20%C	6	642	617	609
	9	651	612	598
	12	623	643	601
	15	621	648	600

5.6 COATING POROSITY:

Table 5.5 Coating porosity for different coating type

Precursor Type	Operating Power level (kW)	Porosity (%)
100% red mud	6	12.89
	9	12.02
	12	11.87
	15	13.02
90% red mud+10% fly ash	6	11.52
	9	11.12
	12	10.90
	15	12.98
80% red mud+20% fly ash	6	10.89
	9	10.54
	12	10.17
	15	11.78
50% red mud+50% fly ash	6	10.56
	9	10.21
	12	09.58
	15	10.98
80% red mud+20% Aluminium	6	09.89
	9	09.55
	12	09.44
	15	10.44
80% red mud+20% Carbon	6	09.97
	9	09.78
	12	09.58
	15	10.13

The porosity data for the prevailing coatings are shown in [Table 5.5](#). From the digitized image obtained by this system, coating porosity was determined using VOIS image analysis software. Results reveal the pure red mud coating have high porosity among others. Red mud-Aluminium composite coatings possess the minimum porosity. The magnitude of porosity was found to be maximum in case of all coating compositions prepared at 15 kW power level. At 6 kW operating power level, there is poor melting of particles subjected to relatively low plasma gas temperature exhibiting non-uniform mixing of molten particles. The improper distribution of molten particles on the substrate at low plasma torch power causes to develop reasonably porous coating layer. On the other hand, at a highest operating power level (15 kW) the high plasma gas temperature caused faster deposition of molten particles by creating a thickened coating layer with high porosity. Porosity level was found to be higher in case of pure red mud compared to the composite coatings made of the mixture of fly ash-red mud and carbon-red mud. As literature reveals, porosity value for atmospheric plasma sprayed ceramic materials ranges about 3 -12 % [187]. So the results obtained here are in acceptable standards.

5.7 COATING DEPOSITION EFFICIENCY:

In the present work plasma torch input power is considered as the influencing factor on the coating deposition efficiency. Data pertaining to the deposition efficiency of prepared coatings are reported in [Table 5.6](#). It is important to mention here that, the data reported in [Table 5.6](#) is corresponds to plasma coating of the prevailing coating powders on mild steel substrate only. The results reveal, the coating deposition efficiency increases with operating power in a sigmoidal fashion. The experimental outcomes show that, the coating deposition efficiency is improved with fly ash reinforcement to pure red mud. The RM+50% FA coating show the maximum value (29.05 %) of deposition efficiency at 15 kW, where as pure red mud posses the minimum (6 %) at 6 kW operating power. Probably the RM+FA coatings melt faster than other coatings in the study and adhere to the substrate in higher amount and hence improve the deposition efficiency.

Table 5.6 Effect of operating power on coating deposition efficiency

Coating Type	Operating Power kW	Deposition Efficiency (%)
RM 100%	6	8
	9	14.3
	12	24
	15	26.2
RM+20%FA	6	9.42
	9	15.92
	12	25
	15	27.5
RM+50%FA	6	10.942
	9	17.192
	12	27.08
	15	29.05
RM+20%C	6	9.92
	9	16.292
	12	25.998
	15	27.979
RM+20%Al	6	8.799
	9	15.65
	12	25.02
	15	27.08

5.8 COATING ADHESION STRENGTH:

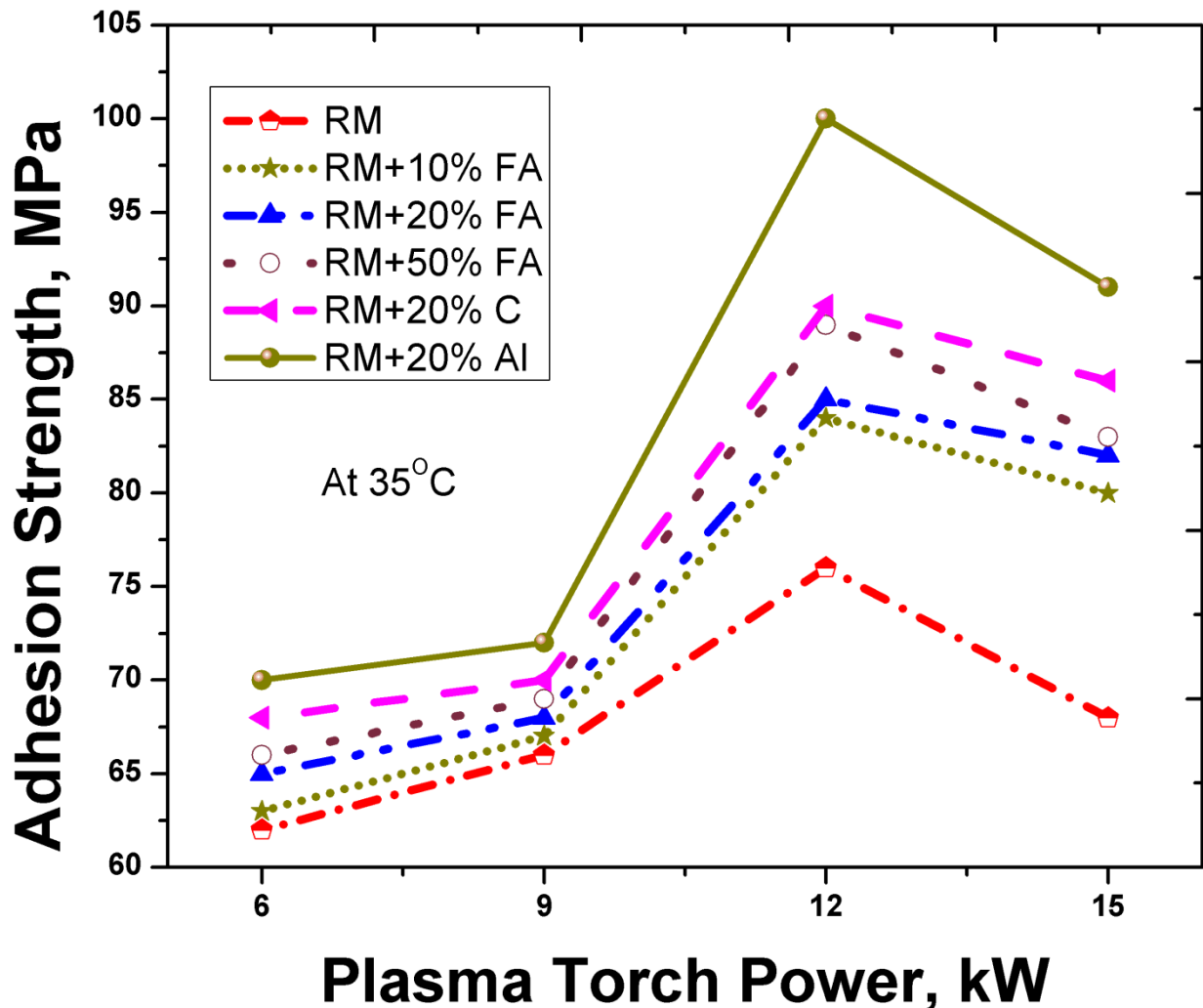


Figure 5.30 Effect of Plasma Torch Power on adhesion strengths of prepared coatings.

In this section the investigation is focused to evaluate the adhesion strength at normal laboratory condition. The room temperature during the experiment was 35°C. Figure 5.30 reveals the outcomes of the tests. The result shows that at low operating power, i.e. at 6 kW the adhesion strength is minimum for all the prepared coatings. The adhesion strength improves with torch input power. But it is interesting to discuss here that, the improvement of adhesion strength is observable up to 12 kW power. Beyond 12 kW the adhesion strength decreases. Reinforcement of fly ash to red mud enhances the bond strength. The red mud-aluminium coatings have the maximum bond strength (100 MPa, at 12 kW) at the interface of the mild steel substrate. Pure red mud coatings do not have sufficient bond strength, and has a minimum value of 62 MPa at 6 kW.

The results are attributing to the fact that, as the operating power increases the fraction of molten particles rises and the velocity of impingement on the substrate improves. There by better splashing of the molten particles occur and improvement of the mechanical interlocking with the mild steel surface. But at 15 kW operating power level, (maximum in this investigation) molten particles fragments and vaporises. There is greater chance for the precursor particles to fly off and causes the improvement of coating porosity. This results in reduced adhesion strength for all coatings at high plasma torch input power. In conclusion, the presence of aluminium plays a vital role for strength of the coatings. Augmentation of fly ash increases the aluminium and silicon content of the precursor powder and at the time of plasma spraying new phases like alumina is formed. This causes the enhancement of interface bond strength with mild steel substrate.

5.9 TGA, DSC AND BOND STRENGTH ANALYSIS AT ELEVATED TEMPERATURES:

Thermal behaviour of the coatings are studied by conducting experiments like thermogravimetric analysis (TGA) as per ASTM E-2008 standards and differential scanning calorimeter (DSC) applying Setaram DSC 131 analyser. The DSC experiments are carried from room temperature to 1000°C at a rate of 10°C/min in oxidative environment, with air flow rate 10 ml/min. The thermal behaviour is studied considering the coatings made at 12 kW operating power. Originated TGA curve for the prevailing coatings are shown in [Figure 5.31](#). Weight loss is maximum (up to 89.6 %) for RM + 50 % FA coatings whereas minimum (up to 95 %) for red mud-aluminium coatings. It is observed that, for all coatings up to about 250°C, no significant weight loss is seen. Here after, the loss is abrupt and becomes stagnant at around 600°C. Reinforcement of FA to RM results in enrichment in Si and Al content, building a more hygroscopic composite. The Si enriched coatings, tends to carry supplementary moisture and dehydrates in great.

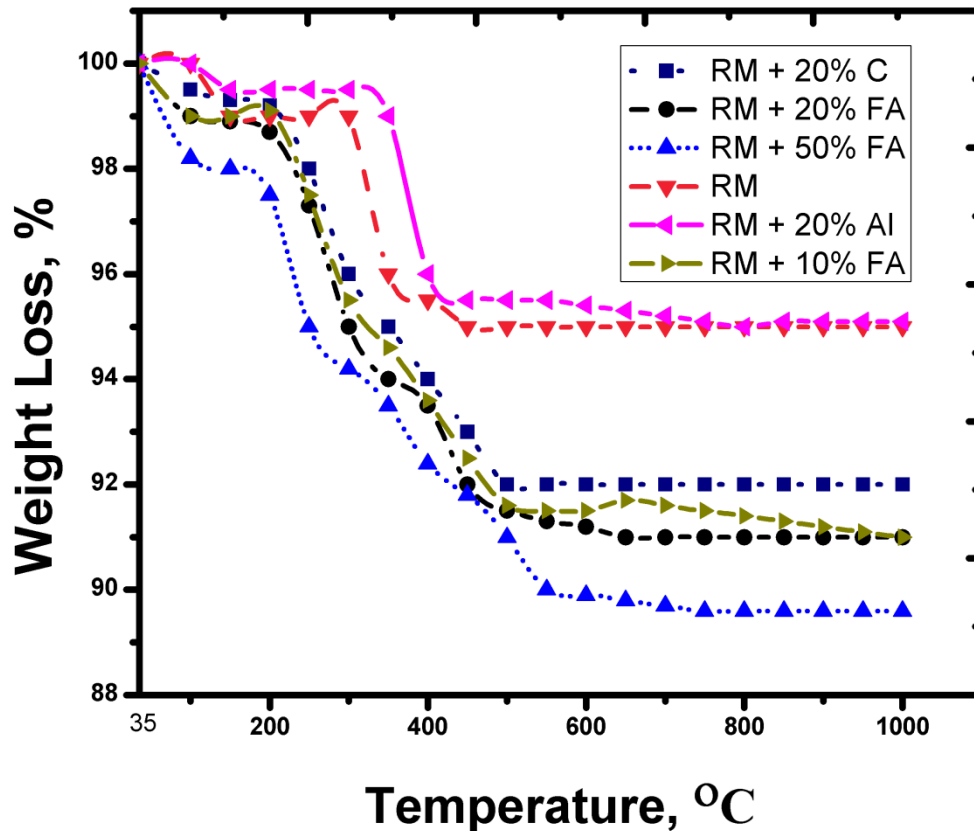


Figure 5.31 TG analyses of coatings

Behavior of the coatings to heat exposure is revealed in Figure 5.32. Heat carrying capacity is highest for Al composited coatings where as minimum for red mud-carbon coatings. The carbon based coating absorbs heat up to 550°C and is least in the observations. The heat carrying capacity of red mud-carbon composite coatings is low. This is because the charcoal considered as carbon in the experiment has less thermal conductivity and absorbs heat at lower rate. Pure RM coatings absorb heat up to a critical temperature of approximately 650°C and then start to release. Whereas the FA (10 %) based coatings continue to gain heat till 750°C. Results are presuming to higher Al content of the FA composited coatings, leading a film of intensified thermal conductivity. The critical temperature of red mud-aluminium coatings originates at 800°C. But the cause of alternation of heating behaviour at critical point is not recognizable.

Finally experiments are conducted to measure adhesion strength of coatings at elevated temperatures. Data is collected at an interval of 100°C up to 1000°C placing the coatings in a muffle furnace. Coated specimens are kept at the each desired

temperature in furnace for 2 hour. Specimens are allowed to cool under normal atmosphere to reach air temperature. Adhesion strength is measured after heat treatment at each temperature interval, using a Caltech BGD 1520 digital pull off adhesion tester with 10 mm dolly as per ASTM D4541 standards. Both resin and hardener mixed in equal proportion and used as adhesive. Adhesion strengths are reported corresponding to adhesive failure of coatings. Figure 5.33 reveals the strength results of coatings. RM-Al coating have adequate strength in compared to others. Adherence falls with temperature. Reinforcement of FA boosts the adhesive strength, might be due to enhancement of interfacial affinity of fly ash molecules to mild steel during melting and origination of coating. Interfacial strength between coating and metal declines linearly with rise in temperature and stabilises at approximately 800°C.

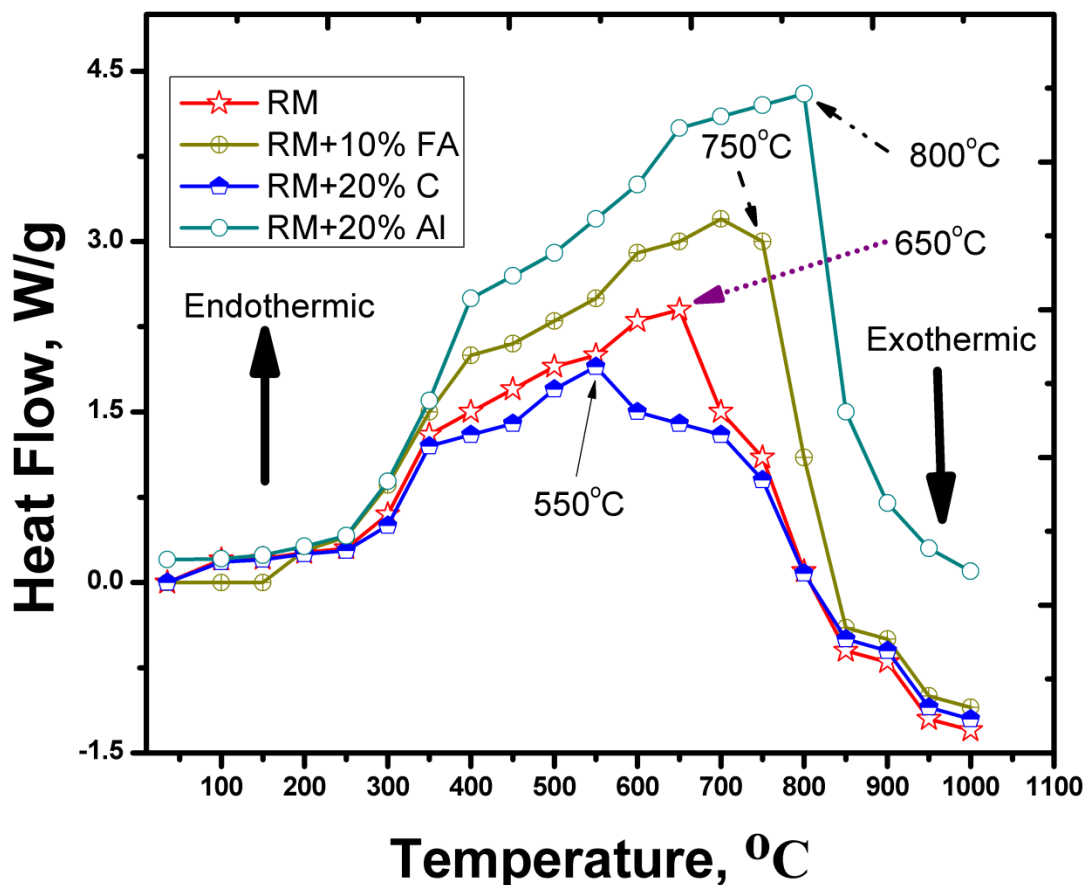


Figure 5.32 Originated DSC plots of coatings

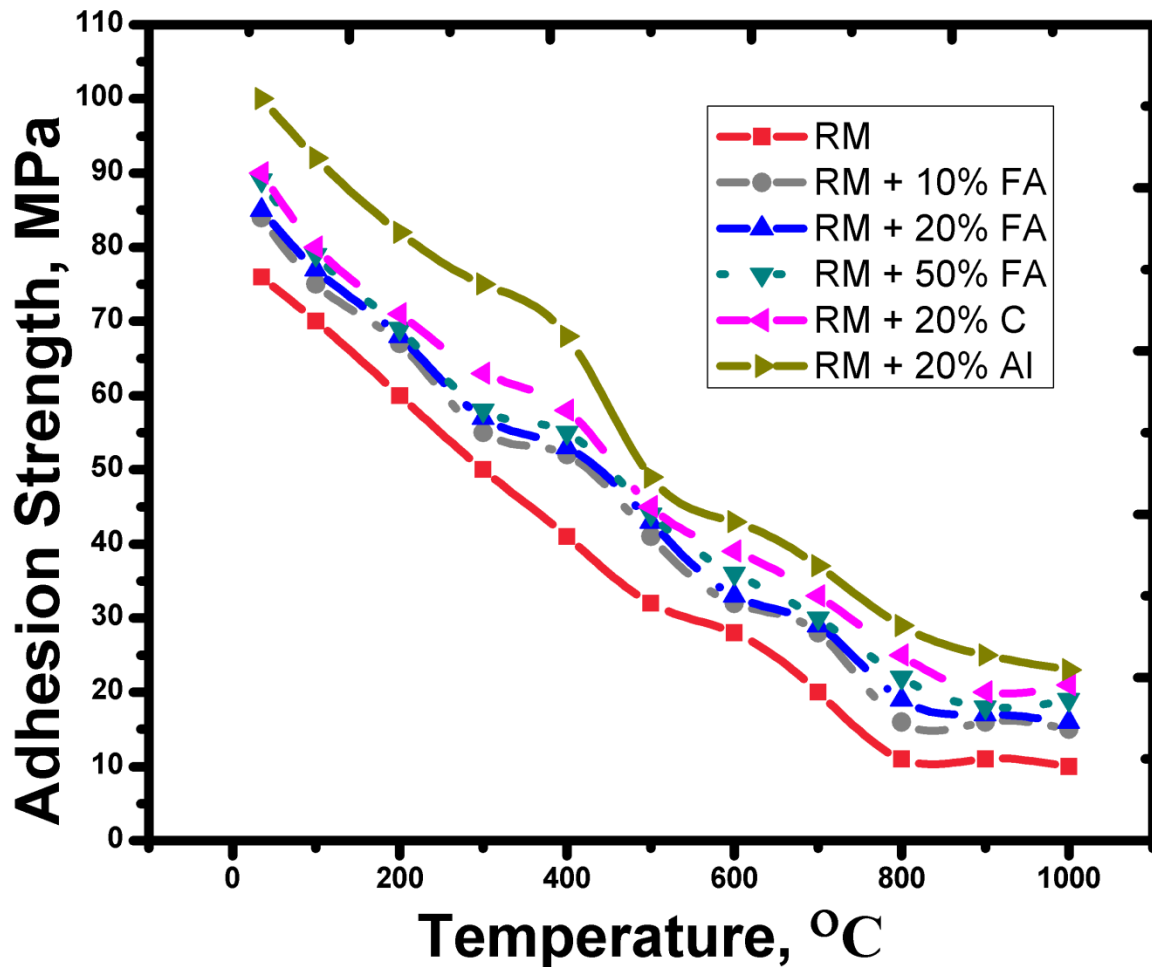


Figure 5.33 Influence of temperature on adhesion strength.

Micro-structural stability is a critical factor influencing the thermal and mechanical behaviour of ceramic coatings. Modifications of coating surfaces are seen after 600°C. To recognize the surface morphology at high temperatures few microscopic images are captured for red mud-fly ash and red mud-aluminium coatings and shown in [Figure 5.34](#) and [Figure 5.35](#) respectively. It is observed that, at elevated temperature (>800°C) the coatings “soften” causing sheets to stick and fuse. However, the most common associated problem is “cracking”. Web-like pattern of fine cracks develop on coating, causing it to resemble cracked and a leathery skin. Enrichment of fly ash leads to increase Si and Al content, resulting the formation of brittle phases which may reduce the scale adherence due to continuous heat exposure. Probably Si reacts with the other species, forming damaging compounds and destroys the bonding between the mild steel and the coating.

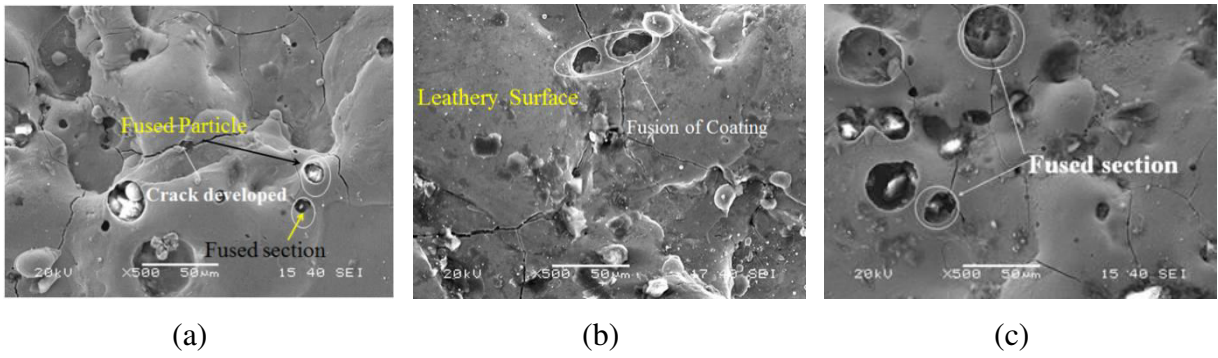


Figure 5.34 Cracked surfaces of RM + 10% FA coatings at (a) 800°C, (b) 900°C and (c) 1000°C

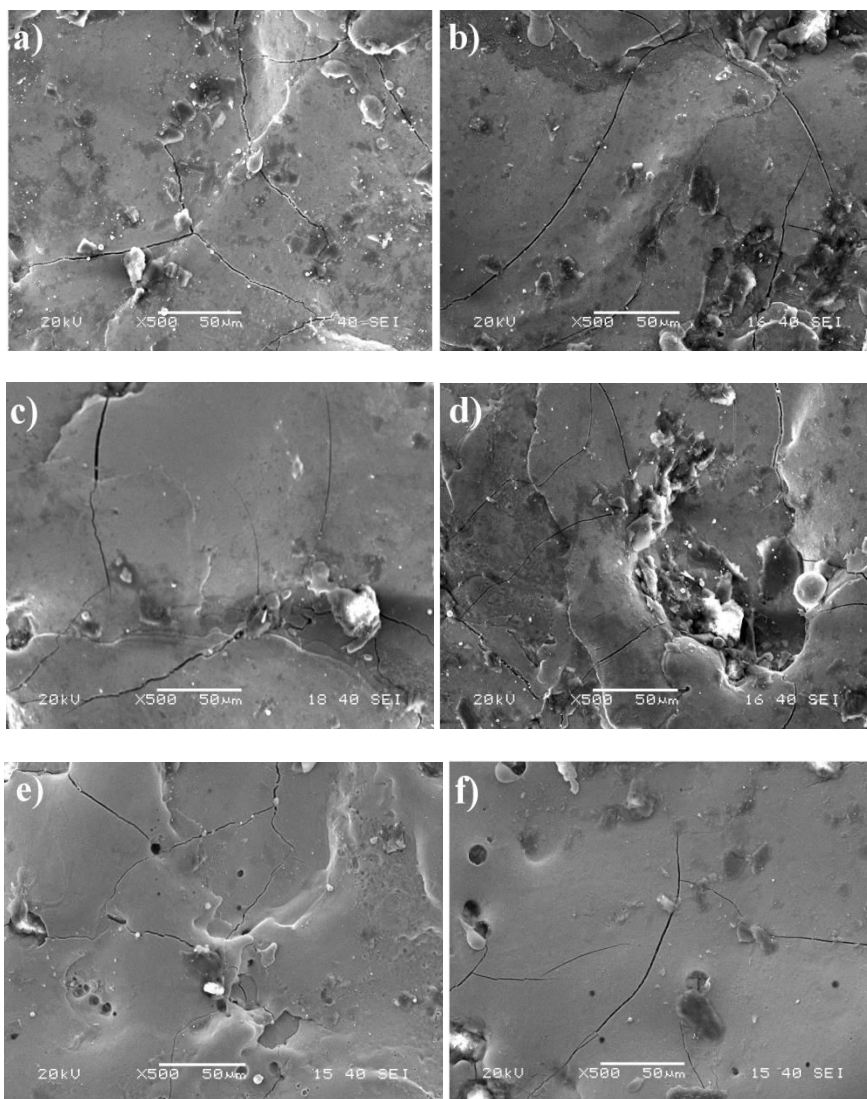


Figure 5.35 Microstructures of RM + 20% Al coatings at (a) 500°C, (b) 600°C, (c) 700°C, (d) 800°C, (e) 900°C and (f) 1000°C

5.10 DESIGN OF EXPERIMENT BY TAGUCHI METHOD:

Design of Experiments (DOE) is one of the important and powerful statistical techniques to study the influence the various controlling factors on performance output. All designed experiments require a certain number of combinations of factors and levels be tested in order to observe the results of those test combination. Taguchi optimization procedure is employed to find the optimum operating parameters influencing the wear using MINITAB-16. Optimization is conducted considering time, power and fly ash content as controlling factors. Operating power chosen are 9, 12 and 15 kW. In this project as the dry sliding wear tests are carried out up to a minimum time of 51 minutes, so in order to understand the effect of time on wear rate the time intervals of 15, 30 and 45 minutes are considered to fit the design performance. The operating conditions implemented are given in [Table 5.7](#).

[Table 5.7](#) Levels of the variables used in the experiment.

Control Factors	Level			
	I	II	III	Units
A: Time	15	30	45	Minute
B: Power	9	12	15	kW
C: FA Content	10	20	50	Wt %

Design is conducted in accordance with $L_{27} (3^{13})$ orthogonal array and corresponding linear graph is shown in [Figure 5.36](#). The S/N ratios for minimum wear rate “in gm” under ‘smaller is the better characteristic’, can be calculated as the logarithmic transformation of the loss function (equation no-1) as shown below.

Smaller is the better characteristic:

$$\frac{S}{N} = -10 \log \frac{1}{n} (\sum y^2) \quad (1)$$

Where ‘n’ is the repeated number trial conditions and ‘y’ is the sliding wear data.

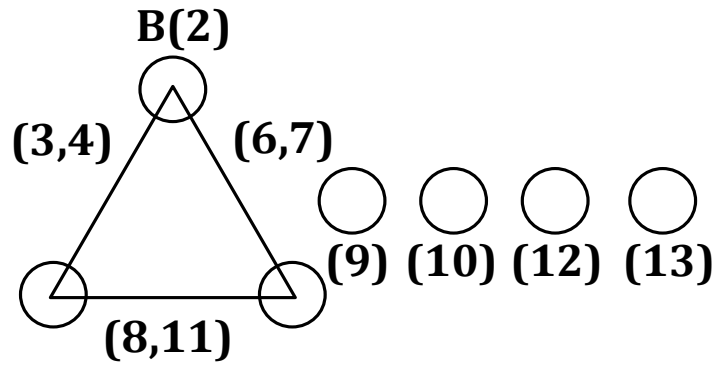


Figure 5.36 Standard linear graphs for L₂₇array

The sliding wear behaviour is designed and published in Table 5.8. The mean of the S/N ratios is found to be 35.30 dB. Figure 5.37 shows graphically the effects of controlling factors on wear rate. Smaller the better characteristic was taken for this analysis. The responses for signal to noise ratios to wear rates are reported in Table 5.9. It is concluded that, time is the most dominating factor to wear, followed by composition and power.

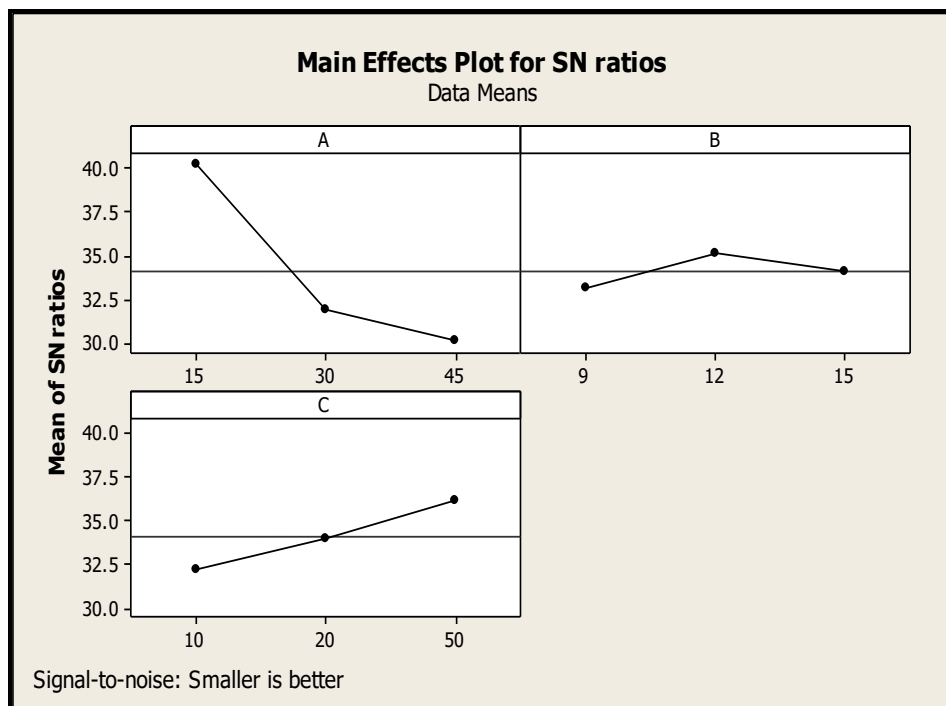


Figure 5.37 Effect of control factors on wear rate

Table 5.8 Experimental design using L₂₇orthogonal array

L ₂₇ (3 ¹³)	Time (Min)	Power(kW)	FA Content %	Wear rate(gm)	S/N Ratio (dB)
1	15	9	10	0.0150794	36.4323
2	15	9	20	0.0125000	38.0618
3	15	9	50	0.0088000	41.1103
4	15	12	10	0.0130000	37.7211
5	15	12	20	0.0100000	40.0000
6	15	12	50	0.0040000	47.9588
7	15	15	10	0.0141000	37.0156
8	15	15	20	0.0110000	39.1721
9	15	15	50	0.0060000	44.4370
10	30	9	10	0.0329865	29.6333
11	30	9	20	0.0250000	32.0412
12	30	9	50	0.0242000	32.3237
13	30	12	10	0.0281000	31.0259
14	30	12	20	0.0222000	33.0729
15	30	12	50	0.0200000	33.9794
16	30	15	10	0.0300000	30.4576
17	30	15	20	0.0248000	32.1110
18	30	15	50	0.0230000	32.7654
19	45	9	10	0.0365480	28.7427
20	45	9	20	0.0320000	29.8970
21	45	9	50	0.0317000	29.9788

22	45	12	10	0.0326000	29.7356
23	45	12	20	0.0282000	30.9950
24	45	12	50	0.0267000	31.4698
25	45	15	10	0.0360000	28.8739
26	45	15	20	0.0299000	30.4866
27	45	15	50	0.0281000	31.0259

Result analysis from [Figure 5.37](#) concludes that a factor combination of A_1 , B_2 and C_3 shows a minimum wear rate. The interaction plots are shown in [Figure 5.38](#). The analysis of variance (ANOVA) was used to analyze the influence of wear parameter.

Table 5.9 Response table to wear

LEVEL	A	B	C
1	40.21	33.14	32.18
2	31.93	35.11	33.98
3	30.13	34.04	36.12
Delta	10.08	1.97	3.93
Rank	1	3	2

The ANOVA establishes the relative significances of factors in terms of their percentage contribution to the response. This analysis was carried out for a level of significance of 5% (the level of confidence 95%). ‘P’ value, less than 0.05 for a particular parameter, indicates that it has the major effect on the responses. Last column in [Table 5.10](#) shows the effect of individual parameters on the responses. Observations from [Figure 5.38](#) and [Table 5.10](#) conclude that the interaction between $A \times B$ shows minimum effect on wear.

Table 5.10 ANOVA table for wear rate

Source	DF	Seq SS	Adj SS	Adj MS	F	P	% P	Rank
A	2	0.0020801	0.0020801	0.0010400	1747.64	0.000	86.06	1
B	2	0.0000644	0.0000644	0.0000322	54.08	0.000	2.66	3
C	2	0.0002486	0.0002486	0.0001243	208.84	0.000	10.27	2
A×B	4	0.0000016	0.0000016	0.0000004	0.65	0.642	0.07	3
B×C	4	0.0000024	0.0000024	0.0000006	0.99	0.465	0.09	2
A×C	4	0.0000162	0.0000162	0.0000041	6.81	0.011	0.66	1
Error	8	0.0000048	0.0000048	0.0000006			0.19	
Total	26	0.002417						

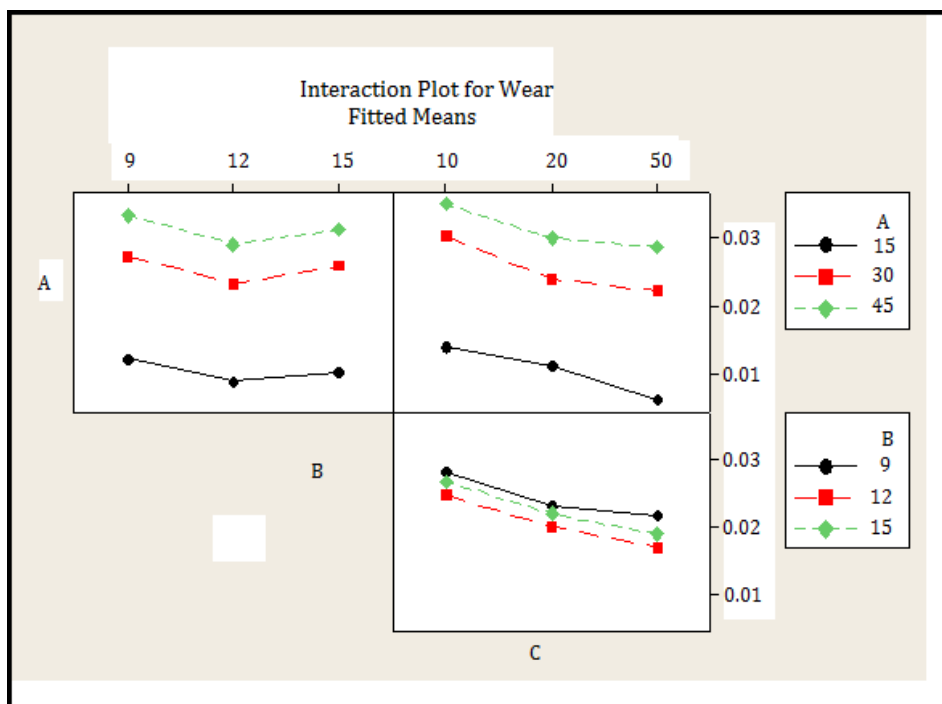


Figure 5.38 Interaction graph between A×B×C for wear rate

The combination of factors A and C has the major effect on wear. The factor B has least contribution on wear rate. But its combination with factor ‘C’ has significant effect on wear rate. The correlation between coating removal rate, CRR (non-variable factor) and variable factors (time, power and FA content) was found by multiple linear regressions from the equation no-2.

$$CRR = K_0 + K_1A + K_2B + K_3C. \quad (2)$$

Where, K_i ($i= 0, 1, 2, 3, \dots$) is a model constant. The regression equation is

$$CRR \text{ (gm)} = 0.00947 + 0.000694 A - 0.000295 B - 0.000161 C. \quad (3)$$

Table 5.11 Results of the confirmation experiments

	Optimal control parameters	
	Prediction	Experimental
Level	$A_1B_2C_3$	$A_1B_2C_3$
S/N ratio of wear rate, dB	46.8563	47.9588

From equation-3 it is observed that time has a major impact on wear, followed by composition and operating power. Confirmation experiment is the final test in the design of the experiment process. The purpose of confirmation experiment is to validate the conclusions drawn during the analysis phase. From the model, result of confirmation test is reported in [Table 5.11](#). An error of 2.35 % for the S/N ratio of wear rate is observed.

CHAPTER-6

CONCLUSIONS

AND

SCOPE FOR FUTURE WORK

6.1 CONCLUSIONS

The present study allows for some salient concluding remarks noted as follows.

Red mud, the waste generated from alumina plants, is coatable on mild steel metal substrates by employing thermal plasma spraying (PS) technique with *excellent wear resistance and high temperature thermal stability*. The addition of fly ash to red mud reduces the wear rate by enhancing the coating property. Addition of carbon and aluminium to red mud further improves the wear resistance by altering the interface properties.

In regard to **micro-structural characteristics** of the obtained coatings it is concluded that, plasma generating power, adversely affect the coating morphology. At low operating power a non uniform, rough surface and cavities are noticed. Increase in power develops a splat and uniform surface. Plasma torch power has no significant effect on coating thickness. There is a marginal increase of thickness with power. XRD analysis reveals the formation of new phases during spraying with varying operating power.

With respect to the **mechanical characteristics** we may conclude that changes in the phases alter the coating physical properties like adhesion strength, deposition efficiency, hardness and porosity. Aluminium addition to red mud maximises the bond strength. The value stands up to 100 MPa at 12 kW. Amount of molten particles increases with operating power up to 12 kW and improves the mechanical interlocking of coating with mild steel. But at 15 kW, molten particles flashes off, increasing the porosity and hence the fall of adhesion strength results.

From the study and analysis of **thermal behaviour** it is concluded that, the prepared coatings can withstand high temperatures in the DSC and TGA experiments. The prevailing coatings sustain high temperature environment up to 1000°C. The coatings stand up to about 500°C without developing crack. Above 800°C however, coatings start to fuse and develops web like structures.

In regard to the **wear behaviour** study it is found for all coating types that in the early stage of the experiment the wear rate increases slowly but then rises drastically with sliding distance for all coating types. The coating wear resistance (reverse of wear rate) increases until an optimum value at 12 kW, afterwards indicating some other dominating parameters. The findings reveal that, red mud + 20 % carbon coating survives up to a sliding time of 120 minute which is maximum among all coatings studied. The frictional force is found to be maximum at 6 kW and minimum at 12 kW operating power. At 15 kW of operating power, the frictional force was found to be in the range of values for the power levels between 9 to 12 kW. These results are in accordance with the findings observed for wear rates.

In wear mechanism study, it is concluded that the wear takes place by the phenomenon of adhesion and abrasion due to the development of shear stresses between the hard asperities of the two surfaces in contact. Design of experiment by Taguchi method and associated optimization reveals that time is the most dominating factor for wear, followed by coating composition and power.

Overall, it may be concluded that, the prepared coatings may be an effective alternative to replace the conventional ceramic coatings. Red mud and its composite coatings possess acceptable thermal properties. Fly ash is a beneficial reinforcing agent for red mud, and the composite can be coatable with favourable surface properties. These coatings can be used at high temperature. These composite coatings can also be employed for suitable tribological applications.

6.2 SCOPE FOR FUTURE WORK:

Although the present study has investigated most of the important features of the RM and RM composite coatings, there is scope for future work to determine some other coating features. The investigations that may be performed for further understandings of these coatings are noted bellow.

Corrosion wear of the coatings may be studied under different corrosive environments to find out its application areas. Erosion wear at different operating condition may be examined to evaluate its resistances to erosion. Contact angles of the said coatings may also be examined with respect to various liquid mediums to check ability of the liquid to maintain contact with the prepared coating surfaces. Surface roughness may also be quantified with the help of a profilometer to understand the surface profile. Properties like abrasion resistance, ability of expand and contract, weather resistance, resistance to bacteria and fungus, radiation resistance may also be studied to explore better application areas.

CHAPTER-7

REFERENCES

- [1] P.R. Taylor; *Thermal Plasma Processing of Materials— Power Beams and Materials Processing PBAMP 2002*, Ed. A.K. Das et al., Allied Publishers Pvt. Ltd., Mumbai, India, pp. 13-20 (**2002**)
- [2] P.P. Bandopadhyaya; *Processing and Characterization of Plasma Sprayed Ceramic Coatings on Steel Substrate—Ph.D. Thesis* , IIT,Kharagpur, India (**2000**)
- [3] R.B. Heiman, ‘*Plasma Spray Coating, Principle and Application*’, VCH, Weinheim, Germany, **1996**.
- [4] A Satapathy-Thermal spray coating of red mud on metals, PhD Thesis, National Institute of Technology, Rourkela, Odisha, India; (**2005**).
- [5] R. Edwards, *Cutting Tools*, The Institute of Materials, UK, **1993**.
- [6] K. G. Budinski, *Surface Engg. For Wear Resistance*, N.J., USA, **1988**.
- [7] K. N. Stratford, **1984**, *Coatings and Surface Treatments for Corrosion and Wear Resistance*, Inst. Of Corrosion Sc. And Tech., Birmingham,UK.
- [8] L. J. Durney, **1984**, *Electroplating Engineering Handbook*, Van Nor stand, NY, USA.
- [9] T. Biestek and J. Weber, **1976**, *Electrolytic and Chemical Conversion Coating*, Portcullis Press Ltd, Warsaw, Poland.
- [10] N. A. Tape, E. A. Baker and B. C. Jackson, **1976**, *Plating and Surface Finishing*, October, p 30.
- [11] N. Fieldstein, **1981**, *Materials Engg.*, July, P 38.
- [12] C. F. Spencer, **1975**, *Metal Finishing*, January, P 38.
- [13] J. Mcdermott, **1972**, *Electroless Plating and Coating of Metals*, Noyes Data Corp, NJ., USA.
- [14] M. F. Ashby and D. R. H. Jones, **1980**, *Engineering Materials*, Pergamon press, NY, USA.
- [15] C. R. Brooks, **1979**, *Heat Treatment of Ferrous Metals*, Hemisphere Publishing Co., Washington, USA.
- [16] C. Dawes and D. F. Tranter, **1983**, *Metal Progress*, December, P 17.
- [17] A. V. Linial and H. E. Hunterman, **1979**, *Wear of Materials*, ASME, NY, USA.

- [18] S. Bhattacharya and F. D. Seaman, **1985**, *Laser Heat Treatment for Gear Application in "Laser Processing of Materials"*, The Metallurgical. Soc. Of AIME, p 211.
- [19] F. A. Smidt, **1983**, *Ion Implantation for Material Processing*, Noyes Data Corp, NJ, USA.
- [20] R. F. Bunshah, **1982**, *Deposition Technologies for Films and Coatings*, Noyes Publications, NJ, USA.
- [21] J. Vossen and W.Kern, **1978**, *Thin Film Processes*, Academic Press, NY, USA.
- [22] H. S. Legg and K. O. Legg, **1989**, *Ion Beam Based Techniques for Surface Modification in "Surface Modification Technologies"*, by T.S.Sudarsan (ed), Marcell Dekker Inc, USA, p 219.
- [23] J. M. Blocher, **1966**, *Vapour Deposited Materials in "Vapour Deposition"*, by C. F. Powell, J. H. Oxley and J. M. Blocher (eds), Willwy, NY, USA.
- [24] D. G. Bhatt, **1989**, *Chemical Vapour Deposition, in "Surface Modification Technologies"*, by T. S. Sudarsan (ed), Marcell DekkerInc, USA, p 141.
- [25] R. L. Little, **1979**, *Welding and Welding Technology*, TMH Publications, New Delhi, India.
- [26] The Welding Handbook, **1980**, American Welding Soc., USA.
- [27] P. T. Houldcroft, **1967**, *Welding Process Tech.*, Welding Process Tech., Cambridge Univ Press, UK.
- [28] L. F. Longo, **1985**, *Thermal Spray Coatings*, ASM, USA.
- [29] V. Meringolo, **1983**, *Thermal Spray Coating*, Tappi Press, Atlanta, USA.
- [30] J. L. Morris, **1951**, *Welding Principle for Engineers*, Prentice Hall, USA.
- [31] G. Shrijit; Procedure of Metal Spraying: 4 Steps | Metallurgy, **2019**;
<http://www.yourarticlelibrary.com/welding/spraying/procedure-of-metal-spraying-4-steps-metallurgy/97716>
- [32] L. Powloski, **1995**, *The Sc. And Engg. Of Thermal Spraying*, Willey, USA.
- [33] E. Lugscheider, **1992**, *Technica*, v 19, p 19.
- [34] D. G. McCartney, **1998**, *Surf. Engg.*, v 14(2), p 204.

- [35] V. V.Sobolev, J.M. Guilemany, J. Nutting and J.R. Miquel, **1997**, *Int. Mat. Rev*, v 42(3), p117.
- [36] B. Xu, M. Shinning and J. Wang, **1995**, *Surf. Engg.*, v 11(1), p 38.
- [37] *Metco Plasma Spraying Manual*,**1993**, Metco, USA.
- [38] J. Wrigren, **1991**, *Surf. Coat. Tech.*, v 45, p 263.
- [39] M. G. Nicholas and K. T. Scott, **1981**, *Surfacing Journal*, v 12, p 5.
- [40] W. Funk and F. Goebe, **1985**, *Thin Solid Film*, v 128, p 45.
- [41] B. Wielage, V. Hofmann, A. Steinhauser and G. Zimmerman, **1998**,*Wear*, v 14(2), P 136.
- [42] N. Y. Lee, D. P. Stinton, C. C. Brandt, F. Erdogan, Y. D. Lee and Z. Mutasim**1996**, *J. Am. Cer. Soc.*, v 79(12), P, 3003.
- [43] A. Pajares, L. Wei, B.R. Lawn and C.C. Berndt., **1996**, *J. Am. Cer. Soc.*, 79(7), p 1907.
- [44] R. C. Novak, **1988**, *J. Gas Turbines and Power*, v-110, p 110.
- [45] A. R. Nash, N. E. Weare and D. L. Walker, July, **1961**, *J. Metals*, July, p 473.
- [46] H. Gruner, **1984**, *Thin Solid Film*, v 118, p 409.
- [47] H. Eaton and R. C. Novak, **1986**, *Surf. And Coating Technology* , v 27, p 257.
- [48] H. Eaton and R. C. Novak, *Proc. Int. Conf on metallurgical Coatings*, San Diego, USA.
- [49] K. Ramchandran and P. A. Selvarajan, **1998**, *Thin Solid Film*, v 315, p 149.
- [50] H. S. Ingham and A. J. Fabel, February, **1975**, *Welding Journal*, p 101.
- [51] S. Oki, S. Gonda and M. Yanokawa, **1998**, *Proc. 15th International Thermal Spray Conference*, 25 – 29th May, France, p 593.
- [52] A. F. Puzryakov, S. A. Levitin and V. A. Garanov, **1985**, *Poroshkovaya Metallurgya*, v 8 (272), p 55.
- [53] J. Hennaut, J. Othzemouri and J. Charlier, **1995**, *Mat. Sc and Tech.*, 1995, v 11, p 174.
- [54] S. Sampath, R. A. Neiser, H. Herman, J. P. Kirkland and W. T. Elan., **1993**, *J. Mat. Res.*, v 8(1), p 78.
- [55] J. Hennaut, J. Othmezouri and J. Charlier, **1995**, *Mat. Sc and Tech.*, 1995, v11, p 174.

- [56] B. Elvers, S. Hawkins and G. Schultz (eds), **1990**, Uhlmann's Encyclopedia of Industrial Chemistry, v 1/16, VCH, p 433.
- [57] C. J. Kubel, Adv. Mat. Proc., **1990**, v12, p 24.
- [58] M. Codenas, R. Vijande, H. J. Montes and J. M. Sierra, **1997**, *Wear*, v 212, p 244.
- [59] Nolan, P. Mercer, and M. Samadi, **1998**, Surf. Engg, v11 (2), p 124.
- [60] Y.Naerheim, C. Coddet and P. Droit, **1995**, Surf. Engg, v11 (1), p 66.
- [61] K. Hojmrle and M. Dorfman, **1985**, *Mod. Dev. Powder. Met.*, v 15(15), p 609.
- [62] O. Knotek, E. Lugscheder and H. Reiman, **1975**; J. Vac. Sc. Tech A, v 12(4), p 75.
- [63] M. Roy, C.V.S. Rao, D. S. Rao and G. Sundarrajan, **1999**; Surface Engineering, v 15(2), p 129.
- [64] Chuanxian, H. Bingtang , L. Huiling, **1984**; Thin Solid Film, v 118, p 485
- [65] J. M. Guilemay, J. M. De Paco, **1998**; Surface Engineering., v.11 (2), p 129.
- [66] Y. Wang, **1993**, *Wear*, v 161, p 69.
- [67] Y. Wang, J. Yuansheng and W. Shizhu, **1988**; *Wear*, v 128, p 265.
- [68] A.Tronche and P. Fauchais, **1988**; *Wear*, v 102, p 1.
- [69] A. A. Stuart, P. H. Shipway and D. G. McCartney, **1999**; *Wear*, v 225-229, p 789.
- [70] S. Economou, M. De Bonte, J. P. Celis, J. R. Roos, R. W. Smith, E. Lugscheider and A. Valencic, **1995**, *Wear*, v185, p 93.
- [71] U. Menne, A. Molar, M. Bonner, C. Varpoort, K. Ebert and R. Bauman, **1993**, Proc. Thermal Spraying – 93, 1993, p 280.
- [72] M. Mohanty, R. W. Smith, M. De Bonte, J. P. Celis and E. Lugscheder, **1996**, *Wear*, v 198, p 251.
- [73] J. F. Li, C. X. Ding, J. Q. Huang and P. Y. Zhang, **1997**, v, p 177.
- [74] J. M. Cuetos, E. Fernandez, R. Vijandez, A. Rucon and M. C. Perez, **1993**,*Wear*, v 169, p 173.
- [75] W. Jainjun and X. Qunji, **1993**, *Wear*, v 162 – 164, p 229.
- [76] J. F. Lin and T. R. Li, **1990**, *Wear*, v 160, p 201.
- [77] A.S. Ahn and O. K. Kwon, **1999**, *Wear*, v 225 – 229, p 814.

- [78] W. Jainjun, X. Qunji and W. Huiling, **1992**, *Wear*, v 152, p 161.
- [79] S. Lathabai, M. Ottmuller , I. Fernandez, **1998**, *Wear*, v 221,p 93.
- [80] L. Zhou, Y. M. Gao, J.E. Zhou, Q.D. Zhou, **1994**, *Wear*, v 176,p 39.
- [81] A.S. Ahn and O. K. Kwon, **1993**, *Wear*, v 162 – 164, p 636.
- [82] T. F. J. Quinn and W. O. Winer, **1985**, *Wear*, v 102, p 67.
- [83] A.Y. Kim, D. S. Lim and H. S. Ahn, **1993**, *J. Kor. Cer. Soc*, v 30, p 1059.
- [84] H. S. Ahn, J. Y. Kim and D. S. Lim, **1997**, *Wear*, v 203 – 204, p 77.
- [85] Y. Fu, A. W. Batchelor, H. Xing and Y. Gu ,**1997**, *Wear*, v 210, p 157.
- [86] Y. Sun, B. Li, D. Yang, T. Wang, Y. Sasaki and K. Ishii, **1998**, *Wear*, v 215, p 232.
- [87] Y. S. Song, J. C. Han, M.H. Park, B.H. Ro, K. H. Lee, E. S. Byun, S. Sasaki, **1998**, Proc. 15thInternational Thermal Spray Conference, 25th– 29thMay, France, p 225.
- [88] M. I. Mendelson, **1978**, *Wear*, v 50, p 71.
- [89] *Metco Technical Bulletin on TiO₂*,**1971**, Metco Inc., NY, USA.
- [90] W. W. Dai, C. X. Ding, J. F. Li, Y.F. Zhang and P. Y. Zhang, **1996**, *Wear*, 196, p 238.
- [91] N. P. Suh, **1973**, *Wear*, v 25, p 111.
- [92] H. So, **1995**, *Wear*, v 184, p 161.
- [93] T. S. Eyre, **1975**, *Wear*, v 34, p 383.
- [94] Halling, Principles of Tribology, TheMcmillan Press Ltd, NY, USA, **1975**.
- [95] Y. Guilmad, J. Denape and J. A. Patil, **1993**, *Trib. Int.* v 26, P 29.
- [96] M. G. Gee, **1992**, *Wear*, v 153, p 201.
- [97] R. Mcpherson, **1973**, *J. Mat. Sc.*, v 8, P 859.
- [98] R. Mcpherson, **1980**, *J. Mat. Sc.*, v 15, P 3141.
- [99] A.R.D.A. Lopez, K. T. Faber, **1999**, *J. Am. Cer. Soc.*, v 82(8), p 2204.
- [100] H. Ono, T. Teramoto and T. Shinoda, **1993**, *Mat and Mfg. Processes*, v 8(4&5), p 451.
- [101] S. Musikant, **1991**, *What Every Engineer Should Know AboutCeramics*, Marcell Dekker Inc, NY, USA.
- [102] R. P. Wahi, and B. Lischner, **1980**, *J. Mat. Sc*, v 15, p 875.

- [103] T. Yamamota, M. Olsson, S. Hogmark, **1994**, *Wear*, v – 174, p 21.
- [104] A. Lamy and T. N. Sopkow, **1990**, Proc. 3rd National Thermal Spray Conference, Long Beach, CA, USA, 20 – 25th May, p 491.
- [105] D. Matejka and B. Bonko, *Plasma Spraying of Metallic and Ceramic Materials*, Willey, Chichester, UK, **1989**.
- [106] M. A. Moore and F. A. King, **1980**, *Wear*, v 60, p 123.
- [107] Cheo, W. D. Kulhmann and D. M. David, **1994**, *Wear*, v 173, p 1
- [108] A. L. Fernandez, R. Rodriguez, Y. Wang, R. Vijande and A. Rincan, **1995**, *Wear*, v 181 – 183, p 417.
- [109] Y. S. Wang, S. M. Hsu and R. G. Munro, **1991**, *J. Soc. Of Tribologists and Lubri. Engg.*, v 47(1), p 63.
- [110] Metals Handbook, ASM, Metals Park, Ohio, USA.
- [111] S. Atamert and J. Stekly, Microstructure, **1993**, *Surf. Engg.*, v 9(3), p 231.
- [112] M. O. Price, T. A. Wolfla and R. C. Tucker, **1977**, *Thin Solid Films*, v 45, p 309.
- [113] M. A. Moore, **1994**, *Wear*, v 28, p 59.
- [114] P. L. Hurricks, **1972**, *Wear*, v 22, p 291.
- [115] M. G. Habsur and R. V. Miner, **1986**, *Mat. Sc. Engg*, v 83, p 239.
- [116] A. E. Spear, **1989**, *J. Am. Cer. Soc.*, v 72, p171.
- [117] A. Marakawa, **1997**, *Mat. Sc. Forum*, v 247, p 1.
- [118] K. Oyoda, S. Komatsu, S. Matsumoto, Y. Moriyoshi, **1991**, *J. Mat. Sc.*, V 26, p 3081.
- [119] W. Zhu, B. H. Tan and H. S. Tan, **1993**, *Thin Solid Films*, v 236, p 106.
- [120] P. Hollman, A. Alhelisteten, T. Bjorke and S. Hogmark, **1994**, *Wear*, v 179, p 11.
- [121] A. Alhelisten, *Abrasion of Hot Flame Deposited Diamond Coatings*, *Wear*, **1995**, v 185, p 213.
- [122] M. R. Dorfman, (**2018**). Thermal Spray Coatings, Chap-22, Hand Book of Environmental Degradation of Materials, p 469-488.

- [123] H. Sutar, D. Roy, and S. C Mishra; Effect of fly ash and carbon reinforcement on dry sliding wear behaviour of red mud. *Indian Journal of Materials Science*, **2015**.
- [124] K. Holmberg, A. Matthews, and H. Ronkainen. (1998). Coatings Tribology—contact mechanisms and surface design. *Tribology international*, 31(1-3), 107-120.
- [125] K. P. S. S. K Umanath, K. Palanikumar, and S. T. Selvamani, (2013). Analysis of dry sliding wear behaviour of Al6061/SiC/Al₂O₃ hybrid metal matrix composites. *Composites Part B: Engineering*, 53, 159-168.
- [126] B. A Kushner, E. R. Novinski. Thermal spray coating. *ASM Hand book*. **1992**; 18:829-833.
- [127] P. Crook. Friction and wear of Hard facing Alloy. *ASM Hand book*. **1992**; 18:758-765.
- [128] S. C. Mishra, S. Das, A. Satapathy, P. V. Ananthapadmanabhan, K. P. Sreekumar; Erosion wear analysis of plasma sprayed ceramic coating using the taguchi technique. *Tribology Transactions*. **2009**; 52(3):401-404.
- [129] J. Temuujin, A. Minjigmaa, W. Rickard, M. Lee, I. Williams, A. V. Riessen, “Fly ash based geopolymer thin coatings on metal substrates and its thermal evaluation”, *Journal of Hazardous Materials*, Vol. 180, 748-752, **2010**.
- [130] N. Ay, O. NuriÇelik, Y. Göncü. Wear characteristics of traditional manganese phosphate and composite hBN coatings. *Tribology Transactions*. **2013**; 56(6):1109-1118.
- [131] M. Afzal, M. Ajmal, A.N. Khan. Wear behavior of WC-12% Co coatings produced by air plasma spraying at different standoff distances. *Tribology Transactions*. **2014**; 57(1):94-103.
- [132] S. F. Wayne, S. Sampath, V. Anand. Wear mechanisms in thermally sprayed mo-based coatings. *Tribology Transactions*. **1994**; 37(3):636-640.
- [133] S. M. Kondawar and V. W. Khond “Fly Ash Utilization Technologies and Use as Thermal Composite Insulation”, *Indian Streams Research Journal*, v - II, ISSUE – III, **2012**, <http://www.isrj.net/PublishArticles/647.aspx>.

- [134] Y. Wang, Y. Jin, S. Wen. The analysis of the friction and wear mechanisms of plasma-sprayed coatings at 450°C. *Wear*. **1998**; 128:265–276.
- [135] Y. Wang, Y. Jin, S. Wen. The analysis of the chemical structure and properties of ceramic surface films in friction using SEM, AES and Micro-region X-ray diffraction. *Wear*. **1998**; 128:277–290.
- [136] Y. Wang, Y. Jin, S. Wen. The inspection of sliding surface and subsurface of plasma-sprayed using scanning acoustic microscopy. *Wear*. **1998**; 134:399–411.
- [137] R. Vijande-Diaz, J. Belzunce, E. Fernandez, A. Rincon, M. C. Pérez. Wear and microstructure in fine ceramic coatings. *Wear*. **1991**; 148:233–331.
- [138] J. Wei, Q. Xue; Effects of additives on friction and wear behaviour of Cr₂O₃ coatings. *Wear*. **1993**; 160:61–65.
- [139] K. Homberg, A. Mathews, H. Ronkainen. Coating's tribology-contact mechanisms and surface design. *Tribology International*. **1998**; 31(1-3):107-120.
- [140] H. Sutar, S. C. Mishra, S. K Sahoo, A. P. Chakraverty, H.S. Maharana; Progress of red mud utilization: An overview. *American Chemical Science Journal*. **2014**; 4(3):255-279.
- [141] A. Satapathy, S. P. Sahu, and D. Mishra; Development of protective coatings using fly ash premixed with metal powder on aluminium substrates. *Waste Management and Research*, **2010**, 28(7), 660-666.
- [142] K. Srinivasulu, S. Manisha Vidyavathy; Microstructure and Thermal Wear behaviour of Plasma Sprayed Fly Ash Coating on AISI 304 Stainless Steel, *International Journal of Engineering Research and Technology*, **2016** ,5(1), 471-476.
- [143] H. Sutar, S. C. Mishra, S. K. Sahoo, A. Satapathy, V. Kumar; Morphology and solid particle erosion wear behaviour of red mud composite coatings. *Natural Science*. **2012**; 4(11):832-838.
- [144] A. Satapathy, H. Sutar, S. C. Mishra, S. K. Sahoo; Characterization of plasma sprayed pure red mud coatings: An analysis. *American Chemical Science Journal*. **2013**; 3(2):151-163.

- [145] N. Prasad, H. Sutar, S. C. Mishra, S. K. Sahoo, S. K. Acharya; Dry sliding wear behavior of aluminium matrix composite using red mud an industrial waste. *International Research Journal of Pure and Applied Chemistry*.**2013**; 3(1):59-74.
- [146] H. Sutar, S. C. Mishra, S. K. Sahoo, H. S. Maharana, A. P. Chakraverty; Tribological aspects of thermally sprayed red mud-fly ash and red mud-Al coatings on mild steel. *American Chemical Science Journal*. **2014**; 4(6):1014-1031.
- [147] L. Pawlowski. The science and engineering of thermal spray coatings. John Wiley and Sons, New York. **1995**; 218.
- [148] H. Herman and R. A. Sulit. Thermal Spray Coatings, ASM Handbook, Vol. 6, Welding, Brazing, and Soldering, ASM International, **1993**, p 1004-1009
- [149] H. Sutar, D. Roy, S. C. Mishra, S. Patra, R. Murmu. Thermal and Dry Sliding Wear Behavior of Plasma Sprayed Red Mud-Fly Ash Coatings on Mild Steel. *Tribology in Industry*. **2018**; 40(1):117-128.
- [150] C. Richard; Tribological Coatings for high temperature applications; *Encyclopedia of Tribology*, **2013**: 3778-3787.
- [151] M. Gines, F. Williams, C. Schuh; Strategy to Improve the High-Temperature Mechanical Properties of Cr-Alloy Coatings; *Metallurgical and Materials Transactions A*, **2007**; 38: 1367.
- [152] M. Bagwan, (**2013**). *Prediction of adhesive strength, deposition efficiency and wear behaviour of plasma spray coating of low grade mineral on mild steel and copper Substrate by soft computing technique* (Doctoral dissertation).
- [153] W. N. Harrison, D. G. Moore, J. C. Richmond; Ceramic coatings for high-temperature protection of steel; *Journal of Research*; National Bureau of Standards, **1947**, 38, 293–307.
- [154] V. V. Sobolev, J. M. Guilemany, J Nutting, J. R. Miquel; Development of substrate-coating adhesion in thermal spraying ; *International Materials Reviews*, **1997**, 42(3), 117-136.

- [155] S. Adachi, K. Nakata; Study of Bonding Strength of Plasma-Sprayed Ti-Al Coating on Mild Steel Substrate; *Plasma Processes and Polymers*, **2007**, 4: S512–S515.
- [156] Y. Y. Wang, C. J. Li, A. Ohmori; Influence of substrate roughness on the bonding mechanisms of high velocity oxy-fuel sprayed coatings; *Thin Solid Films*; **2005**, 485, 141-147.
- [157] J. Wu, J. Yang, H. Fang, S. Yoon, C. Lee; Bond Strength of Al-Si Coatings on mild steel by kinetic spray deposition; *Applied Surface Science.*, **2006**;205, 7809-7814.
- [158] A. Behera, S.C. Mishra; “Dependence of Adhesion Strength of Plasma Spray on Coating Surface Properties”, *Journal of Materials and Metallurgical Engineering*, Vol. 2, Issue 1, 23-30, **2012**.
- [159] P. Pokorny, L. Mastny, V. Sykora, Z. Pala, V. Brozek; Bond Strength of Plasma Sprayed ceramic coatings on phosphate steels; *Metalurgija*, **2015**, 54(2), 411-414.
- [160] S. K. Rahimi, R. Potrekar, N. K. Dutta, N. R. Choudhury; Anticorrosive interfacial coatings for metallic substrates; *Surface Innovations*, **2013**, 1(2), 112-137
- [161] M. Szuch, A. Lewis, H. Pulido, and A. Asymtek; (2006). New Coating Technologies and Advanced Techniques in Conformal Coating. *Asymtek, ANordson Company, Carlsbad, CA*, 1-6.
- [162] P. Nguyen, S.Y. Ho, A. Kotousov; Slurry spray technique for manufacturing thermal barrier coatings, *Surface Innovations*, **2013**, 1(3), 190-199.
- [163] J. Drelich, A. Marmur; Physics and applications of superhydrophobic and superhydrophilic surfaces and coatings; *Surface Innovations*, **2014**, 2(4), 211-227.
- [164] A. Behera, S.C. Mishra; Characteristic study of fly-ash+quartz+illmenite composite coatings on copper substrates; *Emerging Materials Research*; **2013**, 2(1), 39-44.
- [165] D. R. Chinloy and R. K. Holzwarth, **1984**, “Steady state simulation of the bayer Process”, *LIGHT METALS* pp. 13 – 26.

- [166] C. M. Hall, **1889**, US Patent 400766.
- [167] B. K. Mahapatra, M. B. S. Rao, R. BhimaRao, and A. K. Paul, “*Characteristics of red mud generated at NALCO refinery, Damanjodi, India*”, LIGHT METALS, **2000**, pp. 161 -165.
- [168] K. Solimar, I. Sajo, J. Steiner and J. Zoldi, **1992**; “*Characteristics and separability of red mud,*” LIGHT METALS, pp.209 - 223.
- [169] S. Sahin, **1998**, *Correlation between silicon-dioxide and iron-oxide contents of red mud samples*, Hydrometallurgy, 47, pp.371 – 376.
- [170] Q. Wang, S. Gu, Z. Han and D. Li; *Irreversible thixotropic behaviour of red mud slurry and exploitation in dry disposal process Nonferrous Metals (China)*, 50(2), **1998**, pp. 85 – 91.
- [171] R. S. Thakur, and S. N. Das, *Red Mud – Analysis and Utilization -- Publication and Information Directorate*, New Delhi and Wiley Eastern Limited, New Delhi, India. (1994).
- [172] G. Banvolgyi, and P. Siklosi, **1998**, *The improved low temperature digestion (ILTD) process: An economic and environmentally sustainable way of processing gibbsitic bauxites*, LIGHT METALS, pp.45 – 53.
- [173] R. A. Galarraga, R. R. Carneiro, R. E. Keane, and G. Nguyen, **2002**; “*CVG – Bauxilum red mud neutralization*”, LIGHT METALS, pp. 133 – 137.
- [174] S. O. Brown and D. B. Kirkpatrick, **1999**; “*Red mud product development*”, LIGHT METALS, pp. 25 – 30.
- [175] D. B. Kirkpatrick, 1996; *Red mud Product Development*, LIGHT METALS, pp. 75 – 80.
- [176] G. L. Goldstein, and R. S. Reimers, 1999; “*Trace element partitioning and bioavailability in red mud synthetic free water sediment*”, LIGHT METALS, PP. 19 – 24.
- [177] E. P. Kovalenko, 1998, “*Improvement of the process of alumina production at Nilolaev alumina plant*”, LIGHT METALS, pp.55 – 58.
- [178] D. Patel, B. K. Padhi, P. Vidyasagar, A. K. Pattnaik; Res. Ind. 37 (**1992**) 154.
- [179] J. Pera, R. Boumaza, J. Ambroise, Cem. Conc. Res. 34 (**1997**) 1513.
- [180] R. N. Summers, N. R. Guise, D. D. Smirk; Fert. Res. 34 (**1993**) 85.

- [181] D. I. Smirnov, T. V. Molchanova, and L. I. Vodolazov, **1999**; “*Associated components of bauxites and ways for their utilization*”, *Tsvetnaya Metallurgia*, 4, pp. 31 – 34.
- [182] V. Martinent – Catalot, J. M. Lamerant, G. Tilmant, M. S. Bacou, J. P. Ambrosi, **2002**; *Bauxaline: a new product for applications of Bayer process red mud*, *LIGHTMETALS*, pp.125– 131.
- [183] S. Liu, **1998**; “*Removal of Toxic Metals from Landfill Leachate and Wastewater by Spent Bauxite*”, Ph. D. Thesis, Tulane University.
- [184] J. Pradhan, S.N. Das, R.S. Thakur, **2000**; *Removal of Ni from aqueous solution using activated red mud* , *LIGHT METALS*, pp.157 – 160.
- [185] A. I. Zouboulis, K. A. Matis, P. M. Solozhenkin, V. P. Nebera, **1999**; *Removal of ions of toxic metals from solutions using industrial solid waste products*,--*TsvetnyeMetally*, 12, pp.45-48.
- [186] N. Yalcin and V. Sevinc, **2000**; “*Utilization of bauxite waste inceramic glass*,” *Ceramics International*, 26(5), pp.485-493.
- [187] G. Balasubramanian, M. T. Nimje and V. V. Kutumbarao, **2000**; “*Conversion of aluminium industry wastes into glass-ceramic products*”, Fourth Int. Symposium on Recycling of Metals and Engineered Materials, Warrendale, USA, pp.1223 – 1228.
- [188] T. Mahata, B. P. Sharma, S. R. Nair and D. Prakash, **2000**; “*Formation of aluminium titanatemullite composite from bauxite red mud*”, *Met.Mat. Trans. B*, 318, pp. 551 – 553.
- [189] T. Laszlo and K. Jozsef., **1957**; “*Chlorination of red mud (from the manufacture of alumina)*”, *KohaszatiLapok*, 90, 460 – 465; cited from *Chem. Abstr.* 195852, 19035.
- [190] C. Heck, **1953**; “*Iron powder from Bayer-process waste*”, *Ger. Pat.* 894 843, 29 Oct.: cited from *Chem. Abstr.* 1958, 52, 11722 h.
- [191] J. U. Marvin, **1958**; “*Recovery of iron, titanium oxide, and alumina from ores and wastes*”, *U. S. Pat.* 2, 830, 892, 15 Apr. 1958; cited from *Chem. Abstr.* 1959, 53, 13847 f.

- [192] L. P. Ni, **1960**; “*The extaction of aluminium, iron and sodium oxide from red mud*”, Izvest. Akad. Nauk. Kazakh, S.S.R. Ser. Met.Obogashchen. I Ogneuporov., 1, pp. 21 – 26., cited from Chem. Abstr. 1961, 55, 16316 a.
- [193] T. Watanabe and E. Yuki, **1960**; Jap. Pat. 13202, **1960**; cited from Chem. Abstr.1962, 56, 4477 g.
- [194] M. Braithwait; *Benefication of iron oxide waste*. GB Patent No. 2078211 – A., Jan. **1982**.
- [195] Agency of Ind. Sci. Tech., J, Patent No. 52152896 – A., Dec. **1977**.
- [196] N. M. Mozharensko, V A. Noskov, **2001**; “*Possible directions in the use of red mud in metallurgical production*”, Metallurgicheskaya I Gornorudnaya Prom, 2, pp. 127 – 128.
- [197] Q. Xiang, X. Liang, M.E. Schlesinger, J.L. Watson, **2001**; *Low temperature reduction of ferric iron in red mud*, *LIGHT METALS*, pp 157-16.
- [198] B. Mishra, A. Staley and D. Kirtepatrick, **2001**; “*Recovery and utilization of iron from red mud*”, *LIGHT METALS*, pp.149 – 156.
- [199] P. Liu, Z. Huo, S. Gu, J. Ding, J. Zhu and G. Liu, **1995**; “*Magnetic dressing iron mineral concentrate from Bayer red mud*”, *LIGHTMETALS*, pp. 149 – 153.
- [200] D. Dobos, J. Jambo and L. Vishn’ovskii, **1964**; *Utilization of Bayer Process red mud for the production of Fe and Al.*, Tsvent. Metall.,37(2), pp. 36 – 40.
- [201] V. Tathavadkar, M. P. Antony and A. Jha, **2002**; “*Improved extraction of aluminium oxide from bauxite and red mud*,” *LIGHT METALS*, pp.199-203.
- [202] P. Kasliwal and P. S. T. Sai; “*Enrichment of titanium dioxide in red mud: a kinetic study*”, *Hydrometallurgy*, 53, (1), pp. 73 – 87.
- [203] E. Sayan and M. Bayramoglu, **2000**; “*statistical modeling of sulfuric acid leaching of TiO₂ from red mud*”, *Hydrometallurgy*, 57, pp. 181 – 186.
- [204] V. L. Rayzman and I. K. Filipovich, **1999**; “*Intigrating coal combustion and red mud sintering at an alumina refinery*”, *JOM*,51(8), pp. 16 – 18.
- [205] B. Mishra, D. Kirtepatrick and M. Slavik, **2000**; “*Pyrometallurgical extraction of alumina and iron from red mud*”, (Eds): Taylor, P. R.,EPD Congress 2000 (TMS – AIME, Warrandale, PA), pp. 369 – 381.

- [206] S. C. Mishra, K. C. Rout, P. V. Ananthapadmanabhan and B. Mills; *Plasma Spray Coating of Fly Ash Pre-Mixed with Aluminium Powder Deposited on Metal Substrates*. J. Material Processing Technology **2000**. 102, 1 – 3, pp. 9 – 13.
- [207] L. Ramakrishna, D. Sen, D. SrinivasaRao, and G. Sundararajan; *Cotability and Characterization of Fly Ash Deposited on Mild Steel by Detonation Spraying*. J. of Thermal Spray Technology Volume 12 (1) March **2003**, pp. 77 – 79.

LIST OF PUBLICATIONS

BOOK CHAPTER:

- a) Plasma Sprayed Red Mud-Fly Ash Composite Coatings on Mild Steel: A Comprehensive Outline; H. Sutar, R. Murmu, D. Roy, S.C. Mishra; *Advances and Trends in Physical Science Research*, Chapter-13, Vol-2, 2019, Print ISBN: 978-93-89246-00-1, Editor: Dr. Mohd Rafatullah , Book Publisher International, London.

PAPERS PUBLISHED IN REFEREED JOURNAL:

- a) Thermal and Dry Sliding Wear Behavior of Plasma Sprayed Red Mud-Fly Ash Coatings on Mild Steel; **H. Sutar**, D. Roy, S.C. Mishra, S. Patra, R. Murmu; *Tribology in Industry*; 40(1), 117-128, **2018**.
SCOPUS CITE SCORE: 1.29, SNIP: 1.14, ICV: 126.11
JOURNAL OF SERBIAN TRIBOLOGICAL SOCIETY
- b) Sliding Wear Performance Evaluation of Red Mud (RM), RM + Fly Ash (FA) and RM + FA + Al Coatings on Mild Steel; **H. Sutar**, D. Roy, S.C. Mishra, R.R. Murmu; *Materials Sciences and Applications*; 7(3), 171-179, **2016**.
GOOGLE BASE IMPACT FACTOR: 1.08
SCIENTIFIC RESEARCH PUBLICATION, USA
- c) Friction and Wear Behaviour of Plasma Sprayed Fly Ash Added Red Mud Coatings: **H. Sutar**, D. Roy, S. C. Mishra, A. P. Chakraverty and H. Maharana; *Physical Science International Journal*; 5(1), 61-63, **2016**.
NAAS SCORE: 4.69, ICV: 100
SCIENCEDOMAIN INTERNATIONAL PUBLISHER, LONDON, UK.
- d) Effect of fly ash and carbon reinforcement on dry sliding wear behaviour of red mud; **H. Sutar**, D Roy and S.C. Mishra; *Indian Journal of Materials Science*; Article ID 296324, 7 pages, **2015**.
HINDAWI PUBLISHER, USA

THE END